



SERRI Report 70015-010

TEMPORARY EARTHEN LEVEE PROTECTION FROM OVERTOPPING USING A RAPIDLY DEPLOYABLE ARMORING SYSTEM



SERRI Project: *Increasing Community
Disaster Resilience Through Targeted
Strengthening of Critical Infrastructure*

Project Principal Investigator:
Isaac L. Howard, PhD

Report Written and Performed By:

Amanda C. Bilberry - Mississippi State University
Isaac L. Howard - Mississippi State University
Philip M. Gullett - Mississippi State University



This material is based upon work supported by the U.S. Department of Homeland Security under U.S. Department of Energy Interagency Agreement 43WT10301. The views and conclusions contained in this document are those of the authors and should not be interpreted as necessarily representing the official policies, either expressed or implied, of the U.S. Department of Homeland Security.

SERRI Project: Increasing Community Disaster Resilience
Through Targeted Strengthening of Critical Infrastructure

**TEMPORARY EARTHEN LEVEE PROTECTION FROM
OVERTOPPING USING A RAPIDLY DEPLOYABLE ARMORING SYSTEM**

Performing Organization Report No. CMRC-11-01

Written By:

Amanda C. Bilberry, Graduate Research Assistant, Mississippi State University
Isaac L. Howard, PhD, Assistant Professor, Mississippi State University
Philip M. Gullett, PhD, P.E., Associate Professor, Mississippi State University

Date Published:

July 2012

Prepared for
U.S. Department of Homeland Security
Under U.S. Department of Energy Interagency Agreement 43WT10301

Prepared by
OAK RIDGE NATIONAL LABORATORY
Oak Ridge, Tennessee 37831-6283
managed by
UT-BATTELLE, LLC
for the
U.S DEPARTMENT OF ENERGY
under contract DE-AC05-00OR22725

This page was intentionally left blank.

TABLE OF CONTENTS

LIST OF FIGURES	viii
LIST OF TABLES	x
ACKNOWLEDGEMENTS	xi
SYMBOLS	xii
ACRONYMS	xiv
EXECUTIVE SUMMARY	xvi
CHAPTER 1 – INTRODUCTION.....	1
1.1 General and Background Information	1
1.2 Objectives	1
1.3 Scope.....	2
1.4 Incorporation into the National Response Framework	3
1.5 Problem Statement	5
CHAPTER 2 – LITERATURE REVIEW.....	7
2.1 Introduction.....	7
2.2 Hurricane Katrina Storm Surge	7
2.3 Properties of Geosynthetics	8
2.3.1 Fundamental Properties	9
2.3.2 Strength Properties.....	9
2.3.3 Hydraulic Properties	11
2.4 Properties of Available Anchors	12
2.5 Levee Material Properties	13
2.6 Conventional Levee Armoring	14
2.7 Geotextile and Erosion Control Blanket Installation Guidelines.....	15
2.8 Case Studies of Geotextile Anchoring Systems.....	18
2.9 Anchor Design	20

2.10	Seaming Options	21
2.11	Pile Analysis Techniques	22
2.12	Numerical Modeling of Geotextiles and Anchors	23
2.13	Summary of Literature Review.....	24

**CHAPTER 3 – RAPID LEVEE ARMORING CASE STUDY OF
2011 MISSISSIPPI RIVER FLOOD.....25**

3.1	Introduction to Mississippi River Flooding Armoring System.....	25
3.2	Levee Protection Design	25
3.3	Installation of Armoring System.....	26
3.4	Armoring Removal and Project Summary.....	29

CHAPTER 4 – SHALLOW ANCHOR TESTING30

4.1	Anchor Testing Introduction.....	30
4.2	Anchors Tested	30
4.3	Test Section.....	31
4.4	Instrumentation, Data Acquisition, and Terminology	32
4.5	Instrument Calibration	34
4.6	Anchor Testing Procedures and Test Matrix	35
4.7	Effect of Anchor Type	37
4.8	Simulating Sustained Loading	43
4.9	Summary of Anchor Tests for Use in Numerical Modeling.....	45

**CHAPTER 5 – CONCEPT AND CONSTRUCTION OF ARMORING
SYSTEM.....46**

5.1	<i>RDAS</i> Concept	46
5.2	Preliminary Armoring Approaches.....	46
5.3	<i>RDAS</i> Construction Materials	47
5.4	<i>RDAS</i> Construction Guidance.....	48
5.4.1	Material Selection and Setup	49

5.4.2	Excavate Trench.....	49
5.4.3	Roll Down Geotextile Panel	49
5.4.4	Cut Excess and Repeat Geotextile Laydown	49
5.4.5	Trench Burial (1 of 2)	49
5.4.6	Anchor and Seam Geotextile Panels.....	50
5.4.7	Anchoring Installation Recommendations.....	51
5.4.8	Trench Burial (2 of 2) and End Connection.....	52
5.5	Estimation of Installation Rates for <i>RDAS</i>	52
5.6	Summary.....	53

CHAPTER 6 – FINITE ELEMENT MODELING APPROACH54

6.1	Overview of Finite Element Modeling Approach	54
6.2	Model Type 1 – <i>SLEMM-FL-RA</i>	54
6.2.1	<i>SLEMM-FL-RA</i> Model Geometry	55
6.2.2	<i>SLEMM-FL-RA</i> Material Properties	55
6.2.3	<i>SLEMM-FL-RA</i> Contact Interactions.....	56
6.2.4	<i>SLEMM-FL-RA</i> Steps	56
6.2.5	<i>SLEMM-FL-RA</i> Boundary Conditions.....	56
6.2.6	<i>SLEMM-FL-RA</i> Mesh	56
6.3	Model Type 2 – <i>SLEMM-RL-RA</i>	57
6.3.1	<i>SLEMM-RL-RA</i> Model Geometries	59
6.3.2	<i>SLEMM-RL-RA</i> Contact Interactions.....	59
6.3.3	<i>SLEMM-RL-RA</i> Material Properties	60
6.3.4	<i>SLEMM-RL-RA</i> Boundary Conditions.....	61
6.3.5	<i>SLEMM-RL-RA</i> Mesh	61
6.3.6	<i>SLEMM-RL-RA</i> Loads	64
6.3.7	<i>SLEMM-RL-RA</i> External Python Job Submittal Program	66
6.3.8	<i>SLEMM-RL-RA</i> External Python Results Search Programs	69
6.4	Model Type 3 – <i>SLEMM-RL-FA</i>	74
6.5	Model Type 4 – <i>DLEMM</i>	75

6.6	Modeling Results	75
6.7	Summary of Modeling	77
CHAPTER 7 – Conclusions and Recommendations		78
7.1	Summary of Research	78
7.2	Conclusions	79
7.3	Recommendations	80
CHAPTER 8 – REFERENCES		81

LIST OF FIGURES

Figure 1.1.	Levee Considered for <i>RDAS</i>	6
Figure 1.2.	Overview of <i>RDAS</i> Concept	6
Figure 2.1.	Geotextile Terminology	8
Figure 2.2.	Typical Anchors	13
Figure 2.3.	Geotextile to Slope Connection	16
Figure 2.4.	ArmorMax [®] Overlap and Connection Guidelines	16
Figure 2.5.	Geotextile Staple and Stake Details	17
Figure 2.6.	Suggested Anchor Spacing Based on Slope	17
Figure 2.7.	Anchor Connection Used for Kentucky AGS	19
Figure 2.8.	Commonly Used Seam Types	22
Figure 2.9.	Generic p-y Curve in Stiff Clays	23
Figure 3.1.	Attachment of Liner at Crest and Toe of Levee	25
Figure 3.2.	Geomembrane Armoring of Landward Side of Backwater Levee	26
Figure 3.3.	Trench Excavation	26
Figure 3.4.	Overview of Levee Protection Installation	27
Figure 3.5.	Geomembrane Pull Holes and Heat Seams	27
Figure 3.6.	Trench of Armored Levee Protection	28
Figure 3.7.	Pinned Toe of Geomembrane	28
Figure 3.8.	Panel Installation in Curve Portions of Protection	29
Figure 3.9.	Levee Protection During Removal	29
Figure 4.1.	Photographs of Anchors Tested	30
Figure 4.2.	Anchor Test Site at USACE-ERDC	31
Figure 4.3.	Strain Gage Locations	33
Figure 4.4.	Load Cell Calibration	34
Figure 4.5.	Deflection Calibration of Potentiometer	35
Figure 4.6.	Installation of Mobi Stakes and Photos of Data Acquisitions Approach	35
Figure 4.7.	Mobi Stake (0.6 m) Anchor During Testing	36
Figure 4.8.	Installation of 0.3 m Star Picket	36
Figure 4.9.	Star Picket (0.3 m) Anchor During Testing	36
Figure 4.10.	Installation of 0.6 Threaded Bar Anchor	36
Figure 4.11.	Threaded Bar Anchor During Testing	37
Figure 4.12.	Anchor Type Load Deflection Comparison for 0.3 m Length	39
Figure 4.13.	Anchor Type Load Deflection Comparison for 0.6 m Length	40
Figure 4.14.	Load Deflection Curve for Taped and Non-Taped Specimens	42
Figure 4.15.	Load Deflection Behavior within linear Portion of Curves	43
Figure 4.16.	Load Deflection Behavior of Sustained Loading Comparison	44
Figure 4.17.	Overview of Load Deflection Curve Used in Numerical Modeling	45
Figure 5.1.	Preliminary Design Anchoring and End Connection Concepts	47
Figure 5.2.	Summary of <i>RDAS</i> Construction Sequencing	48
Figure 5.3.	Sequences for Anchoring and Seaming of Geotextile Panels	50
Figure 5.4.	Modifications to Vitton et al. (1998) Anchor Connection Cup	51
Figure 5.5.	Recommended End Connection Approaches	52
Figure 6.1.	Model Type 1 – Geometry	55

Figure 6.2.	Model Type 1 – Geotextile and Earthen Levee Mesh	57
Figure 6.3.	Flow Diagram of Rigid Levee Model.....	58
Figure 6.4.	Model Type 1 – Assembly of Model Parts	59
Figure 6.5.	Frictional Resistance for a Range of Friction Factors	59
Figure 6.6.	Undeformed Specimen During ASTM D4595 Testing	60
Figure 6.7.	Load vs. Percent Strain Plot from Product Specifications.....	60
Figure 6.8.	Model Type 2 – Boundary Conditions.....	61
Figure 6.9.	Model Type 2 – Geotextile Mesh	62
Figure 6.10.	Mesh Convergence Curve.....	62
Figure 6.11.	Shear Stress Distribution for Mesh Size = 2.47 m ²	63
Figure 6.12.	Shear Stress Distribution for Mesh Size = 0.45 m ²	63
Figure 6.13.	Shear Stress Distribution for Mesh Size = 0.18 m ²	63
Figure 6.14.	Model Type 2 – Applied Loads	64
Figure 6.15.	Shear Stress Profiles on Levee.....	65
Figure 6.16.	UTRACLOAD Subroutine (Waveload.f).....	65
Figure 6.17.	Job Submittal Program (<i>JSP</i>) Flowchart.....	67
Figure 6.18.	<i>JSP</i> Code Lines 1 to 31 of 91.....	67
Figure 6.19.	<i>JSP</i> Code Lines 32 to 91 of 91.....	68
Figure 6.20.	Flowcharts of Output Search Programs	69
Figure 6.21.	<i>OSSS</i> Program Code Lines 1 to 69 of 113	70
Figure 6.22.	<i>OSSS</i> Program Code Lines 69 to 113 of 113	71
Figure 6.23.	<i>ORS</i> Program Code Lines 1 to 24 of 143.....	71
Figure 6.24.	<i>ORS</i> Program Code Lines 25 to 87 of 143.....	72
Figure 6.25.	<i>ORS</i> Program Code Lines 88 to 143 of 143.....	73
Figure 6.26.	Model Type 3 Mesh Convergence.....	74
Figure 6.27.	Model Evaluation Rectangle for Dual Layer Geotextile Model.....	75

LIST OF TABLES

Table 2.1.	Product Details of Geosynthetics Investigated	9
Table 2.2.	Fundamental Properties of Applicable Geosynthetics	9
Table 2.3.	Strength Properties of Applicable Geosynthetics	10
Table 2.4.	Interface Friction Testing Test Data	10
Table 2.5.	Manning's n of Applicable <i>TRM</i> 's from North American Green [®]	11
Table 2.6.	Manning's n from Kilgore and Cotton.....	11
Table 2.7.	Erosion Control Material Properties	12
Table 2.8.	Overview of Available Anchor Types	12
Table 2.9.	Installation Procedures for Anchors.....	12
Table 2.10.	Levee Fill Material Properties	14
Table 2.11.	Typical Undrained Embankment Fill Properties	14
Table 2.12.	Suggested Length of Anchors Based on Soil Type	18
Table 2.13.	Overlap Requirements Based on Subgrade CBR.....	21
Table 2.14.	Model Parameters Used by Huang et al.....	24
Table 2.15.	Geotextile Material Properties Used in Seay Model.....	24
Table 4.1.	Drive Sleeve Test Results	32
Table 4.2.	Dynamic Cone Penetrometer Test Results	32
Table 4.3.	Anchor Pull Schedule	37
Table 4.4.	Comparison of Anchor Type Effectation.....	38
Table 4.5.	ϵ_{max} Strain Gage Data for 0.3 m Length Rods.....	41
Table 4.6.	ϵ_{max} Strain Gage Data for 0.6 m Length Rods.....	41
Table 4.7.	Load Deflection Data for Sustained Loading Effects Comparison	44
Table 6.1.	Material Property Values for Earthen Levee Model.....	55
Table 6.2.	Results of <i>SLEMM</i>	76
Table 6.3.	Reaction Forces from Dual Layer Rectangle Validation Model	77

ACKNOWLEDGEMENTS

Thanks are due to many for the successful completion of this project. The authors are especially grateful for the financial support provided by the *SERRI* program. In addition, due gratitude is extended to everyone employed at *DHS* and *ORNL* who worked diligently with the authors to make this project a success. A great deal of the success of this research can be attributed to the efforts of *DHS* and *ORNL* personnel.

Thanks are due to USACE-ERDC-APB under the direction of Dr. Gary Anderton for hosting the anchor testing portion of the project, providing the test site, and providing technical contributions. Additional thanks are owed to the following ERDC employees who supported the research by assisting in planning, providing technical guidance, building the test site, and conducting the needed testing: Chase Bradley, Civil Engineering Technician-APB; Daniel Butler, Model Maker-DPW; Tommy Carr, Electronics Technician-ISD; Chad Gartrell; Research Civil Engineer-APB; Quint Mason, Civil Engineering Technician-APB; and Greg Norwood, Research Civil Engineer-APB.

Dr. William H. McAnally, Research Professor at Mississippi State University, Jeremy A. Sharp, Research Hydraulic Engineer at USACE-ERDC-CHL, and Freddie Pinkard, Chief of the River Engineering Section and Mississippi River Channel Improvement Coordinator at the USACE Vicksburg District provided assistance in visiting the Yazoo River Backwater Levee while armored during the Mississippi River flooding of 2011. Mr. Pinkard also helped assemble information regarding the levee armoring and provided technical guidance for this portion of the project.

Many others supported the efforts presented in this report and are owed due thanks. Joe Ables, consultant, assisted in wiring sensors and data acquisition. Thanks are due to the Vicksburg, Memphis, and New Orleans USACE districts for providing levee material data and Eddie Templeton of Burns Cooley Dennis, Inc. for helping define needed levee cap material properties. Randy Lord, former MSU student, assisted with several test items including attaching strain gages to the threaded rods. Thanks are also due to Marneisha Richard, former graduate student, who assisted in literature review for anchoring.

Thanks are owed to Freddie Pinkard and Dr. Robert Hall (consultant, retired from USACE-ERDC as Chief, Geosciences and Structures Division) for technical and editorial review of this report. Mr. Pinkard reviewed Chapter 3, while Dr. Hall reviewed technical content from all chapters. The contributions of Mr. Pinkard and Dr. Hall are reflected in this document and they were invaluable.

SYMBOLS

A	Area of geotextile for Wide Width Tensile Test
A_A	Area of anchor plate
A_{D1}	Distance anchored on first panel
A_{D2}	Distance anchored on first panel plus the width of one geotextile panel
A_g	Section area of geogrid
B	Length /width of the square anchor place
C	Width of levee crest
C_D	Cross direction
$Coords(l)$	x -Coordinate of node (m)
D	Embedment depth
E	Young's modulus
F_c	Breakout factor
G_s	Specific gravity
G_w	Geotextile Width for Modeling
H	Horizontal
H_1	Levee height
H_2	Berm height
LL	Liquid Limit
LL_{avg}	Average Liquid Limit
L_1	Width of geotextile specimen during Wide Width Tensile Test
L_2	Length of geotextile specimen during Wide Width Tensile Test
M_D	Machine direction
ML	Sandy silt
P	Axial load
$P@_{ef}$	Load corresponding to the beginning of yielding
P_{max}	Maximum anchor load
PL	Plastic Limit
Q_u	Net ultimate holding capacity
R^2	Coefficient of Determination
R_L	Geotextile roll length
R_W	Geotextile roll width
RF_{max}	Maximum reaction force over entire geotextile
$S_{100\%}$	Stiffness at 100% of maximum load
$S_{75\%}$	Stiffness at 75% of maximum load
$S_{50\%}$	Stiffness at 50% of maximum load
$S_{25\%}$	Stiffness at 25% of maximum load
S_x'	Anchor spacing in wave overtopping direction along landward slope of the levee
S_z'	Anchor spacing in z -direction along levee
T	Depth of anchor trench
TL	Trendline equation for linear portion of anchor pull
T_g	Geotextile thickness
T_{seam}	Geotextile seam strength

V	Vertical
W_{α}	Weight of soil immediately above anchor
W	Total width of levee including berm width
W_1	Width of levee only
W_2	Width of berm only
a	Adhesion
c_{a-p}	Peak adhesion during ASTM D 5321 (kPa)
c_{a-r}	Residual adhesion during ASTM D 5321 (kPa)
c_u	Undrained cohesion of clay
d_1	Depth of levee
f	Coefficient of friction for geotextile-soil interaction
h	Overtopping height
k	Coefficient of lateral earth pressure
m	Slope
n	Manning's coefficient of roughness
t_{ef}	Total time of yielding
w	Moisture content
β	Angle of slope with ground
γ	Unit Weight of Soil
γ_{avg}	Average density
γ_d	Standard Proctor density
γ_{dry}	Dry Density
γ_{water}	Unit weight of water
$\Delta @ P_{max}$	Deflection at maximum load
ΔL_1	Change in width of geotextile specimen during Wide Width Tensile Test
ΔL_2	Change in length of geotextile specimen during Wide Width Tensile Test
δ_p	Peak angle of friction during ASTM D 5321 (°)
δ_r	Residual angle of friction during ASTM D 5321 (°)
ε	Strain
$\varepsilon @ P_{max}$	Largest strain gage reading at maximum load for any location on anchor
ε_{max}	Maximum strain of each gage throughout entire test
θ	Inclination of anchor with respect to the horizontal
τ	In-Plane von mises shear stress
$\tau_{avg,90\%}$	Average von mises stress of bottom 90% of data
τ_F	Frictional resistance
τ_{gross}	Gross applied shear stress
$\tau_{max,all}$	Maximum shear stress over entire geotextile
$\tau_{max,90\%}$	Maximum shear stress excluding top 10% of data
τ_{net}	Net shear stress
Φ	Friction angle
ν	Poisson's ratio

ACRONYMS

2D	Two Dimensional
3D	Three Dimensional
AdH	Adaptive Hydraulics
AGS	Anchored Geotextile System
APB	Airfields and Pavements Branch
AASHTO	American Association of State Highway and Transportation Officials
ASCE	American Society of Civil Engineers
ASTM	American Society for Testing and Materials
ATV	All Terrain Vehicle
BMP	Best Management Practices
C3D9R	3 dimensional, 9 node continuum element with reduced integration
CAE	Complete Abaqus Environment
CBR	California Bearing Ratio
CEE	Civil and Environmental Engineering
CL	Low Plasticity Clay
CH	High Plasticity Clay
DCP	Dynamic Cone Penetrometer
DHS	Department of Homeland Security
DLEMM	Double Layer Elastic Membrane Model
ERDC	Engineering Research and Development Center
FA	Flexible Anchor
FEA	Finite Element Analysis
FEMA	Federal Emergency Management Agency
FL	Flexible Levee
FSR	Factor of Safety Ratio
<i>GUI</i>	Graphical User Interface
HDPE	High Density Polyethylene
HPTRM	High Performance Turf Reinforcement Mat
HTL	Hurricane Liaison Team
HWL	High Water Level

<i>JSP</i>	Job Submittal Program
M3D9R	3 dimensional, 9 node membrane element with reduced integration
MSU	Mississippi State University
NICC	National Infrastructure Coordinating Center
NRF	National Response Framework
OMC	Optimum Moisture Content at Standard Proctor density
<i>ORS</i>	Output Reactions Search
ORNL	Oak Ridge National Laboratory
<i>OSSS</i>	Output Shear Stress Search
<i>PI</i>	Plasticity Index
PVC	Polyvinyl Chloride
RA	Rigid Anchor
<i>RDAS</i>	Rapidly Deployable Armoring System
<i>RECP</i>	Rolled Erosion Control Products
<i>RF</i>	Reaction Force
RL	Rigid Levee
S4R	4 node reduced integration shell element
SERRI	Southeast Regional Research Initiative
SLEMM	Single Layer Elastic Membrane Model
TRM	Turf Reinforcement Mat
USACE	United States Army Corps of Engineers
USCS	Unified Soil Classification System
WC	Wave Case

EXECUTIVE SUMMARY

This document describes the development of a Rapidly Deployable Armoring System (*RDAS*) used to temporarily protect the landward side of critical portions of earthen levee systems against storm surge overtopping. An *RDAS* could improve resilience of the current levee systems in the U.S. The research was broken into four parts: collecting shear stress profiles for wave and surge overtopping, determine the feasibility of *RDAS* construction, performing anchor testing to determine load deflection behavior in representative levee soil, and conducting numerical modeling of an *RDAS* with typical levee dimensions, anchor behaviors, and shear stress profiles.

Shear stress profiles used in this report were collected by flume testing provided in SERRI Report 70015-009. Constructability of an *RDAS* was verified by performing a case study on the Yazoo Backwater levee protection performed by the USACE. Full scale anchor testing was performed and typical load deflection behavior was determined for use in modeling. A finite element model of an *RDAS* was developed, although further modeling is required for the current model to be able to provide design guidance. A new element formulation could be required to accommodate shear and surface loading to further develop the model for design use.

Research performed for this document validated an *RDAS* has merit for emergency applications for levee protection, although further research is needed for field use. The research team recommends giving an *RDAS* serious consideration for temporary protection of select levee sections although further investigations are needed before deployment. Full scale testing of an *RDAS* system is needed to determine the interactions and behaviors of the anchors, geotextile strength mobilization, friction resistance, and wave conditions.

CHAPTER 1 – INTRODUCTION

1.1 General and Background Information

The work presented in this report was developed in partial fulfillment of the requirements of Task Order 4000064719 sponsored by the *Department of Homeland Security (DHS)* through its *Southeast Region Research Initiative (SERRI)* program administered by *UT-Battelle* at the *Oak Ridge National Laboratory (ORNL)* in Oak Ridge, Tennessee. The research was proposed by members of the *Department of Civil and Environmental Engineering (CEE)* at *Mississippi State University (MSU)* to *SERRI* in a document dated 1 June 2007. The proposed research was authorized by *UT-Battelle* in its task order dated 10 December 2007. Work on the project was initiated on 1 January 2008. A modification of Task Order 4000064719 was proposed on 9 September 2008 and agreed upon on 29 September 2008. A second Task Order modification dated 22 June 2010 was also performed, which is the Task Order used to generate this report.

The scope of work associated with Task Order 4000064719 included several related components. The general project objectives were to investigate means for rapidly using on-site materials and methods in ways that would most effectively enable local communities to rebuild in the wake of a flooding disaster. Within this general framework, several key work components were associated with Task Order 4000064719. Specifically, the scope of work dated 22 June 2010 includes research efforts in the following six task groups:

Task 1: Erosion Control-Erosion Protection for Earthen Levees.

Task 2: Bridge Stability-Lateral & Uplift Stability of Gravity-Supported Bridge Decks.

Task 3: Levee Breach Repair-Closure of Breaches in Flood Protection Systems.

Task 4: Pavement Characterization and Repair.

Task 5: Emergency Construction Material Development-Staging Platform Construction.

Task 6: Fresh Water Reservoir-Restoration of Fresh Water Supplies.

The research described in this report was associated with Task 1. The report of this work was the 10th deliverable of the research project, hence the designation of the report as *SERRI Report 70015-010* of Task Order 4000064719. Work related to Task 1 was also delivered in *SERRI Report 70015-009*. The research contract was delivered in a series of reports to allow users to more efficiently obtain the information of interest.

1.2 Objectives

A key component of this research was to develop solutions which may be rapidly deployed to achieve maximum benefit to the community, typically through use of on-site materials, pre-engineered components, and innovative construction materials and techniques. This research aimed to develop solutions for protecting and/or expeditiously reconstituting critical civil infrastructure components. In this context, the specific objective of the total

effort of Task Order 4000064719 was to develop specialty materials and design and construction procedures which may be rapidly deployed to protect and restore selected key civil infrastructure components.

The primary objective of this report was to provide guidance for a Rapidly Deployable Armoring System (*RDAS*) for the landward side of earthen levees to mitigate the effects of storm surge and overtopping waves. To accomplish the primary objective, the following four items were identified as secondary objectives.

- 1) Conduct literature review.
- 2) Investigate anchoring geosynthetics to a levee face via full scale testing.
- 3) Provide construction guidance for using geotextiles as rapidly deployable temporary armoring for earthen levees.
- 4) Conduct parametric numerical modeling of levees and their protection mechanisms to establish design parameters such as anchor depth, anchor spacing, and geotextile strength. Writing user subroutines to increase modeling efficiency was also part of this secondary objective.

1.3 Scope

The revised Task 1 scope of work dated 22 June 2010 includes the eight items listed below. These eight items are the full deliverable of Task 1. *SERRI Report 70015-009* partially addressed item a) and fully addressed items b) through e). This report addresses the remainder of item a) and fully addresses items f) through h). With regard to item a), literature review related to waves and loading were addressed in SR 70015-009, while all items related to a rapid armoring system were addressed in SR 70015-010.

- a) Conduct a literature review to investigate key parameters related to levee overtopping. Items of interest could include erosion, anchoring, geosynthetics, storm surge, mechanical connection, adhesive connections, and/or a range of appropriate field conditions.
- b) Produce a scale model representing a typical flood protection levee. The model shall be constructed within an existing modeling flume outfitted with a controlled wave generator.
- c) Use the scale model from b) to conduct instrumented testing to characterize parameters associated with wave and surge overtopping under a range of conditions associated with hurricane events. Instrumentation will be used to measure pressure and velocity profiles on the protected side of earthen levees.
- d) Perform adaptive hydraulics (AdH) simulations to compliment the data from c).
- e) Use information from c) and d) to develop shear stress profiles along key portions of an earthen levee.
- f) Investigate anchoring geosynthetics to a levee face. The investigation could include physical testing, practice review coupled with fundamental design principles using adaptations of existing technology, and/or numerical modeling as appropriate to investigate anchoring a geotextile system to the protected side of an earthen levee. Testing options include large scale investigations using a portal frame system and evaluation of the connection mechanism between the anchor and the geosynthetic. The connection could also be evaluated with a number of other approaches; the research

team will select an approach or approaches. Connection schemes could vary from pinned/bolted to cables to adhesive depending on the information obtained. Numerical modeling will be considered to investigate anchor/geosynthetic/soil interaction in conjunction with or in place of physical testing.

- g) Conduct parametric numerical modeling of levees and their protection mechanisms to establish parameters such as required anchor depth, required anchor spacing, and similar. The intent is to use information from a) to f) within the model as inputs for calibration.
- h) Provide construction guidance for using geotextiles as a rapidly deployable temporary armoring for earthen levees.

In an overall sense, Task 1 was divided into 4 parts. The first part was *SERRI Report 70015-009* where the focus was obtaining levee face shear stress profiles during overtopping via flume testing to determine expected conditions during overtopping events (Hughes et al. 2011). The second part of the project was to determine construction feasibility for an *RDAS* considering emergency field conditions alongside time and material constraints. A project presented in Chapter 3 of this report on rapid levee armoring of the Yazoo Backwater Levee by the United States Army Corps of Engineers (USACE) validated construction was feasible. Chapter 5 of this report builds on Chapter 3 and provides *RDAS* construction guidance. The third part of the project was to perform full scale shallow anchor pullout testing to obtain anchor capacities in field conditions expected during wave overtopping (Chapter 4). The final part of the project was to incorporate the shear stress profiles and shallow anchor capacities into a finite element model of the levee to aid in *RDAS* design (Chapters 6 and 7). The technical content found in this report parallels the thesis written by Bilberry (2012).

1.4 Incorporation into the *National Response Framework*

The *National Response Framework (NRF)* is a document that guides the United States when conducting all-hazards response [response refers to immediate actions to save lives, protect property and the environment, and meet basic human needs (NRF 2008)]. The *NRF* is a continuation of previous federal level planning documents (e.g. Federal Response Plan of 1992), and serves as the state of the art in responding to disaster events. The following paragraphs summarize how the research within Task 1 could be applicable to the *NRF* and in what manner. The tone of the paragraphs assumes the reader is at least casually familiar with the *NRF* and supporting documentation.

According to NRF (2008), “Resilient communities begin with prepared individuals and depend on the leadership and engagement of local government, nongovernmental organizations, and the private sector.” The word “prepared” in the previous sentence is very powerful and could refer to numerous components. The current state of practice in emergency strengthening prior to a water based catastrophe is an area where the authors feel the United States is not fully “prepared”. To approach a state of readiness where the United States is “prepared” for these events, concepts need to be developed that are studied to reasonable resolution where design methods and materials are developed (primarily laboratory scale and analytical studies). These methods and materials then need to be demonstrated at full scale, and thereafter training needs to be performed to ensure construction responders can perform the needed tasks. In present day, this level of preparedness does not exist.

The *NRF* is primarily oriented toward implementing nationwide response policy and operational coordination for any domestic event. *NRF* (2008) focuses on responding to and recovering from incidents that do occur, which is one of four major parts of a larger *National Strategy for Homeland Security*. *NRF* (2008) states that although some risk may be unavoidable, first responders can effectively anticipate and manage risk through proper training and planning. An entire chapter of *NRF* (2008) addresses planning. One of the three principal benefits that is listed for planning is “it contributes to unity of effort by providing a common blueprint for activity in the event of an emergency. Planning is a foundational element of both preparedness and response and thus is an essential homeland security activity.

Neither training nor planning appears to be performed to any significant extent related to emergency design and construction for the purpose of rapidly strengthening and/or repairing civil infrastructure. Training programs that result in certifications to perform certain activities would expedite selection of qualified groups in the highly time sensitive environment of a disaster. Having known quantities of certified contractors in place would also be valuable during planning exercises. The end products of the work within Task 1 would need to be further developed into full scale demonstrations. Contractors and design firms could then be certified to perform the tasks.

The goals of the research conducted in this report possibly align with the needs of the *Hurricane Liaison Team (HLT)*, whose goal is to enhance hurricane disaster response. Response was stated earlier to refer to immediate actions to save lives, protect property and the environment, and meet basic human needs. The *NRF* is not specific as to whether response refers to actions immediately prior to an event that temporarily strengthen key infrastructure (i.e. work presented in this report). Task 1 does align with *Scenario 10: National Disaster-Major Hurricane* of the National Planning Scenarios that have been established in *NRF* (2008).

The National Infrastructure Coordinating Center (NICC) monitors the Nation’s critical infrastructure and key resources on an ongoing basis. During an incident, the NICC provides a coordinating forum to share information across infrastructure and key resources sectors through appropriate information-sharing entities such as the Information Sharing and Analysis Centers and the Sector Coordinating Councils.” Selection of which levees to temporarily strengthen were outside of the scope of the research, but in future activities this selection process could be coordinated with the *NICC*.

Repeatedly preparedness is stated (directly or indirectly) as an essential precursor to response. The *RESPONSE ACTIONS* chapter of *NRF* (2008) shows a circular preparedness cycle consisting of the following four categories: 1) plan; 2) organize, train, and equip; 3) exercise; and 4) evaluate and improve. Under the organize category, assembling well-qualified teams of paid and volunteer staff for essential response and recovery tasks is listed. Also under the organize category is discussion of *Pre-Scripted Mission Assignments*. They are used to assist in planning for and reduction in time necessary to deploy resources that can be tailored for training, development, and to exercise rosters of deployable resources. These assignments would need to be developed for Task 1.

Advanced Readiness Contracting is used to ensure contracts are in place before an incident for often needed commodities (a list is provided that does not include construction materials). Geosynthetics and anchors are construction items that would need to be included

in *Advanced Readiness Contracting*. This could be an essential step for successful construction of a rapid levee armoring system.

1.5 Problem Statement

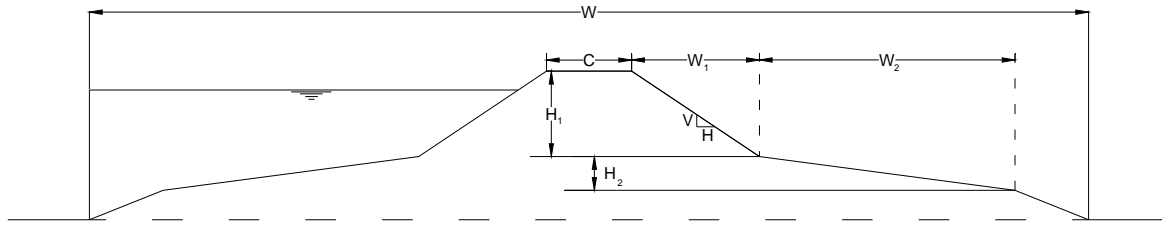
Many hurricane protection earthen levees such as those in present day New Orleans are in potential danger from erosion due to storm surge, wave overtopping, and flooding from large storms. As an example, wave overtopping and storm surge during Hurricane Katrina caused numerous failures in the levee system. If levees can stand against overtopping without failure, or at least stand for the longest possible time, numerous benefits can be reaped by minimizing loss of life and property damage. Design and implementation of a Rapidly Deployable Armoring System (*RDAS*) used to temporarily protect the landward side of critical portions of earthen levee systems against storm surge could improve resilience of a levee system and in turn minimize loss of life and property damage. Many areas such as those along the Mississippi River, the Sacramento River basin, and the region around Lake Okeechobee would benefit from an *RDAS*.

United States levees are currently given an “F” letter grade rating in the American Society of Civil Engineers (ASCE) Annual Infrastructure Report Card. United States flood defenses are rated at the very lowest levels of adequacy and reliability, and natural disasters such as Hurricane Katrina have caused levee repair and protection to become a key issue in civil engineering (Seed et al. 2012).

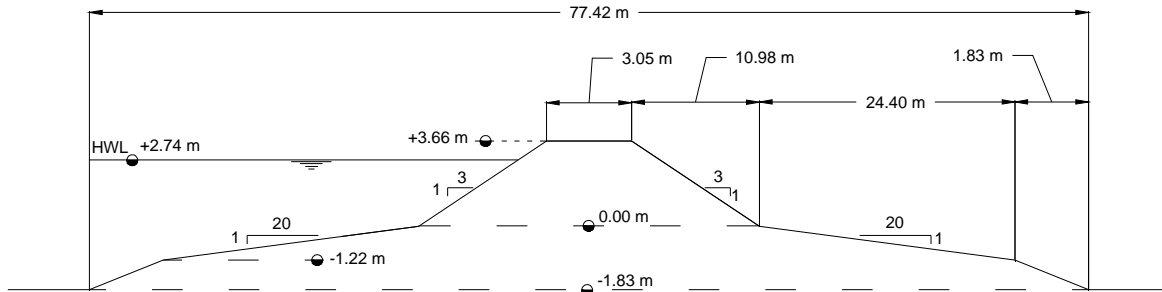
Options for permanent levee repair and protection include, but are not limited to, seeding, placement of loose stone riprap, rock-filled mattresses, articulated concrete mattresses, paving, permanent erosion protection using geotextiles, and turf reinforcement mats. Most protection and armoring is placed on the seaward side of levees. A commonly used *RDAS* has not been identified by the authors. The *RDAS* will ideally prevent levee failure from overtopping, but if not it will lengthen the time to failure, which will allow more time to get people safely out of the affected area.

This study focused on protecting the levee shown in Figure 1.1 (typical New Orleans levee section) by developing a landward side protection system. One slope was considered; 3 horizontal to 1 vertical (3H:1V). Figure 1.2 presents an overview of the *RDAS* design concept with terminology used in the remainder of this report. The *RDAS* essentially consists of anchoring a geotextile to the landward side of the levee to protect against surge and wave overtopping.

Levee dimensions analyzed in this study were limited to those in Figure 1.1b. Woven geotextiles were the only armoring material considered. Square and rectangular anchor spacing patterns were the only configurations considered for the *RDAS*. Additionally, the finite element modeling software Abaqus was used alongside Fortran and Python programming languages to perform the necessary computations.



a) Typical Levee



b) Typical Levee with Dimensions

Figure 1.1. Levee Considered for RDAS

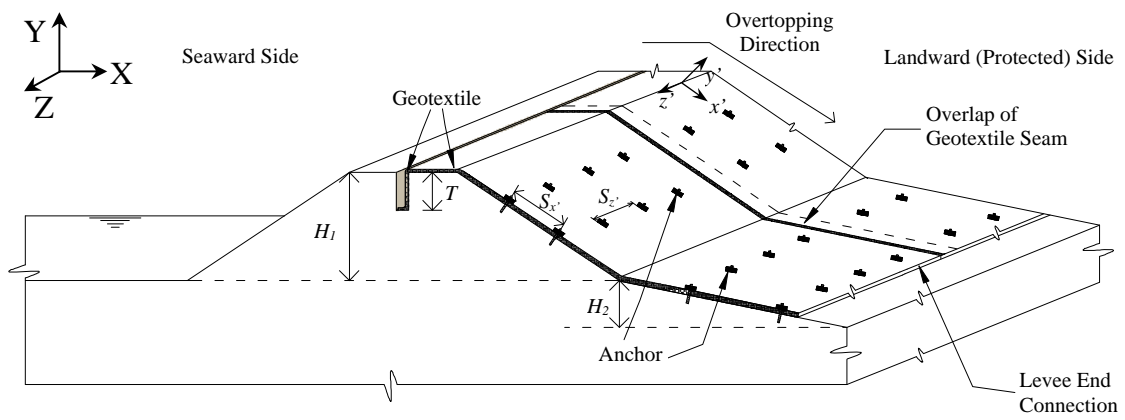


Figure 1.2. Overview of RDAS Concept

CHAPTER 2 – LITERATURE REVIEW

2.1 Introduction

A literature review was conducted to ascertain information that would be useful in developing a rapidly deployable armoring system for the landward side of an earthen levee. Pertinent literature related to wave overtopping was, in general, precluded from this document as it was provided in *SERRI Report 70015-009*. Key items of investigation in this report were erosion of unprotected levees, use of geosynthetics within levees and key properties that would be pertinent to a geotextile armoring system, mechanical and/or adhesive connection of anchors to geotextile, shallow anchors, conventional levee armoring systems, testing of armoring systems, and numerical simulation of waves on levees with emphasis on information related to modeling armoring systems.

2.2 Hurricane Katrina Storm Surge

Hurricane Katrina made landfall on August 29, 2005 near Buras, LA as a Category 3 storm with winds near 110 knots. The 16.8 m high waves and massive storm surge produced were the largest ever recorded to hit North America. The hurricane protection system failure during Hurricane Katrina has been documented as costly resulting in many deaths, many left homeless, and billions of dollars in direct damage (Briaud et al. 2008, Seed et al. 2008, Fritz et al. 2008, Heerden 2007). According to Manous et al. (2009) the southeast Louisiana hurricane protection system was 567 km long at the time of Hurricane Katrina, but was a complex assemblage of many components that was neither designed nor operated as a system.

It took 43 days to remove the water from the city of New Orleans immediately after failure of the hurricane protection system. Heerden (2007) reported over half of the greater New Orleans protection levees were damaged. Nicholson (2006) reported on a team of independent experts assembled and sent to New Orleans in September 2005. The group observed a number of failure mechanisms including overtopping scour erosion, seepage, and piping. Sills et al. (2008) reported that the storm surge and waves caused dozens of major breaches of the hurricane protection system, and that the majority of these breaches were attributed to overtopping and erosion. Levees were able to last only a few hours at most prior to failure from the high velocity and overtopping flow volumes. Erosion due to overtopping also increased instability problems of weak soil foundations (Sasanakul et al. 2008). According to Carter (2005) and Seed et al. (2008) a considerable breach during Hurricane Katrina was in the 17th Street Canal which was at a levee-flood wall combination spanning 137 m.

Briaud et al. (2008) defines erodibility as the soil erosion rate corresponding to the water flow velocity over the soil. Researchers have analyzed the erodibility of material sampled from New Orleans levees, and an erosion chart was developed that included categories from very high erodibility (Category I) to Non-Erosive (Category VI). The chart was based on soil erosion rate versus applied shear stresses. Results from erosion testing showed that the levees in New Orleans contained soil ranging from Category I to Category

IV. These results suggest a reason for some levees failing from and some levees withstanding the storm surge.

The USACE reported that St. Charles and Jefferson levees, which were reinforced with geotextiles at the time of Hurricane Katrina, were loaded by the storm but were not breached like other unreinforced levees in the same area (Woodward and Dendrent 2009a, 2009b; Bygness 2008). The geotextile reinforcement included placing layers of geotextiles within the soil layers of the levee during construction.

2.3 Properties of Geosynthetics

Geotextiles are woven or nonwoven fabrics used in construction for purpose(s) including: separating aggregate and soil layers, reinforcement, filtration, drainage, and/or containment. The first documented use of geotextiles was 1958 under concrete erosion control blocks. The geotextile was used as an economical replacement of a granular filter behind concrete blocks to prevent erosion (Theisen 1992). Since then, geotextile use has been extended into many construction projects.

Geotextiles are stored in rolls with common roll lengths (R_L) of 46, 91, and 110 m, while roll widths (R_W) usually range between 3.8 to 4.5 m. Geotextiles can be manufactured to project specific requirements, but pre-ordering would be necessary in these cases likely making it an impractical option for disaster response. General dimensions and directional terms used in the geotextile industry are provided in Figure 2.1.

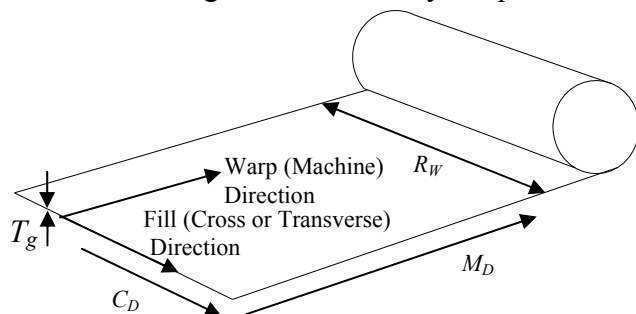


Figure 2.1. Geotextile Terminology

Table 2.1 summarizes several geosynthetics pertinent to this effort; a product ID was assigned to each geosynthetic for identification purposes in the rest of this document.

Most geotextiles are made of polypropylene; polyester is also used for some applications. Geotextile thicknesses (T_g) can range from 0.25 to 7.5 mm, and the specific gravity (G_s) of polypropylene geotextile is 0.91 (Koerner 2005).

Many types of erosion control blankets are available including temporary or permanent fabrics. Temporary erosion control blankets made by North American Green[®] are made of straw. These types of blankets are placed on moderate slopes or low-flow channels. Extended degradable erosion control blankets are made of straw and coconut fibers. Permanent turf reinforcement mats (TRMs) are made of straw and a coconut fiber matrix or straw and a polypropylene fiber matrix (North American Green[®] 2004).

Table 2.1. Product Details of Geosynthetics Investigated

Product ID	Manufacturer	Model	Product Type
<i>GT-1</i>	TenCate Mirafi®	HP270	Geotextile
<i>GT-2</i>	TenCate Mirafi®	HP570	Geotextile
<i>GT-3</i>	TenCate Mirafi®	PP200/40	Geotextile
<i>GT-4</i>	TenCate Mirafi®	HP565	Geotextile
<i>GT-5</i>	TenCate Mirafi®	HP370	Geotextile
<i>GT-6</i>	TenCate Mirafi®	HP665	Geotextile
<i>GT-7</i>	TenCate Mirafi®	HP770	Geotextile
<i>GT-8</i>	TenCate Mirafi®	HP465	Geotextile
<i>TRM-1</i>	Propex ArmorMax™	HPTRM	Turf Reinforcement Mat
<i>TRM-2</i>	North American Green®	SC250	Turf Reinforcement Mat
<i>TRM-3</i>	North American Green®	C350	Turf Reinforcement Mat
<i>TRM-4</i>	North American Green®	P550	Turf Reinforcement Mat
<i>TRM-5</i>	North American Green®	P300	Turf Reinforcement Mat

2.3.1 Fundamental Properties

Table 2.2 outlines fundamental geosynthetic properties including roll length (R_L), roll width (R_W), geosynthetic thickness (T_g), and estimated roll weight.

Table 2.2. Fundamental Properties of Applicable Geosynthetics (TenCate Mirafi® 2010a-h, North American Green® 2009a-d, and Propex® 2010b)

Product ID	R_L (m)	R_W (m)	T_g (mm)	Roll Weight (kg)
<i>GT-1</i>	91	4.5	--- ⁽¹⁾	100
<i>GT-2</i>	91	4.5	--- ⁽¹⁾	215
<i>GT-3</i>	91	4.5	--- ⁽¹⁾	620
<i>GT-4</i>	91	4.5	--- ⁽¹⁾	202
<i>GT-5</i>	91	4.5	--- ⁽¹⁾	121
<i>GT-6</i>	91	4.5	--- ⁽¹⁾	253
<i>GT-7</i>	91	4.5	--- ⁽¹⁾	242
<i>GT-8</i>	200	5.2	--- ⁽¹⁾	156
<i>TRM-1</i>	27.4	2.6	10.2	32.4
<i>TRM-2</i>	16.9	2.0	18.3	15.4
<i>TRM-3</i>	16.9	2.0	17.0	16.8
<i>TRM-4</i>	16.9	2.0	19.3	23.6
<i>TRM-5</i>	32.9	2.0	13.7	27.7

1: T_g not provided on product data sheets; a variety of HP products were measured with calipers to be between 1.2 to 3.5 mm.

2.3.2 Strength Properties

Table 2.3 outlines geosynthetic strength properties including maximum permissible shear stress, maximum permissible velocity, seam strength (T_{seam}), tensile strength in the machine direction (M_D), and cross direction (C_D) at various strain (ϵ) levels.

Table 2.3. Strength Properties of Applicable Geosynthetics (TenCate Mirafi® 2010a-h, North American Green 2009a-d, and Propex® 2010b)

Product ID	Shear Stress (Pa) ⁽¹⁾⁽²⁾	Velocity (m/s) ⁽¹⁾⁽³⁾	T_{seam} (kN/m)	M_D/C_D Tensile Strength			
				@ 2% ϵ (kN/m)	@ 5% ϵ (kN/m)	@ 10% ϵ (kN/m)	@ Ult. ϵ (kN/m)
GT-1	---/---/---	---/---	18.4	7.0/8.6	17.7/19.8	34.1/35.2	38.5/35.9
GT-2	---/---/---	---/---	43.8	14.0/19.3	35.0/39.4	70.0/70.0	70.0/70.0
GT-3	---/---/---	---/---	20.0	25.0/---	80.0/---	---/---	200.0/40.0
GT-4	---/---/---	---/---	35.0	7.9/19.3	22.8/35.0	61.3/70.0	66.5/70.0
GT-5	---/---/---	---/---	24.6	7.9/7.9	21.9/22.8	35.0/35.0	52.5/39.4
GT-6	---/---/---	---/---	52.5	---/---	17.5/61.3	43.8/96.3	70.0/96.3
GT-7	---/---/---	---/---	43.8	16.6/22.8	52.5/52.5	96.3/84.0	105.1/84.0
GT-8	---/---/---	---/---	26.3	8.8/8.8	21.9/21.9	52.5/47.3	---/---
TRM-1	---/---/718	---/7.6	---	---/---	---/---	---/---	58.4/43.8
TRM-2	144/383/480	2.9/4.6	---	---/---	---/---	---/---	9.01/10.7
TRM-3	153/480/576	3.2/6.0	---	---/---	---/---	---/---	9.1/11.2
TRM-4	191/576/672	3.8/7.6	---	---/---	---/---	---/---	11.2/16.6
TRM-5	144/383/383	2.7/4.9	---	---/---	---/---	---/---	7.0/6.2

1: Values based on max permissible short duration of 0.5 hr

2: Unvegetated / Partially Vegetated / Fully Vegetated

3: Unvegated Velocity / Vegetated Velocity

Kim et al. (2004) and Kim et al. (2005) performed interface testing according to ASTM D 5321 except a 10 cm square test box was utilized. Test results are provided in Table 2.4. Shearing occurred at 0.9 mm/min to displacements of 1.0 to 1.3 cm. Kim et al. (2004) noted the materials were immediately inundated and then sheared after placement into the test box, while Kim et al. (2005) made no mention of whether the test specimens were inundated during testing. Kim et al. (2004) noted sand was placed below the *PVC Tube* during testing, while four straps were attached to a plywood block for testing of *Strap to PVC Tube* interface properties. *PVC Tube to PVC Tube* testing incorporated normal weights of 45 to 260 N, while *Strap to PVC Tube* testing incorporated 145 to 260 N normal weights. Residual displacement was reached at approximately 0.4 cm deformation. The high value of peak friction (54°) between two tube sections was noted to be likely due to interlocking of the polyester reinforcing strands since the material was textured.

Table 2.4. Interface Friction Testing Test Data (Kim et al. 2004, 2005)

Source	Interface Material Description	c_{a-p} (kPa)	δ_p (°)	c_{a-r} (kPa)	δ_r (°)
Kim et al. (2004)	Sand: 6% fines, D_{60} of 0.16 mm, D_{10} of 0.08 mm, 15.5 kN/m ³ test density, 15% compaction moisture	0.00	34	0.00	32
	Monofilament: woven polypropylene (AOS of 0.21 mm)	1.24	17	0.00	17
	Silty Sand: 48% fines, 17.9 kN/m ³ test density, 12.5% OMC	2.76	32	0.00	32
	Silt: 77% fines, LL of 51, PI of 16, 17.9 kN/m ³ test density, 25.0% OMC	3.45	30	0.00	27
	Grass: Healthy fine-bladed <i>festuca sp.</i>	0.00	22	0.00	22
Kim et al. (2005)	Strap: Woven nylon 2.5 cm wide and 1.6 mm thick	---	25	---	18
	PVC Tube: PVC with 7.5 parallel interwoven reinforcement strands per cm (0.5 mm) (610 g/m ² coated vinyl)	---	54	---	14

Notes: Interface material tested relative to the PVC geomembrane tube listed in the last row.

Test listed in the last row was PVC Tube interfacing with PVC Tube.

Ghiassian (1995) developed a test to determine the interface resistance between fabric and soil. An arc-shaped fabric was placed over a Muskegon dune sand and equal loads were applied to both ends of the geosynthetic. Fabrics tested were cotton fabric, fiberglass mesh, and Geolon N35 filter cloth. The interface resistance was determined by the tension at the ends of the geosynthetic when it began to slip and was a function of the radius of the circular arc, the angular curvature of the arc, adhesion between soil and fabric, and tensions at the end of the fabric at the time of sliding. Test results showed interface friction between 30 and 36 degrees for all fabrics tested.

2.3.3 Hydraulic Properties

Table 2.5 presents the available Manning’s n values for the select TRM’s. No Manning’s n data was available for GT-1 to GT-8. According to Sprague et al. (2002), n for unvegetated rolled erosion control products (RECPs) typically vary between 0.02 to 0.04 with material type and flow depth. Kilgore and Cotton (2005) used typical roughness coefficients (n) for Manning’s equation in the design of roadside channels with flexible linings (Table 2.6).

Table 2.5. Manning’s n of Applicable TRM’s from North American Green® (2009a-d)

Product ID	Flow Depth (m)		
	≤0.15	0.15 – 0.60	≥0.60
TRM-1	---	0.026	---
TRM-2	0.040	0.040 – 0.012	0.011
TRM-3	0.041	0.040 – 0.013	0.012
TRM-4	0.041	0.040 – 0.014	0.013
TRM-5	0.034	0.034 – 0.020	0.020

Table 2.6. Manning’s n from Kilgore and Cotton (2005)

Type of Rolled Erosion Control Product	Minimum	Typical	Maximum
Open weave textile	0.022	0.025	0.028
Erosion control blankets	0.028	0.035	0.045
Turf reinforcement mat	0.024	0.030	0.036

Chen et al. (2010) performed laboratory testing on seven types of artificial erosion control materials to determine material properties of each including coverage ratio (%), apparent openings (mm), thickness (cm), and Manning’s coefficient (n) as shown in Table 2.7. Woven, non-woven, and composite materials were tested in the study. Material was attached to a block of soil tilted to 35° and 45° angles and measuring 300 cm long, 100 cm wide, and 20 cm thick for testing. An artificial rainfall simulator was used at an intensity of 13 cm/h for a duration of 1 hour. The Manning’s n was estimated by measuring the water velocity under uniform flow over each material placed in a flume. Coverage ratio testing was performed according to ASTM D6567, and the apparent openings test was performed according to ASTM D4751.

Table 2.7. Erosion Control Material Properties (Chen et al. 2010)

Material	Coverage Ratio (%)	Apparent Openings (mm)	Thickness (cm)	<i>n</i>
Non-woven mat	63.64	10.2	1.3	0.080
Wire and plastic net	27.95	10.0	2.0	0.037
Woven geotextile ⁽¹⁾	66.89	10 by 2	3.0	0.163
Composite mat	61.46	10.5	2.0	0.087
Woven mat	83.13	4.2	0.8	0.057
Jute net	64.05	20 by 12	0.3	0.073
Wooden-block net	22.06	120 by 100	5.0	0.150

⁽¹⁾: Fertilizer strips included.

2.4 Properties of Available Anchors

Many lightweight anchors are available for anchoring utility poles, retaining walls, sheet piles, and revetment mats. Table 2.8 presents fundamental properties for a variety of available anchor types from Foresight[®] Products, LLC and Platipus[™] Anchors, while Figure 2.2 provides photos of the anchors. Anchor investigation was limited to those that could be installed in the field with light weight equipment; Table 2.9 outlines general installation for each anchor as specified by product literature.

Table 2.8. Overview of Available Anchor Types (Foresight[®] Products 2001a,b; Platipus[™] Anchors 2010a,b; ArmorMax[®] 2010b)

Product ID	Anchor Name	Manufacturer	Capacity (kg)	Weight (kg)	Typical Driving Depths (m)
A-1	MantaRay [®]	Foresight [®] Products	4,079 – 18,151	2.7-9.5	2-10
A-2	StingRay [®]	Foresight [®] Products	10,197 – 45,377	21-35	5-15
A-3	Duckbill	Foresight [®] Products	122 – 2,243	0.03-1.1	0.5-1.5
A-4	Stealth	Platipus [™] Anchors	255 – 10,197	---	0.4-3
A-5	Type 2	--- ⁽¹⁾	224	---	0.6
A-6	Type 1A	--- ⁽¹⁾	907	---	1.1
A-7	Type 1B	--- ⁽¹⁾	2,264	---	1.1

⁽¹⁾ Anchors described in ArmorMax[®] product literature without specifying a manufacturer.

Table 2.9. Installation Procedures for Anchors (Foresight[®] 2001a,b; Platipus[™] Anchors 2010a,b)

Product ID	Installation Requirements
A-1	Manual, Vehicle Mounted Breaker or Compactor
A-2	Vehicle Mounted Breaker or Compactor
A-3	Hammer or Jackhammer
A-4	Manual or Breaker Installation

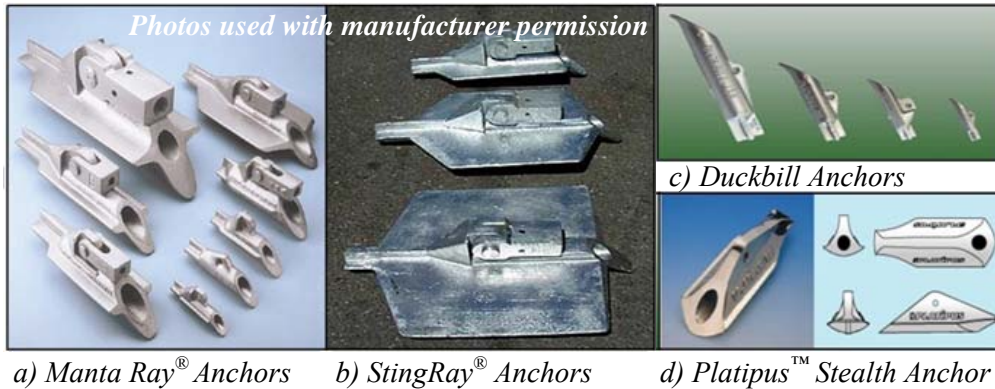


Figure 2.2. Typical Anchors (Foresight® Products, 2001a, Platipus™ Anchors 2010b)

Load plates are commercially available to ensure the geotextile is secured to the slope. Platipus™ Anchors (2010c) offers several types of load plates including galvanized or stainless steel square plates in 10, 15, 20, or 30 cm square dimensions. Polyethylene plates are available in 9 cm diameter, 15 cm square, and 20 cm square sizes.

2.5 Levee Material Properties

Levee surfaces (i.e. capping material) can contain silty soil, lean clay, or plastic clay. Plastic clay is very common in the lower Mississippi valley. Review of the USACE Design and Construction of Levees Manual (EM 1110-2-1913) found no strict set of requirements regarding levee material index properties such as Plasticity Index (*PI*) (USACE 2000). Personal contact with the Memphis, Vicksburg, and New Orleans USACE districts in March of 2011 revealed differences related to common levee capping material requirements. No strict set of specifications for levee capping material seem to exist; rather, the specifications seem to vary by district depending on the most commonly available material within each district.

The New Orleans District requires low plasticity (CL) to high plasticity (CH) material for levee capping based on the Unified Soil Classification System (USCS) with a *PI* greater than 10, organic content less than 9%, and less than 35% sand. It was noted that the New Orleans District did not have a maximum *PI* requirement provided the organic content does not exceed requirements.

The Memphis District indicated in March 2011 there were allowable moisture and organic content limits when they could be issues for a project. Levees in the district were described as made primarily from fat clay including the mainline of the Mississippi River. Some sand levees were said to exist that had a lean to fat clay capping. Material closely available was said to be used in most instances. No set requirements were in place that would limit use of a fat clay with a given *PI* so long as it did not have excessive moisture when placed and the organic content was low.

The Vicksburg District does not specify Atterberg limits for levee construction material. Usually, the Vicksburg District evaluates borrow pits and requires a contractor to obtain capping material from the chosen borrow pit. In determining a borrow pit, the district generally tries to limit the *PI* to 40 because higher values often lead to sluffing of the levee due to wetting and drying. If materials with *PI* higher than 40 are used, flattened slopes are recommended to alleviate maintenance issues.

Table 2.10 presents material properties for levee materials tested from the 17th Street Canal and London Avenue Canal levees in New Orleans. Shear strength values varied widely (≈ 5 kPa to 239 kPa), but a reasonable value was assumed for the levee fill based on data from unconfined compression tests (Duncan et. al 2008 and Brandon et. al 2008). Table 2.11 presents typical assumed undrained soil properties for embankment materials when test data are not available.

Table 2.10. Levee Fill Material Properties (Duncan et. al 2008 and Brandon et. al 2008)

Location	Soil Type	LL _{avg}	γ_{avg} (kN/m ³)	Friction Angle	Cohesion (kPa)
17 th Street Canal and London Avenue	CH and CL	45	17.1	0	43

Table 2.11. Typical Undrained Embankment Fill Properties (USACE 2007)

Soil Type	γ_{avg} (kN/m ³)	Friction Angle	Cohesion (kPa)
Compacted Clay (90%)	17.3	0	19.2
Compacted Clay from Bonnet Carrie ⁽¹⁾	18.1	0	28.7
Uncompacted Clay ⁽¹⁾	15.7	0	9.6

⁽¹⁾ Clays from dry borrow pit and placed on land.

2.6 Conventional Levee Armoring

A variety of methods are used to armor levees for overtopping in current practice. Armoring options include: loose stone riprap, wire baskets filled with small stones, rock-filled mattresses, articulated concrete mattresses, fabric-formed concrete, grout-filled bags, geocell structures filled with soil, soil cement, roller compacted concrete, and asphalt/concrete paving. Conventional methods are not suitable for the current application, though useful information can be taken from them.

Articulated concrete mattresses have proven stable against surge overtopping as documented by full-scale testing. Concrete mattresses are available in different sizes and weights for rapid placement, but placement requires heavy equipment rendering the method ineffective for weak soil. Asphalt and concrete paving is an alternative slope protection that is impermeable and durable enough to withstand wave overtopping, but this option requires heavy installation equipment and is not feasible on weak soils Hughes et al. (2006). Protection options such as gabions and roller compacted concrete protection systems are also used as outlined by dam designs provided by Hill (1997).

Commonly used structural armoring systems, or “hard armor”, for slope stabilization in coastal areas are riprap, gabions, concrete blocks, and tied tires. The confining stresses that heavy armoring systems place on the underlying soil helps protect the slope from erosion. Hard armoring systems can be unsightly, costly, and some coastal communities have regulations against their use.

Soft armoring systems made of geosynthetics are one alternative to hard armoring systems. Koerner and Robins (1986) first introduced the idea of using an anchored geotextile system for slope failure protection. The geosynthetic is anchored with small diameter metal rods at reinforced openings on the geotextile and driven into the slope to create tension in the geotextile. The fabric tensioning provides compressive stresses on the ground surface to further protect the system from erosion. According to Ghiassian et al. (1997), most research

performed for anchored geotextile systems (*AGS*) has been for sandy slopes. The *AGS* is an active tensioning system. Tensioning of the geotextile and resulting normal forces on the protected slope result in soil densification. Granular soils tend to densify much faster as compared to cohesive soils. In cohesive soils, the normal forces cause consolidation which takes longer (Koerner 2005). Gray et al. (1996) suggest using an anchored geonet for protection of coastal sand dunes as an alternative to hard armor such as rock revetments.

2.7 Geotextile and Erosion Control Blanket Installation Guidelines

Based on current practice standards presented by Koerner (2005), geotextiles chosen for slope stability protection should have a minimum 35 kN/m tensile strength based on the Wide Width Tensile Test. If prefabrication is not an option, large anchor plates or fabric reinforcement at each anchor location can be used. The reinforced geotextile area at each anchor location should provide 90 kN/m tensile strength based on the Wide Width Tensile Test for 15 cm around the anchor. Anchors used in traditional applications for connection should have a minimum diameter of 13 mm and be long enough to extend 1.5 m deeper than the expected slope failure plane. Before connecting anchors to the geotextile, the anchor should be driven into the ground a distance of 0.3 to 0.6 m. The remainder of the anchor is driven into the ground after connecting to the geotextile to allow for fabric tensioning as the anchor is driven.

TenCate Mirafi™ outlined installation guidelines for geotextiles used in filtration and drainage applications. The area to be covered by geotextile should first be cleared of debris that could damage the geotextile. Any large depressions along the slope should be filled to ensure the geotextile is placed directly in contact with the soil. At a minimum, a 0.6 m overlap should be used when connecting geotextiles. Trenches used to anchor the geotextile to the slope should be placed at a minimum of 1 m from the top of the slope. For maximum stability, the trench should be at least 0.6 m deep (TenCate Mirafi™ 2001).

North American Green® guidelines for installing TRMs on slopes include anchoring the blanket in a 15 cm by 15 cm trench with staples. The blanket should be stapled along the crest every 30 cm in the *z-direction*, as shown by Figure 1.2 levee crest axis. A 5 to 12.5 cm overlap should be stapled when connecting two adjoining blankets. Connecting blankets down the slope should have a 7.5 cm overlap with a stapled connection across the seam spaced at 30 cm (North American Green® 2004).

The USACE outlines current design procedures for the use of geotextiles in construction (USACE 1995). This manual is aimed at long term uses for geotextiles such as bank erosion protection, pavements, railroad beds, retaining wall earth embankments, and drain construction. In bank erosion protection, the geotextile should be placed on a cleared soil surface with no large depressions. The geotextile is placed with the machine direction (M_D) the same as the slope direction to protect the slope from wave action. Figure 2.3 shows the USACE geotextile-slope connection schematic including trench and pin dimensions. Trench anchoring should be used at the top and ends to prevent uplift.

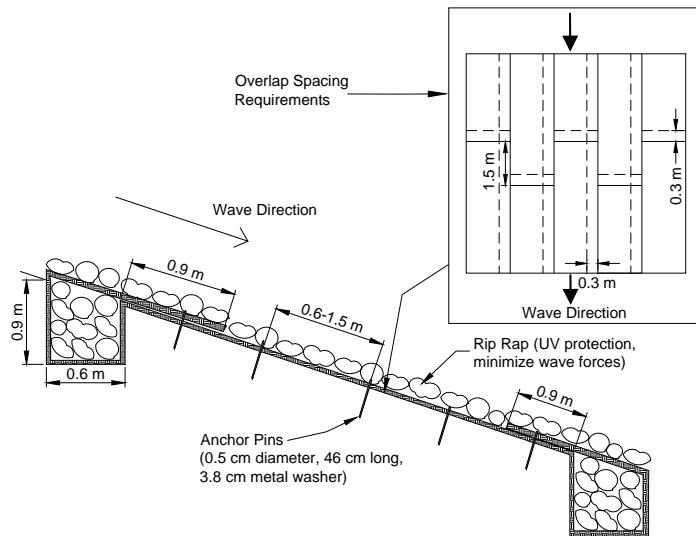


Figure 2.3. Geotextile to Slope Connection (USACE 1995)

The Wisconsin Transportation Bulletin (2010) outlines general construction guidelines for geotextiles including roadbed construction, silt fence installation, and slope protection. The bulletin suggests that geotextile be unrolled down the levee beginning at the crest. Adjoining panels should be overlapped 0.6 to 0.9 m and pinned at 0.9 to 1.5 m intervals down the slope. The geotextile should be buried in a 0.3 m deep trench at the crest and for typical applications, seeding is suggested.

ArmorMax[®] is an erosion protection system made of woven three dimensional high performance turf reinforcement mat (HPTRM) made by ProPex[®]. Installation guidelines suggest that the HPTRM be unrolled up the slope beginning at the toe. All adjoining panel seams should be overlapped a minimum of 0.15 m, and end of roll overlaps should be a minimum of 0.3 m. The HPTRM should be secured by an earth percussion anchor (see Table 2.8 for anchor information) at the toe and crest in a 0.3 m square trench. Metal pins and earth percussion anchors are used to connect the geotextile to the slope; Figure 2.4 outlines overlap and connection guidelines (ArmorMax[®] 2010a).

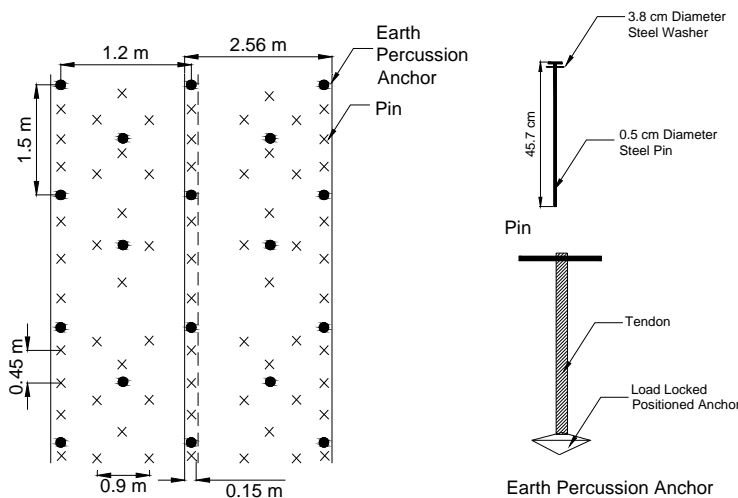
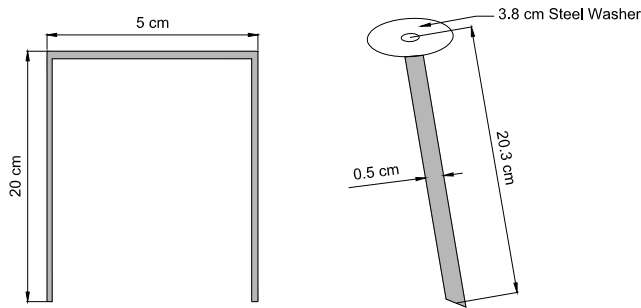


Figure 2.4. ArmorMax[®] Overlap and Connection Guidelines (ArmorMax[®] 2010a)

The California Stormwater BMP Handbook (2003) includes installation guidelines for placing geotextiles and mats on slopes for erosion protection. Woven polypropylene fabric with a minimum thickness (T_g) of 1.5 mm is specified for slope erosion control applications. Geotextile should be secured at the top of the slope in a 15 cm square trench placed 4 m beyond the edge of the crest before unrolling down the levee slope. The geotextile should be secured to the slope on 0.9 m intervals down the slope by either 11 gauge steel wire U-shaped staples or metal stakes driven flush with the ground surface (Figure 2.5).



a) U-Shaped Staple Detail b) Metal Geotextile Stake Detail

Figure 2.5. Geotextile Staple and Stake Details (California Stormwater BMP 2003)

ProPex[®] product installation guidelines for anchoring TRMs and HPTRMs suggest three options for anchor types: U-shaped wire staples, metal geotextile pins, or percussion driven anchors. Figure 2.6 presents recommended anchor frequency and spacing; Table 2.12 presents suggested ground anchor lengths for various soil conditions.

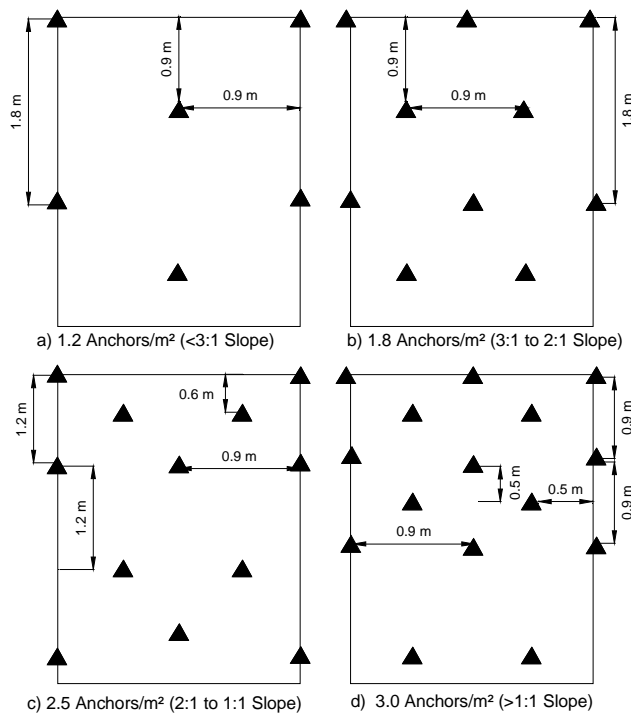


Figure 2.6. Suggested Anchor Spacing Based on Slope (ProPex[®] 2010a)

Table 2.12. Suggested Length of Anchors Based on Soil Type (ProPex[®] 2010a)

<u>Soil Type</u>	<u>Length of Anchor (cm)</u>
Rocky	15
Clayey	15 or 30
Silty	30 or 46
Sandy	46 or 61

2.8 Case Studies of Geotextile Anchoring Systems

Austin and Theisen (1996) described the geotextile protected Atkinson Island levee constructed from dredged material (medium to stiff clay and coarse sand) from the Houston Ship Channel. A woven geotextile fabric used as an erosion protection system on a 122 m sandy section of the 2H:1V levee. Product literature shows the chosen geotextile could withstand 7.5 m/s unidirectional flow velocities and 480 Pa shear stresses (Synthetic Industries 1995).

The geotextile fabric was placed on the levee seaward side approximately one year after construction. To begin installation, levee slopes were smoothed using a track hoe. Anchor trenches were installed at the levee top and toe to attach the geotextile to the anchor. The top trench was 30 by 60 cm, while the toe trench was approximately 45 cm by 130 cm to prevent anchor failure due to sediment migration during the winter months. After the fabric was rolled down the levee (adjacent rolls were overlapped 15 cm), the geotextile was anchored into the trench using Model 68-DB1 duck bill anchors (refer to A-3 in Table 2.8) with 90 cm stainless steel cables. To reinforce the connection, four 45 cm long, 9.5 mm diameter reinforcing steel bars in a hairpin shape were placed at the corners of the fabric. The anchor trenches were subsequently backfilled and compacted to a specified density, and three dry cement bags were placed along the toe of the levee to provide extra support. Approximately half the constructed length was covered with 2.5 cm of dredged material and the other half was left unseeded completely. The crew constructing the erosion protection system averaged approximately 25 linear meters per day across the levee, allowing full installation in five days (Austin and Theisen 1996).

The USACE and Synthetic industries monitored the site as a joint venture. The levee section endured waves 2 m high. In 1995, no significant soil erosion was observed. Even though the levee section was not seeded or planted, native vegetation was present along most of the levee slope.

An AGS was installed on a slope in Kentucky (Vitton et al. 1998). The soil was sandy silt (ML), had average liquid and plastic limits of 28 and 22, respectively, and had an undrained shear strength of 23 kPa. The geotextile tensile strength in the warp and fill directions were 160 kN/m and 140 kN/m, respectively. Two anchor materials were re-bar and A36 cold rolled steel round stock. Re-bar anchors proved too brittle to drive. The anchor was connected to the geotextile through a connection cup pressed from 14-gauge steel. The cup was approximately 130 mm diameter and 50 mm deep with a 22 mm hole for anchor connection (Figure 2.7). Anchors were placed in a hexagonal pattern on 1.4 m spacing. Rods (13, 19, and 25 mm) were tested in stiff clay; a 19 mm rod was chosen based on pullout resistance and ease of installation. Total anchor length was 3.9 m.

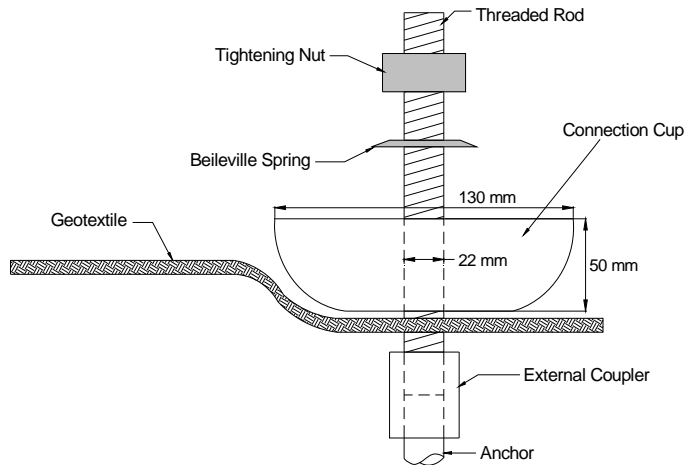


Figure 2.7. Anchor Connection Used for Kentucky AGS (Viton et al. 1998)

Installation was performed using: 1) Hiltel TE804 electric demolition hammer powered by a 4,000-watt generator; and 2) 267 N pneumatic jackhammer and diesel compressor. Dynamic pile driving enlarged the anchor hole to a point where the top portion of the anchor was not in contact with the soil. A total of 360 m² of geotextile was anchored. Installation was spread over 4 months due to bad weather conditions, but overall installation time was approximately 2.5 weeks using a 4 member work crew. The research team monitored the AGS for 1 year to determine field performance. Over time, the geotextile lost tension, which might be attributed to consolidation of the soil around the anchor. The research showed an AGS could be a suitable solution for preventing slope failures, but further research is needed to determine the extent of their applicability.

ArmorMax[®] permanent erosion protection system described in Section 2.7 was placed on the crest and landward slope of the Penn Levee and the Decamp Street Levee in Lafitte, Louisiana after Hurricane Katrina. A total of 2.9 km of armoring was installed on Penn Levee and 0.4 km installed on Decamp Street levee. Before installation, the levee was prepared by mowing, removing obstructions, and smoothing the levee surface. The HPTRM was secured to the levee with earth percussion anchors (labeled A-5 in Table 2.8) in a checkerboard grid pattern at 1.5 m centers. The armor system on Penn Levee did not fail from the 3.66 m storm surges of Hurricane Ike or heavy rain from Hurricane Gustav (ArmorMax[®] 2010b).

Turf erosion control products were installed on 20,234 m² (5 acres) of side slopes of the LaSalle-Grant Landfill in central Louisiana. The turf system was a long term erosion protection system for soil that was highly erodible with a high plasticity index. The system was placed on slopes from 3H:1V to 4H:1V. The turf system included placing geotextile with tufted polyethylene grass on top of a 50 mil geomembrane. Anchoring for stability was not required in this application because the turf system provided sufficient interface friction of 38 degrees. The system has endured rainfall intensities in excess of 0.1 m per hour without failure. Installation time was reported as approximately 4 days for 10,117 m² (2.5 acres) with one crew of workers (Hayes 2010).

2.9 Anchor Design

Reinforcing rod anchors used in *AGS* are typically small diameter steel or iron rods or pipes driven past the expected failure plane of the slope (Koerner and Robins 1986). The rods provide benefit to overall slope stability due to the friction/adhesion along the rod surface and suction at the rod end in saturated soils. In addition, the rods provide bending and torsional resistance from soil mass movement in the slope (Koerner and Robins 1986). Soil anchor capacities depend on soil shear strength, soil moisture conditions, seepage conditions, suction between the soil and anchor, friction between the soil and anchor, anchor geometry, anchor length, and anchor orientation (Hryciw and Haji-Ahmac 1992, Koerner and Robins 1986, and FEMA 2009). According to Ghiassian et al. (1997) the optimum anchor length should be designed based on the skin friction along the anchor beyond the failure plane. In addition, the anchor installation angle should maximize stability and pull-out resistance, while spacing between anchors is small enough to ensure the geotextile remains tensioned (Hryciw and Haji-Ahmac 1992).

Hryciw and Haji-Ahmad (1992) developed a method using charts to determine the optimum length, spacing, and angle embedment orientation requirements for anchored systems. Assumptions were 2 dimensional infinite slopes, cohesionless soils, and shallow failure surfaces. In general, the anchored system was designed for geotextiles placed on slopes with the anchor attached at a reinforced 5.1 cm diameter connector. Variable anchor lengths along the slope can be prescribed; however, it was anticipated that geotextiles for anchoring would be manufactured with reinforced openings at predetermined increments. The required spacing between anchors should match one of these increments (typically S_x of Figure 1.2 is taken as 1.22, 1.52, or 1.83 m).

Hryciw's (1991) equation (Equation 2.1) gives an approximation to the optimum angle (counterclockwise with respect to the y' in Figure 1.2) with a standard deviation of 0.33 degrees.

$$\theta_{opt} = 47.5^\circ - 0.7\beta - 9k + 8FSR \quad (\text{Equation 2.1})$$

Where

β = angle of the slope (in degrees)

k = coefficient of lateral earth pressure

FSR = Factor of Safety Ratio

Merifield et al. (2003) classified soil/anchor failure into 2 cases: 1) immediate breakaway; and 2) no breakaway. The immediate breakaway case does not account for adhesion or suction between the soil and bottom of the anchor, while no the breakaway failure case accounts for these properties. Since the suction force depends on many variables (e.g. embedment depth, soil permeability undrained shear strength, and loading rate) it is impossible to determine an exact value for each anchor location. According to Das and Puri (1989) the net ultimate holding capacity (Q_u) of an inclined square plate anchor is given by Equation 2.2 and the breakout factor (F_c) is given by Equation 2.3.

$$Q_u = (A_A)(c_u)(F_c) - W_\alpha[\cos(\theta)] \quad \text{(Equation 2.2)}$$

$$F_c = \frac{\frac{Q_u}{B^2} - \gamma D \cos^2 \theta}{c_u} \quad \text{(Equation 2.3)}$$

Where

Q_u = net ultimate holding capacity

A_A = area of the anchor plate

c_u = undrained clay cohesion

F_c = breakout factor

W_α = weight of soil immediately above the anchor

θ = inclination of the anchor with respect to the horizontal

B = length/width of the square plate

γ = unit weight of soil above anchor

D = embedment depth

El Sawwaf and Nazir (2006) studied the effect of soil reinforcement placed in front of shallow vertical anchors on pullout resistance. Fifty-four (54) tests on a small scale model included placing rows of piles close to the vertical anchor plate to determine the additional ultimate load obtained from the soil reinforcement around the plate. Study findings show the row of piles installed around the existing anchor plate significantly increased the ultimate capacity of the anchor, but the capacity improvement is dependent on the pile length, diameter, spacing, and location relative to the anchor plate.

2.10 Seaming Options

Typical purposes for overlapping or sewing adjacent geotextile pieces are to ensure full soil coverage and to provide maximum reinforcement strength. The decision to overlap or seam geotextiles is often made based on: soil California Bearing Ratio (CBR); material and labor cost comparison between sewing and purchasing enough material to provide adequate overlapping; and feasibility of each method in reference to the specific application (TenCate™ 2001). Table 2.13 shows AASHTO M288-96 overlap requirements based on subgrade CBR.

Table 2.13. Overlap Requirements Based on Subgrade CBR (AASHTO M288-96)

Soil CBR	Minimum Overlaps (m)
>3	0.3 to 0.5
1 – 3	0.6 to 1
0.5 – 1	1 or sewn
<0.5	sewn
All roll ends	1 or sewn

According to TenCate™ (2001), seams created from sewing two geotextile panels together produce approximately 60% of the ultimate Wide Width Tensile Strength in the cross-machine direction. Standard woven geotextiles used in practice at the time of

TenCate™ (2001) could provide seam strengths up to 52 kN/m. A single thread “chain stitch” or a double thread “lock stitch” with stitch densities of 3 to 6 stitches per 2.5 cm were stated to be commonly used in practice. Small, handheld sewing machines generally provide seam strengths up to 42 kN/m (TenCate™ 2001).

Union Special Corporation produces sewing machines for field and in-plant seaming of a variety of materials including clothing, bags, and geotextiles. The Union Special 2200 is a single needle portable sewing unit designed for sewing geotextiles which operates using either an electric or pneumatic motor. The unit weighs approximately 5 kg. According to manufacturer product data sheets, the 2200 model can seam light to medium weight fabrics up to 9 mm thick at a rate of 1200 to 1700 stitches per minute depending on material type. As outlined by product data sheets, the 2200 model is capable of seaming approximately 9.6 m per minute assuming a standard 8 mm stitch length and 1200 stitches per minute. Larger capacity sewing machines such as the 80200 model are available that can seam fabrics up to 17 mm.

Commonly used seam types as outlined by Union Special Corporation product literature are the SSa “Prayer” Seam, SSn “J” Seam, and SSd “Butterfly Seam” (Figure 2.8). The SSn “J” Seam could be beneficial in the application of an *RDAS* to prevent water penetrating the seams.

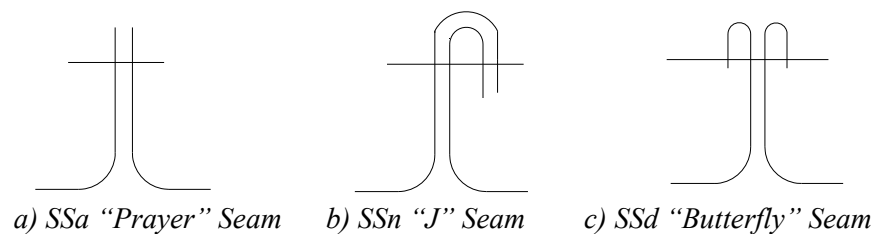


Figure 2.8. Commonly Used Seam Types

2.11 Pile Analysis Techniques

Pile analysis techniques were investigated to assess their pertinence in terms of anchor/soil interaction behavior. Broms Method (1964a, 1964b, 1965) is a hand calculation utilizing static equilibrium equations to develop the ultimate lateral loading of a pile in a homogeneous, isotropic soil through the use of closed form equations, charts, and graphs. Broms (1965) developed a dimensionless laterally loaded pile groundline deflection analysis method based on the subgrade reaction approach. For short dimensionless pile lengths, piles were assumed to be completely rigid, rotating about a point along the pile, and long dimensionless pile lengths were considered infinitely long.

The Beam on Elastic Foundation method has been used to analyze laterally loaded piles by treating the pile as the beam and the soil as elastic springs defined by the modulus of subgrade reaction (k). Matlock and Reese (1960) applied non-linear soil modulus variations to develop general equations and methods of computation for elastic-pile theory and rigid-pile theory.

One of, if not the, most common analysis methods in present day is the p-y method (e.g. Reese et al. 1974). This method addresses the nonlinear nature of soil by allowing for various unique spring stiffness at different depths of the pile being loaded. This method utilizes full-scale testing to make back calculations about soil-pile interaction. A template

curve is typically empirically scaled to produce a unique relationship between soil reaction and lateral displacement at any depth along the pile (e.g. Figure 2.9).

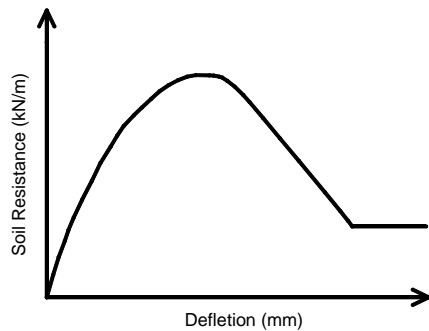


Figure 2.9. Generic p - y Curve in Stiff Clays

Hsiung (2003) developed theoretical solutions for maximum deflection and moment for laterally loaded piles in a uniform subgrade reaction linear-plastic soil where the subgrade modulus was found to be strain dependent. Shen and Teh (2004) developed a variational solution approach to the subgrade reaction method with stiffness increasing with depth. Finite element and finite difference methods have gained popularity recently (Klar and Frydman 2002 and Ng and Zhang 2001). The method allows for 2-D or 3-D interaction through the use of elastic constants and/or nonlinear constitutive models which can better approximate plasticity, adhesion, boundary conditions at the surface, and boundary conditions at the pile tip.

2.12 Numerical Modeling of Geotextiles and Anchors

Most finite element models of soil anchors, soil nails, and piles have used interface elements to describe the interaction between the soil and the modeled structure (Liang and Feng 2002; Hartl and Pernthaner 2002; Smith and Su 1997; Zhang and Zhaoyuan 1999; Cheung and Lee 1991). Zhang and Zhaoyuan (1999) created a finite element model of a soil nail structure supporting an excavation using double spring elements to describe the interface between the soil and soil nail. Xue (2003) used the finite element program CRISP to create an anchor interface element by wrapping a cylindrical slip element around the beam elements of the anchor. Kim et. al (2007) used Abaqus to create a 2D model of ground anchors. Both the soil and anchor strand was modeled using four noded axisymmetric brick elements with reduced integration. The soil failure model was based on the Drucker-Prager failure criterion with the non-associated flow rule.

Huang et al. (2006) performed a 2D finite element analysis of a river dike reinforced with geogrid and metallic bar mats within the soil layers. The analysis used a linear elastic-perfectly plastic approach to model the soil-geosynthetic interaction. Mohr-Coulomb failure criterion was used to model the soil behavior. The geogrid was modeled with rod elements. Table 2.14 presents parameters used for the geogrid and interface material model.

Table 2.14. Model Parameters Used by Huang et al. (2006)

Material	Parameter	Symbol	Value
Geogrid	Young's modulus	E (MPa)	19.6
	Section area	A_g (m ² /m)	5.25×10^{-4}
Soil and Geogrid Interface	Young's modulus	E (MPa)	10.0
	Poisson's ratio	ν	0.33
	Adhesion	a (kPa)	0
	Friction angle	Φ (°)	30

Seay (2009) modeled geotextile tubes filled with slurry using Abaqus. The geotextile tube was meshed with 4 node reduced integration shell elements (S4R). The geotextile tube rested on an elastic foundation meshed with SPRING1 elements. Geotextile material properties used in the model are presented in Table 2.15.

Table 2.15. Geotextile Material Properties Used in Seay Model (2009)

Parameter	Symbol	Value
Young's modulus	E (MPa)	7035
Poisson's Ratio	ν	0.45
Density	γ (kg/m ³)	75.0

2.13 Summary of Literature Review

Review of literature revealed many erosion control products such as geotextiles and turf reinforcement mats are commercially available that could be used to cover an earthen levee face. In addition, small earth anchors, stakes, and threaded bar are available commercially that could be installed without heavy equipment to secure the geosynthetic to the levee. Modifying *AGS* concepts that have confinement functions to be solely for anchoring could have merit to prevent levee breaches and flooding.

Currently, there appears to be little available research on failure models of small earth anchors in clay. Also, available analysis techniques (e.g. p-y curves for piles) may not accurately describe the behavior of a short earth anchor in the face of a levee. Finite element modeling has been performed on anchor soil interactions, but many researchers have reported contact interaction issues. Review of literature did not reveal modeling efforts for an *AGS* (or similar system) on the earthen side of levees with overtopping wave loads applied. Current geotextile models typically use shell and brick elements, while the use of membrane elements may be able to provide more accurate behavior.

CHAPTER 3 – RAPID LEVEE ARMORING CASE STUDY OF 2011 MISSISSIPPI RIVER FLOOD

3.1 Introduction to Mississippi River Flooding Armoring System

During the Mississippi River flooding of 2011, the USACE deployed levee protection to the landward side of the Yazoo River Backwater Levee in Vicksburg, MS. The Yazoo River Backwater Levee was chosen for protection because it was the only levee within the Vicksburg USACE district that was anticipated to overtop. The Yazoo River is a tributary of the Mississippi River and connects to it north of Vicksburg, MS. The Yazoo Backwater Levee extends from the Mississippi River Main Line Levee along the north side of the Yazoo River. The area surrounding the Yazoo Backwater Levee is well vegetated lowlands.

During the 2011 flood, the Mississippi River peaked at a stage of 17.4 m on the Vicksburg gage. This stage was higher than the peak of 17.1 m recorded during the 1927 flood. The 1927 flood stages, however, would have been higher if levees had not failed during that event. At the time of the 2011 flood, the USACE installed temporary armoring to the Yazoo River Backwater Levee. The authorized grade of the Yazoo Backwater Levee is 32.6 m. Therefore, the levee could not be raised above this elevation. However, several sections of the levee were lower than this elevation, so the USACE raised all low sections of the levee to 32.6 m, and armored the landward side of the levee to provide additional protection.

3.2 Levee Protection Design

A typical cross-section of the Yazoo River Backwater Levee includes a 7.3 m levee height with a 6.1 m levee crest and a total levee foot print of approximately 75.6 m. Side slopes are 1 vertical to 5.5 horizontal on the landside and 1 vertical to 4 horizontal on the riverside. Design concepts for securing the liner to the levee are shown in Figure 3.1.

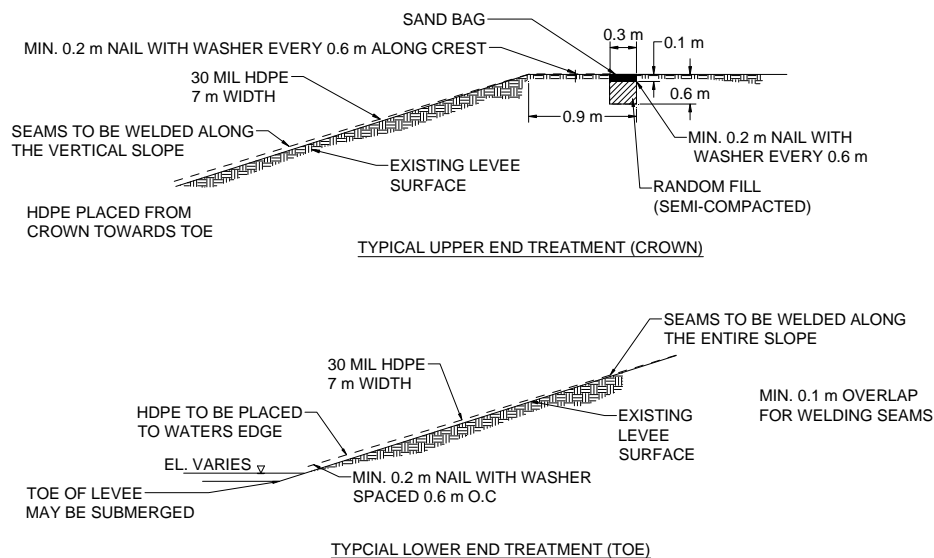


Figure 3.1. Attachment of Liner at Crest and Toe of Levee

3.3 Installation of Armoring System

Approximately 5.6 linear km of temporary armoring was installed beginning Friday May 6, 2011 and was essentially complete by Wednesday May 11; May 12 was needed for clean up and miscellaneous activities. At the time of armoring, the Mississippi River was flowing at approximately 63,700 m³/s. Figure 3.2 shows the armoring along the landward side of the Backwater Levee.



Figure 3.2. Geomembrane Armoring of Landward Side of Backwater Levee

The trench at the top of the levee was initially created using a trackhoe with a 0.3 m wide bucket (Figure 3.3a). This method was too slow, and was replaced by a large trenching device (Figure 3.3b and 3.3c). Producing a straight trench was difficult, so a line was painted along the slope at approximately 1.5 m offset so the operator was able to produce a straight trench by attaching an alignment pole with chain to the trencher.

A 30 mil thick HDPE geomembrane typically used as a landfill liner was installed on the landward levee slope (1 vertical to 5.5 horizontal slope). The geomembrane was placed onto a spreader bar with an excavator at the levee crest and pulled down the slope by construction personnel (Figure 3.4). Small holes were cut at the end of the product to allow workers to grip the membrane roll and pull it down the levee slope. The 7 m wide panels were overlapped 15 cm. Heat seaming (welding) was used to join panels, and where a hole was burned into the product due to the seaming tool being in one place too long, a patch was placed. Construction was performed by approximately 64 people.

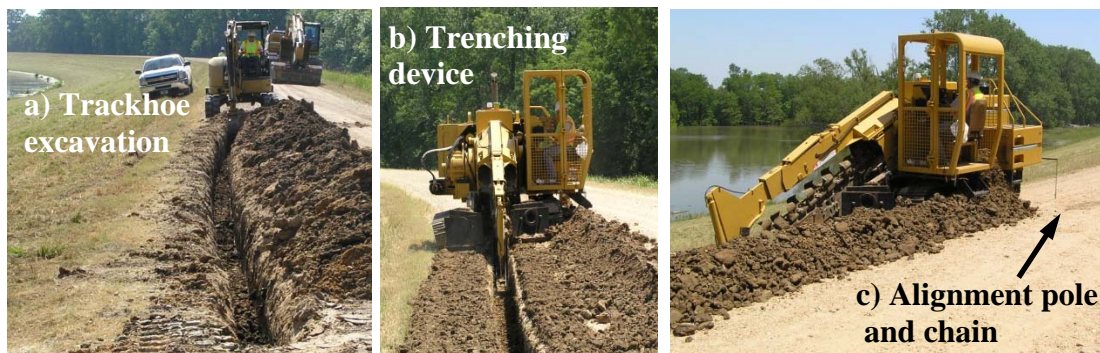


Figure 3.3. Trench Excavation



Figure 3.4. Overview of Levee Protection Installation

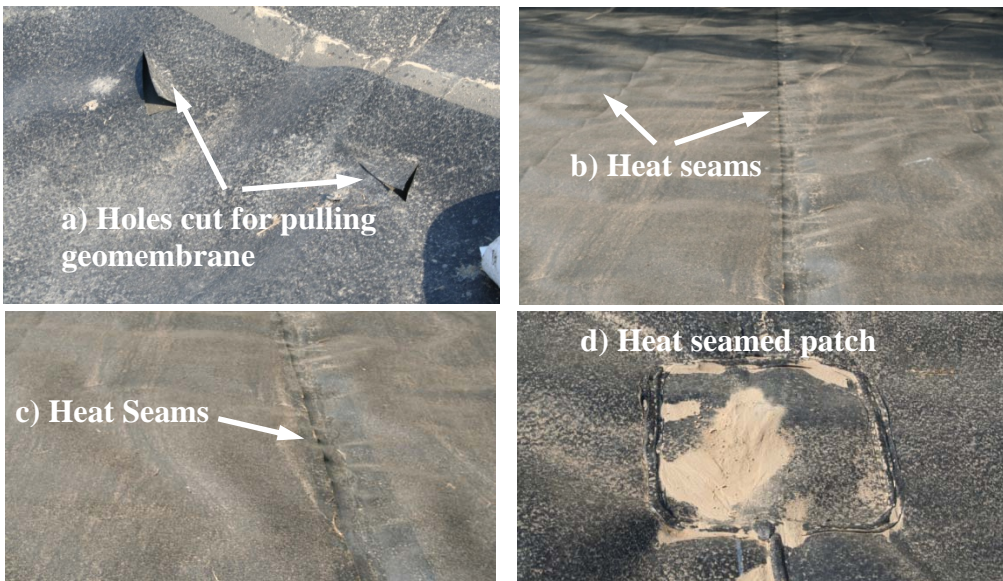


Figure 3.5. Geomembrane Pull Holes and Heat Seams

The geomembrane was placed along the edges of the 0.3 m wide by 0.6 m deep trench and 0.4 m long liner pins were installed on 0.6 m spacing along the trench. Random fill was semi-compacted over the membrane to a height of approximately 0.2 m below the top of the trench. Sandbags were placed over the semi-compacted fill to complete trench filling (Figure 3.6). Achieving a level trench after the sandbag placement was a concern to prevent erosion due to turbulence of the water flowing over this area during overtopping. Cement grout was not used at the top of the armoring system due to fear it would be difficult to remove.

When the membrane was pulled down the levee, it was placed flat on the ground before being cut from the roll with a box cutter. The membrane extended to the levee toe or to the water level present at the time of placement if the toe was submerged. The membrane was pinned along the toe with 0.4 m long liner pins on 0.6 m spacing, and sandbags were placed along the geomembrane for added support as shown in Figure 3.7a. Sandbags were also placed along the levee face on the edges of the geomembrane at the end of the armoring system to prevent removal from water or wind on the levee face as shown in Figure 3.7b.



Figure 3.6. Trench of Armored Levee Protection



Figure 3.7. Pinned Toe of Geomembrane

The levee slope was uneven in some locations, but did not appear to pose problems with temporary armoring placement. Pie shaped pieces of geomembrane were cut and placed in the curved portions of the levee as shown in Figure 3.8. Entrapped air under the geomembrane was noted as a possible concern during an overtopping event.



Figure 3.8. Panel Installation in Curve Portions of Protection

3.4 Armoring Removal and Project Summary

The total cost to place the temporary armoring system was approximately \$1,560,000 including: \$730,000 for linear materials cost, \$495,000 for heat seaming, and \$335,000 for installation (i.e. trenching, nails, etc). Product removal and disposal cost (liner was recycled) were \$100,000. After the temporary armoring was removed, the approximately 200,000 m² area was re-seeded by September 19, 2011 for \$80,000. Total project costs were \$1,740,000. Figure 3.9 shows the levee during lining removal. The Yazoo Backwater Levee was not overtopped during the 2011 flood. Grass is currently growing on the levee face as per February 2012 correspondence with USACE.



Figure 3.9. Levee Protection During Removal

CHAPTER 4 – SHALLOW ANCHOR TESTING

4.1 Anchor Testing Introduction

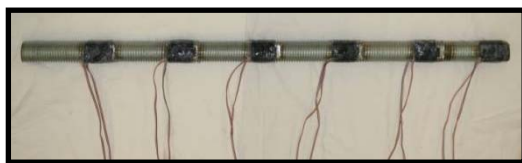
Anchor testing was performed in June of 2011 at the USACE Engineer Research and Development Center (ERDC) in coordination with the Airfields and Pavements Branch (APB). Twenty-seven anchor pulls were performed in soft clay resembling an earthen levee face a few years after construction at high moisture. The purpose of the anchors is to help maintain stability in a geosynthetic based armoring system. The remainder of this chapter describes the testing and analysis of the anchor pull testing.

4.2 Anchors Tested

Three anchor types were tested: Mobi stakes, Star pickets, and threaded bar anchors (Figure 4.1). Mobi stakes have a driving head that is 0.8 cm thick and 6 cm wide, and the end that is driven into the soil is tapered to a point over a distance of approximately 1.3 cm. They are 2.5 cm diameter and weigh ≈ 4.0 kg/m. Two Mobi stake lengths were tested: 30.5 and 61 cm, which had embedment depths approximately 1 cm less than their length when driven into the soil.

Star pickets are Y-shaped when viewed from the end and are fabricated from 6.4 mm thick metal and weigh ≈ 2.1 kg/m. They were 60 cm long, with a hole 33 cm from the end driven into soil and a second hole 57 cm from the end. The driving tip on the anchors was approximately 3.8 cm long. The anchors were pulled parallel to the individual member in the Y-shape. When the anchor was pulled from the 33 cm hole, the embedment depth into soil was approximately 31 cm. When the anchor was pulled from the 57 cm hole, the embedment depth into soil was approximately 55 cm. For the remainder of this chapter, depths are referred to as 0.3 m and 0.6 m, which are approximate.

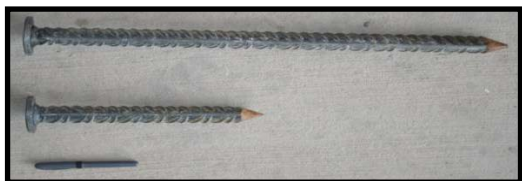
The threaded bar was produced by Vulcan Threaded Products. The bars were made of low carbon steel with a yield stress of 315 to 353 MPa based on data sheets obtained from the supplier. The bar diameter was 2.2 cm not considering threads and 2.5 cm diameter when considering threads. The nominal weight of the bars was ≈ 3.4 kg/m. The bar width was ≈ 1.85 cm after machining where strain gages were installed reducing the area of the 2.2 cm diameter solid portion from 3.80 cm² to 2.60 cm².



(a) Threaded Bar With Strain Gages



(b) Threaded Bar Without Strain Gages



(c) Mobi Stakes



(d) Star Picket

Figure 4.1. Photographs of Anchors Tested

4.3 Test Section

The test section was approximately 15 m square and 75 cm deep (Figure 4.2). Native soil was present below 75 cm as opposed to the prepared soil used for testing. Properties of the soil deposit used to build the test section are shown in bullet form below.

- *USCS Classification:* CH
- *Liquid Limit (LL):* 75 to 86
- *Plastic Limit (PL):* 24 to 27
- *Plasticity Index (PI):* 51 to 62
- *Standard Proctor Density (γ_d):* 1.35 to 1.37 g/cm³
- *Specific Gravity (G_s):* 2.68 to 2.74
- *Optimum Moisture Content at γ_d (OMC):* 25 to 29%
- *Organic Content:* 7.9 to 8.1%
- *Percent Fines:* 97 to 98%
- *Percent Sand:* 2 to 3%
- *Percent Silt:* 18 to 20%
- *Percent Clay:* 77 to 80%

Levee compaction requirements in the Vicksburg USACE district are typically 90% of standard Proctor (ASTM D 698) dry density (γ_d), and go up to 95% of standard proctor in some instances. The average dry density of the material based on two tests was 1.36 g/cm³, making the compaction threshold 1.23 g/cm³ at the time of levee construction. Heavy clay will have noticeable desiccation near the levee surface. This desiccation would reduce the dry density, though how much is not readily available. Dry density of 80 to 85% of standard proctor was deemed reasonable to represent a wet levee face after desiccation during overtopping. The soil condition is believed to be reasonable but isn't based on test data or historical values as they weren't available. The test section target dry density (γ_{dry}) was set at 1.09 to 1.16 g/cm³.

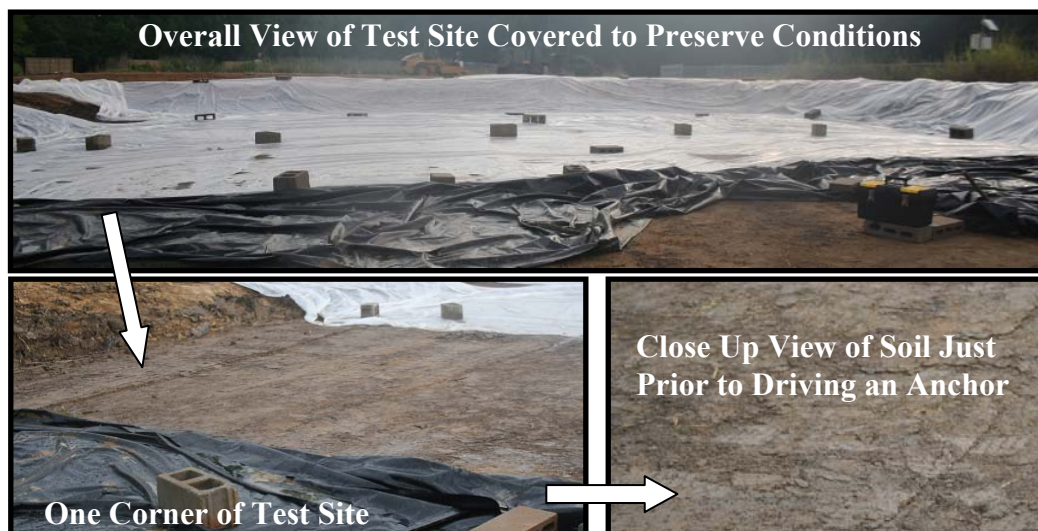


Figure 4.2. Anchor Test Site at USACE-ERDC

The test section was first compacted with an empty Ingram rubber tire roller having seven tires each weighing approximately 1,500 kg while the roller water tank was empty. A Dynapac steel wheel vibratory compactor was then used that weighs approximately 11,300 kg. Three passes of each compactor were used. Drive sleeves (7 cm tall by 7.6 cm diameter) were used to take samples from the test site after construction and measure in-situ density and moisture content (Table 4.1). Test locations were distributed throughout the site, and as seen in Table 4.1 the section met the desired construction requirements. Four Dynamic Cone Penetrometer (DCP) tests were performed using a 4.6 kg hammer within the test section to obtain a correlation to CBR. Correlated CBR values within the top 60 cm are shown in Table 4.2 in 15.2 cm intervals.

Table 4.1. Drive Sleeve Test Results

Depth from Surface (cm)	γ_{dry} (g/cm³)	γ (in-situ) (g/cm³)	w (%)
1 to 8	1.15	1.60	39.3
	1.15	1.61	39.7
	1.10	1.55	40.6
	1.13	1.59	40.4
	1.14	1.59	38.9
	1.17	1.62	38.3
<i>Average</i>	<i>1.14</i>	<i>1.59</i>	<i>39.5</i>
31 to 38	1.13	1.59	40.2
	1.06	1.55	45.7
	1.16	1.52	30.4
<i>Average</i>	<i>1.12</i>	<i>1.55</i>	<i>38.8</i>
61 to 68	1.11	1.58	40.5
	1.21	1.56	28.8
	1.13	1.58	40.4
<i>Average</i>	<i>1.15</i>	<i>1.57</i>	<i>36.6</i>

Table 4.2. Dynamic Cone Penetrometer Test Results

Depth from Surface (cm)	Range of CBR	Average CBR
0 to 15.2 cm	1.7 – 2.7	2.2
15.2 to 30.4 cm	2.2 – 5.8	4.0
30.4 to 45.6 cm	3.9 – 8.7	5.5
45.6 to 60.8 cm	3.9 – 13.9	8.1

4.4 Instrumentation, Data Acquisition, and Terminology

Summaries of the electronic instrumentation used to collect needed test data are summarized as follows.

- *Foil Strain Gages*: Vishay Micro-Measurements type C2A-06-250LW-350 with a gage factor at 24 C of $2.095 \pm 0.5\%$.
- *Cable-Extension Transducer*: Celesco Model PT101-0040-111-1110.
- *Load Cell*: Load Cell Central Model HTC-8k with dual threaded stud mounts.
- *Thermocouple*: Omega TC-TT-T-20 PFA insulated bead type.

A National Instruments™ NI CompaqDaq 9172 chassis was used to acquire all data using a program written for the application in LabView™. Load, displacement, and strain were acquired with NI 9237 I/O modulus, while temperature was acquired with a NI 9211 analog input module. Fifty readings were taken from each sensor, averaged, and the average value was written to a file at a rate of ≈ 32 Hz. This approach provided a stable signal with enough resolution to capture behaviors of interest without producing unnecessarily large files.

Load cell signals were acquired with the following key parameters: gage factor of 2.10, gage resistance of 350Ω , Poisson's ratio of 0.28, full bridge wiring configuration, excitation at 2.5 V, and output range of $\pm 10e^{-3}$. Displacement signals from the cable-extension transducer were acquired with the following key parameters: gage factor of 2.10, gage resistance of 350Ω , Poisson's ratio of 0.28, half bridge wiring configuration, excitation at 2.5 V, and output range of $\pm 11e^{-3}$. Load and displacement outputs from data acquisition were in units of strain (ϵ) that was multiplied by e^6 resulting in a micro-strain ($\mu\epsilon$) value that was calibrated to force or displacement using external calibration described in the next section.

Strain gage signals were acquired with the following key parameters: gage factor of 2.095 (24 C gage factor), gage resistance of 350Ω , Poisson's ratio of 0.28, quarter bridge wiring configuration, excitation at 2.5 V, and output range of $\pm 35e^{-3}$. The NI 9237 module reads strain directly so no external calibration was needed; the signal was reported in micro-strain ($\mu\epsilon$) units. Temperature was acquired with cold junction compensation (*cjc*) performed internal to the NI 9211 module for the type *T* thermocouple. The signal range was set at 5 to 65 C.

Strain gage readings were not adjusted to account for temperature. Test durations were relatively short and readings were taken for several seconds prior to loading the anchors, which served as the reference for all subsequent readings negating the need to account for thermal output effects. Gage factor variations from 24 C would be less than 0.1% for the conditions encountered, which is insignificant for the application.

Threaded bar anchors were instrumented with strain gages (Figure 4.3) to evaluate which anchors reached yielding and what position on the length of the anchor yielding occurred. Threaded bar anchors were wrapped in electrical tape to protect the strain gages from moisture or loading damage during testing. Strain gages were positioned on the rods at 0.1 m spacing with 1 gage positioned on each side of the rod. 0.3 and 0.6 m rods were instrumented with 4 and 12 strain gages, respectively.

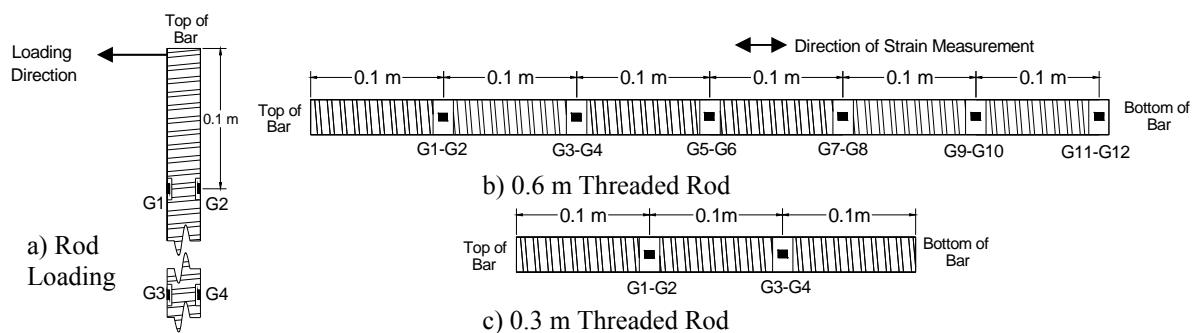


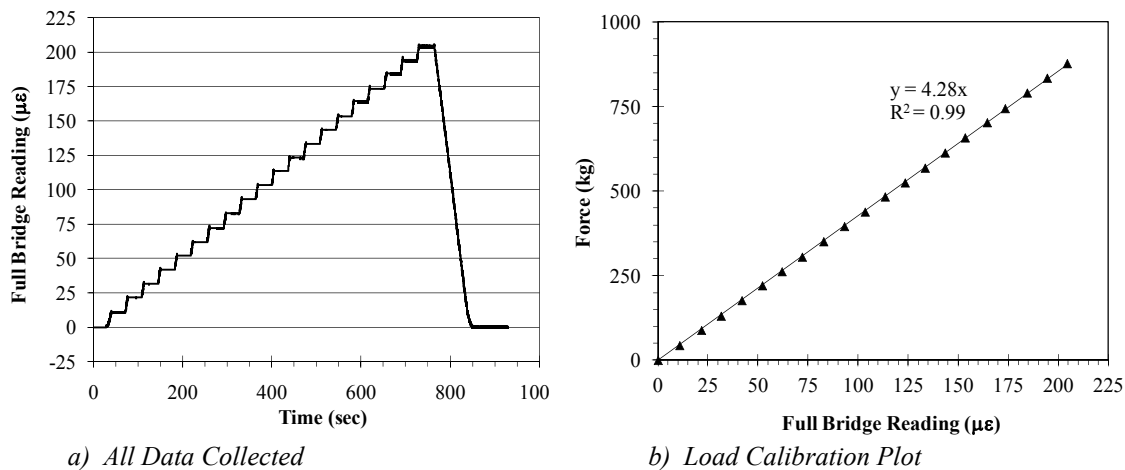
Figure 4.3. Strain Gage Locations

Data collected during testing included: maximum load achieved by the anchor (P_{Max}), deflection corresponding to the maximum load achieved ($\Delta@P_{Max}$), largest strain gauge reading at maximum load for any location on an anchor, $\epsilon_{Max}@P_{Max}$, (the gauge with maximum strain was reported for this value), and maximum strain (not necessarily recorded at P_{Max}) for each individual strain gauge location (ϵ_{Max}). Load (y) versus deflection (x) was plotted for each anchor pull and was used to calculate: the trendline equation for the linear portion of the curve (TL); the coefficient of determination (R^2) of the linear portion of the curve, and four stiffness parameters. Stiffness at maximum load (S_{100}) was defined as P_{Max} divided by $\Delta@P_{Max}$. Similarly, S_{75} , S_{50} , S_{25} were defined as the ratio of load to deflection at 75, 50, and 25% of P_{Max} , respectively.

4.5 Instrument Calibration

A general use multi-meter was used to verify foil strain gage resistance after attachment to the threaded rods. Bonding strain gages to steel at normal temperatures is a routine application so no strain calibration was necessary. Thermocouples were verified using a thermometer calibrated by an external service.

The load cell was calibrated using a load frame to apply approximately 900 kg in 45 kg increments with a 30 second pause after each load increment was increased. Once the full load was applied, loading was held constant for 2 minutes then the load was released at a constant rate. The cable extension transducer was calibrated by extending the string potentiometer in 7.6 cm increments to 84 cm with a 10 second pause after each extension. After the total distance was reached, the string potentiometer was released at a constant rate. Figure 4.4 presents the load cell calibration plot; Figure 4.5 presents the cable extension transducer calibration plot.



a) All Data Collected
Figure 4.4. Load Cell Calibration

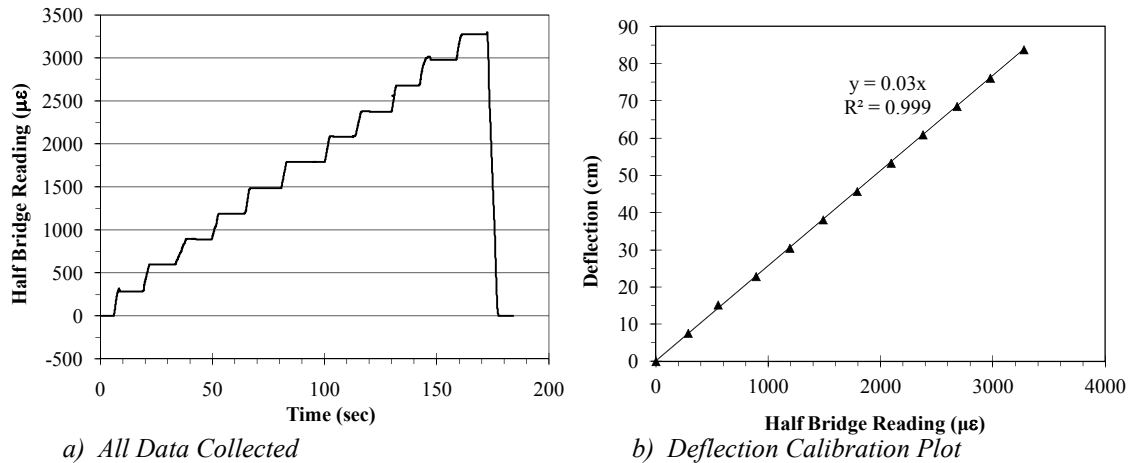


Figure 4.5. Deflection Calibration of Potentiometer

4.6 Anchor Testing Procedures and Test Matrix

An area approximately 0.6 m wide and 1.2 long was allocated to each anchor pull so adjacent anchors did not affect soil properties by changing the compacted state of the soil. All three anchor types were driven into the soil using a sledgehammer until approximately 2.5 cm of anchor was protruding. A wench was used to apply load horizontally until the anchor could not carry load. All anchors failed by slicing through the soil a width on the order of the size of the anchor. An increase in anchor capacity could likely be achieved by installing a plate to the front of the anchors to increase the soil bearing area.

For Mobi stakes, a cable was wrapped around the head of the anchor, attached to the load cell, and driven into the ground until the anchor was fully installed. The string potentiometer was attached to the anchor head, and load was applied horizontally with a wench attached to an All Terrain Vehicle (ATV) (Figures 4.6 and 4.7).

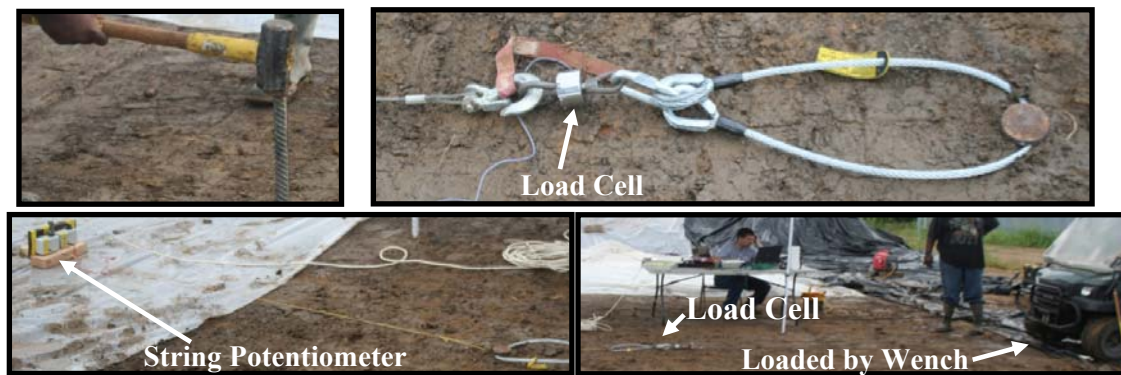


Figure 4.6. Installation of Mobi Stakes and Photos of Data Acquisition Approach



Figure 4.7. Mobi Stake (0.6 m) Anchor During Testing

Star pickets were installed to a depth according to the anchor length being tested since only one size Star picket was tested. The string potentiometer and load cell were attached to an eye hook attached to a drilled hole in the Star picket at the desired embedment depth (Figures 4.8 and 4.9). Threaded bar anchors were installed until 2.5 cm remained and a machined threaded anchor attachment was tightened on the top of the bar. The string potentiometer and load cell were connected to an eye hook on the anchor head (Figures 4.10 and 4.11). Twenty-seven anchor pulls were performed as shown in Table 4.3.



Figure 4.8. Installation of 0.3 m Star Picket



Figure 4.9. Star Picket (0.3 m) Anchor During Testing



Figure 4.10. Installation of 0.6 m Threaded Bar Anchor

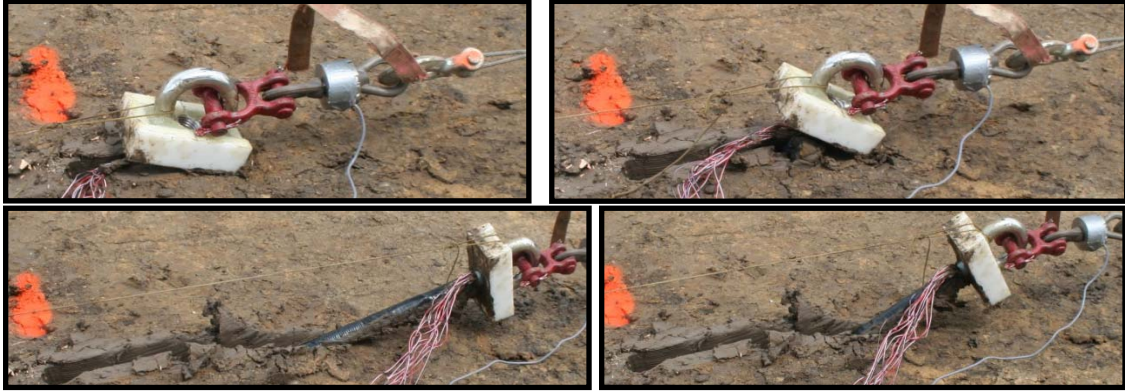


Figure 4.11. Threaded Bar Anchor During Testing

Table 4.3. Anchor Pull Schedule

Pull Number	Anchor Type	Length (m)	Load	Taped (y/n)
1	Mobi Stake	0.6	Continuous	No
2	Mobi Stake	0.6	Continuous	No
3	Mobi Stake	0.6	Continuous	No
4	Mobi Stake	0.3	Continuous	No
5	Mobi Stake	0.3	Continuous	No
6	Mobi Stake	0.3	Continuous	No
7	Star Picket	0.3	Continuous	No
8	Star Picket	0.3	Continuous	No
9	Star Picket	0.3	Continuous	No
10	Star Picket	0.6	Continuous	No
11	Star Picket	0.6	Continuous	No
12	Star Picket	0.6	Continuous	No
13	Threaded Rod	0.6	Continuous	Yes
14	Threaded Rod	0.6	Continuous	Yes
15	Threaded Rod	0.6	Continuous	Yes
16	Threaded Rod	0.3	Continuous	Yes
17	Threaded Rod	0.3	Continuous	Yes
18	Threaded Rod	0.3	Continuous	Yes
19	Threaded Rod	0.6	Continuous	No
20	Threaded Rod	0.6	Continuous	No
21	Threaded Rod	0.6	Continuous	No
22	Threaded Rod	0.3	Continuous	No
23	Threaded Rod	0.3	Continuous	No
24	Threaded Rod	0.3	Continuous	No
25	Threaded Rod	0.6	Sustained Load	No
26	Threaded Rod	0.6	Sustained Load	No
27	Threaded Rod	0.6	Sustained Load	No

4.7 Effect of Anchor Type

Three replicates of each anchor type were tested to determine their differences in loading capacity and deflection behaviors. A typical anchor pull (defined as the beginning of recorded load to ultimate deflection) lasted 3 to 5 seconds and 5 to 10 seconds for 0.3 and 0.6

m anchors, respectively. Average ultimate loads ranged from approximately 145 kg (Threaded Bar anchor) to 155 kg (Mobi Stake anchor) for 0.3 m lengths and 280 kg (Threaded Bar anchor) to 360 kg (Star Picket anchor) for 0.6 m lengths. To aid in determining anchor load deflection behavior at low deflections, a trendline was created for the linear portion of the curves. Large deflections were not of interest, as it is expected the anchors would pull out of the ground if these conditions were sustained for longer time periods. Anchors were essentially rigid at the load rates tested until approximately 20 kg (up to 50 kg) was applied; trendlines include data after deflection was recorded. Table 4.4 presents load deflection information obtained for each anchor test, and Figure 4.12 and 4.13 present a typical load deflection curve and trendline for each anchor type for 0.3 and 0.6 m length anchors, respectively.

Table 4.4. Comparison of Anchor Type Effect

Pull No.	P_{Max} (kg)	$\Delta@P_{Max}$ (cm)	$\epsilon_{Max}@P_{Max}$ ($\mu\epsilon$)	S_{100} (kg/cm)	S_{50} (kg/cm)	S_{75} (kg/cm)	S_{25} (kg/cm)	TL	R^2
0.3 m Mobi Stakes									
4	146	3.7	n/a	40	285	943	*	y=161.2x+48.6	0.93
5	160	2.4	n/a	67	2390	*	*	y=119.2x+115.4	0.96
6	158	2.4	n/a	66	*	*	*	y=138.8x+128.9	0.82
0.3 m Star Pickets									
7	123	20.4	n/a	7	87	113	78	y=94.0x+0.0	0.94
8	173	7.4	n/a	24	173	351	878	y=130.0x+39.5	0.96
9	148	10.7	n/a	16	145	392	370	y=141.5x+35.2	0.94
0.3 m Threaded Bar (Taped)									
16	134	6.8	572	20	65	236	1151	y=86.7x+39.4	0.92
17	151	5.1	711	29	64	102	87	y=45.1x+33.8	0.96
18	130	5.7	658	23	91	232	*	y=51.1x+50.0	0.94
0.3 m Threaded Bar (Non-Taped)									
22	143	3.7	670	28	76	105	97	y=82.6x+5.3	0.96
23	148	9.4	660	16	56	291	726	y=16.0x+79.0	0.96
24	144	3.4	682	42	204	473	*	y=128.7x+45.7	0.94
0.6 m Mobi Stakes									
1	320	5.6	n/a	57	251	499	1682	y=246.0x+68.7	0.96
2	327	5.7	n/a	58	498	1117	*	y=313.2x+108.0	0.85
3	375	18.8	n/a	20	187	539	570	y=206.0x+104.8	0.93
0.6 m Star Pickets									
10	341	18.8	n/a	18	137	237	173	y=194.7+0.0	0.92
11	374	19.8	n/a	19	274	504	562	y=468.2x+0.0	0.86
12	365	9.7	n/a	38	297	734	3182	y=190.7x+130.2	0.93
0.6 m Threaded Bar (Taped)									
13	266	8.9	2593	30	150	210	1734	y=156.0x+25.0	0.95
14	272	3.6	2131	76	192	326	796	y=166.7x+49.4	0.95
15	298	13.3	2679	22	91	167	406	y=107.6x+42.0	0.95
0.6 m Threaded Bar (Non-Taped)									
19	343	15.2	3729	23	64	119	237	y=107.0x+29.4	0.93
20	359	10.4	5036	35	138	192	277	y=148.3x+12.5	0.94
21	321	9.4	3323	34	121	162	163	y=125.6x+19.2	0.98

*No deflection was recorded at this load.

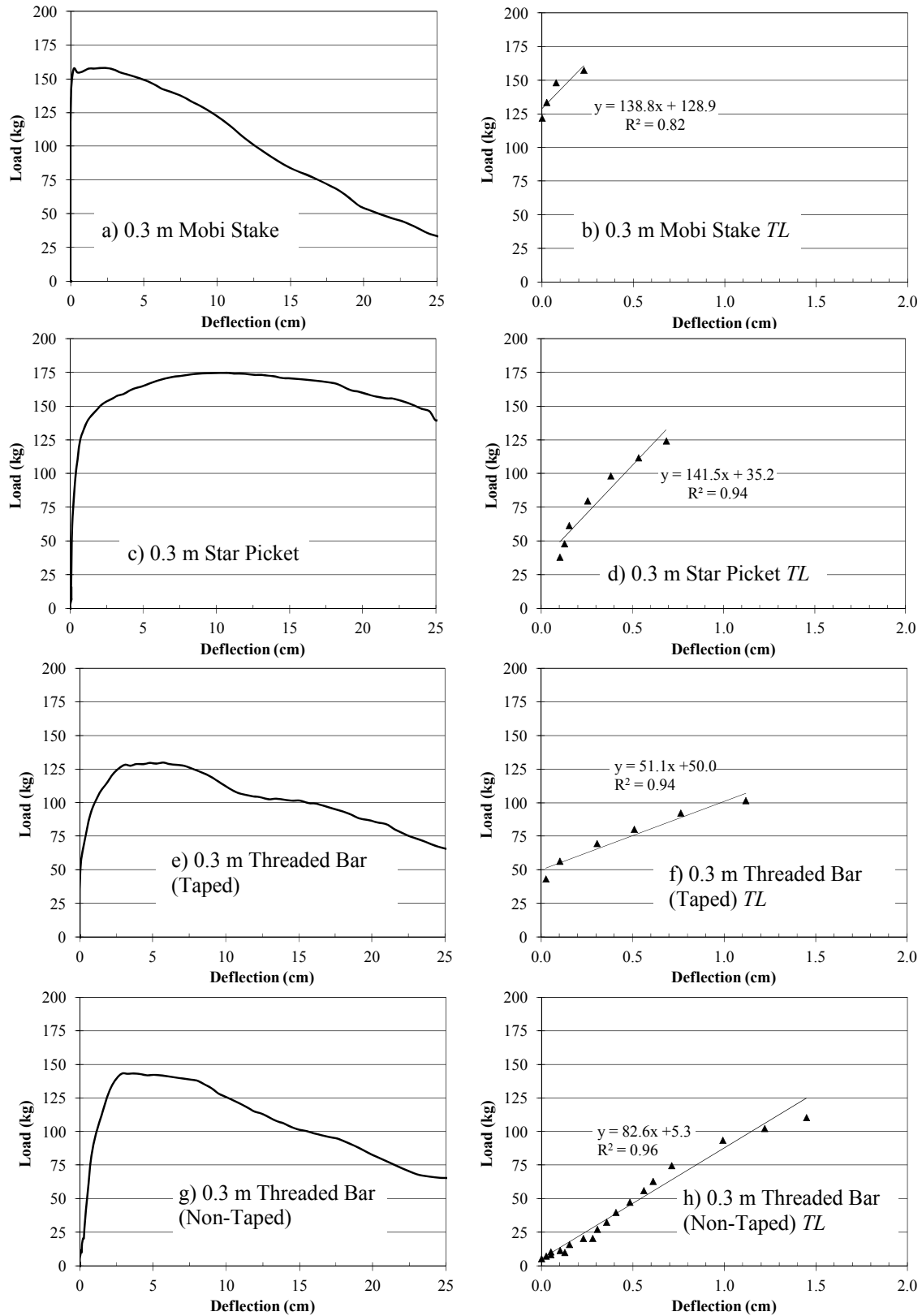


Figure 4.12. Anchor Type Load Deflection Comparison for 0.3 m Length

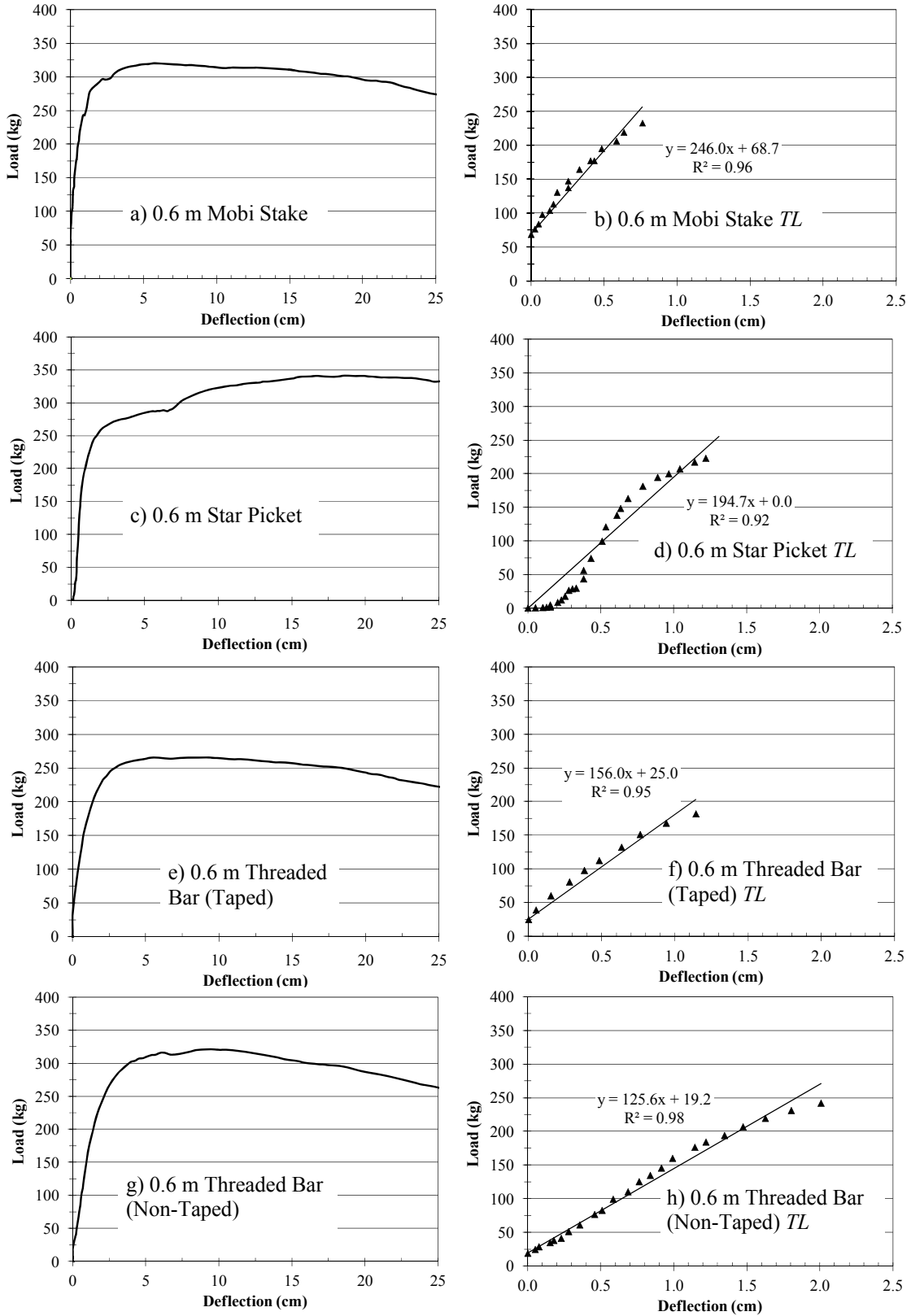


Figure 4.13. Anchor Type Load Deflection Comparison for 0.6 m Length

Tables 4.5 and 4.6 present the strain gage data for 0.3 and 0.6 m length rods, respectively, including the length of time that yielding occurred, t_{ef} , the load corresponding to the beginning of yielding, $P_{@ef}$, and the maximum strain value recorded over the entire pull for each strain gage ($G1$ to $G12$). A yielding strain reference of $1681\mu\epsilon$ to determine when yielding has occurred as used based on a Young's modulus and yield stress of low carbon steel of 210 GPa and 353 MPa, respectively.

Seven non-taped strain gages were damaged during testing, while only one strain gage was damaged of the taped specimens. Strain data collected showed all 0.6 m anchors experienced yielding, and removing the protective tape increased the maximum strain by an average of $1590\mu\epsilon$. The average load at which yielding began was 199 kg and 190 kg for 0.6 m taped and non-taped, respectively. An allowable load of 175 kg (perhaps as high as 225 kg) for 0.6 m long anchors seems reasonable when considering ultimate load and strain gage data, but these values should be investigated before use in a temporary armoring system. Yielding was not an issue for 0.3 m anchors because they pulled out of the soil before considerable bending occurred during testing. Strain gages on opposite sides of the threaded bar (e.g. $G1$ and $G2$ of Figure 4.3) generally were in agreement in terms of strain magnitude. An equal and opposite strain level is reasonable for this loading configuration and is a favorable result from the strain gages.

Table 4.5. ϵ_{Max} Strain Gage Data for 0.3 m Length Rods

Pull Number	16	17	18	22	23	24
Taped	Yes	Yes	Yes	No	No	No
G1	597	732	654	674	686	694
G2	-612	-691	-671	-658	-633	-658
G3	421	520	399	440	439	442
G4	-411	490	-427	-424	-414	-415

Tension (+) and compression (-) signs refer to the strain direction.

Table 4.6. ϵ_{Max} Strain Gage Data for 0.6 m Length Rods

Pull Number	13	14	15	19	20	21
Taped	Yes	Yes	Yes	No	No	No
t_{ef}(sec)	3.1	2.5	3.8	12.7	9.3	4.3
$P_{@ef}$(kg)	194.8	231.0	170.8	212.2	174.4	184.4
G1	-1666	-1510	[-1713]	[-2189]	[-2357]	[-1880]
G2	1585	1519	[1697]	[2187]	--- ⁽¹⁾	[1923]
G3	[-2601]	[-2191]	[-2743]	[-3737]	[-5183]	[-3263]
G4	[2496]	[2210]	[2723]	[3670]	[5033]	[3405]
G5	[-2559]	[-2146]	[-2725]	[-3419]	[-4947]	[-3288]
G6	[2495]	[2128]	[2528]	[3284]	[4755]	[3349]
G7	-1531	-1332	-1550	[-1751]	[-2984]	[-1958]
G8	1475	1364	[1597]	[1746]	[2422]	[1950]
G9	-494	-402	-483	-550	--- ⁽¹⁾	-602
G10	--- ⁽¹⁾	409	512	524	636	602
G11	-23	-10	-31	--- ⁽¹⁾	--- ⁽¹⁾	--- ⁽¹⁾
G12	20	13	32	26	--- ⁽¹⁾	--- ⁽¹⁾

Tension (+) and compression (-) signs refer to the direction of strain.

[] indicate gages that experienced yielding based on $1681\mu\epsilon$ yielding strain reference.

(1) Strain gage damaged during testing.

Three replicates were performed with 0.3 m and 0.6 m Threaded Bars without tape to compare the effects tape had on load deflection characteristics as tape was only present to protect the strain gauges. Figure 4.14 shows load deflection curves for taped and non taped anchors reach a maximum load quickly and begin to pull through the soil until the anchor pulls out of the ground. Average maximum load values of 3 replicates were 145 and 138 kg for taped and non-taped 0.3 m rods, respectively, and 278 and 341 kg for taped and non-taped 0.6 m rods, respectively. For the longer anchors, removal of the tape allowed the threads to improve loading carrying capacity by 23%, while no meaningful change was observed for the shorter anchors.

Figure 4.15 presents the load deflection trendlines for taped and non-taped anchors. Maximum loads ranged between 130 and 160 kg and 260 and 360 kg for 0.3 and 0.6 m rods, respectively. Deflections at each load varied from 3.4 to 15.2 cm. Taping anchors produced noticeable but not drastic changes in the linear portion of the load deflection curves.

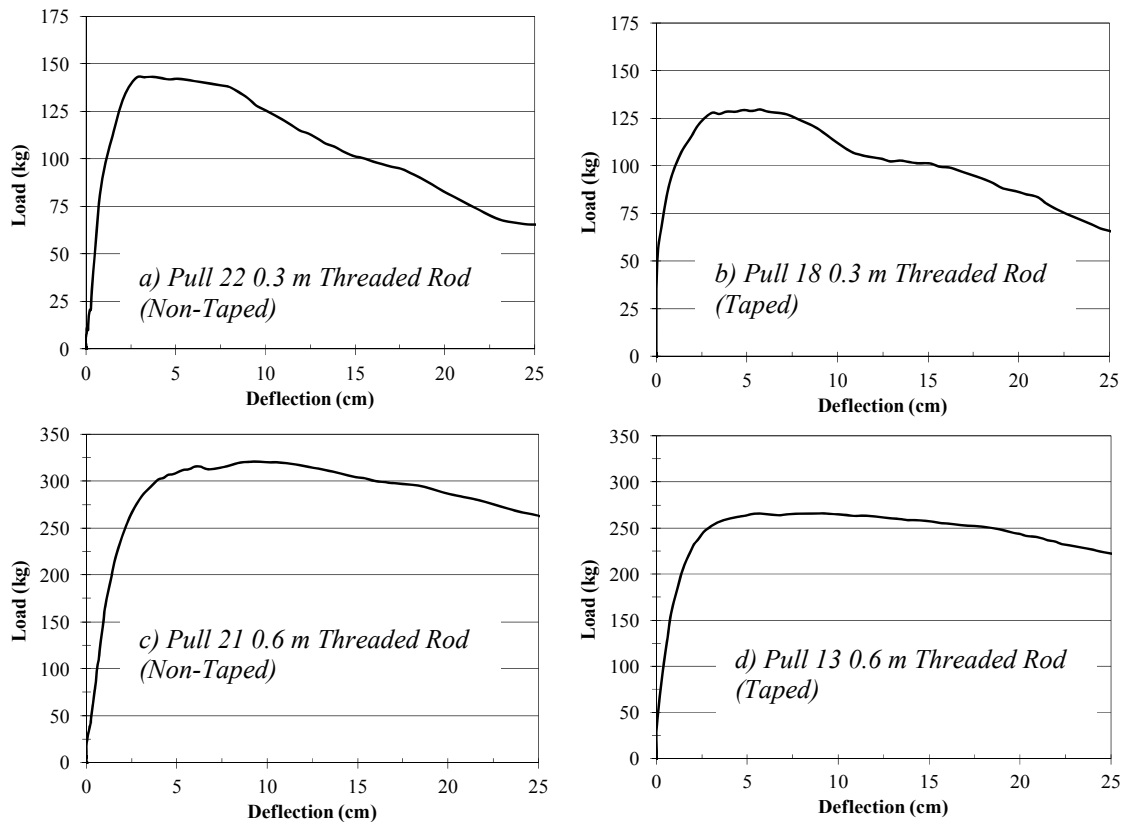


Figure 4.14. Load Deflection Curve for Taped and Non-Taped Specimens

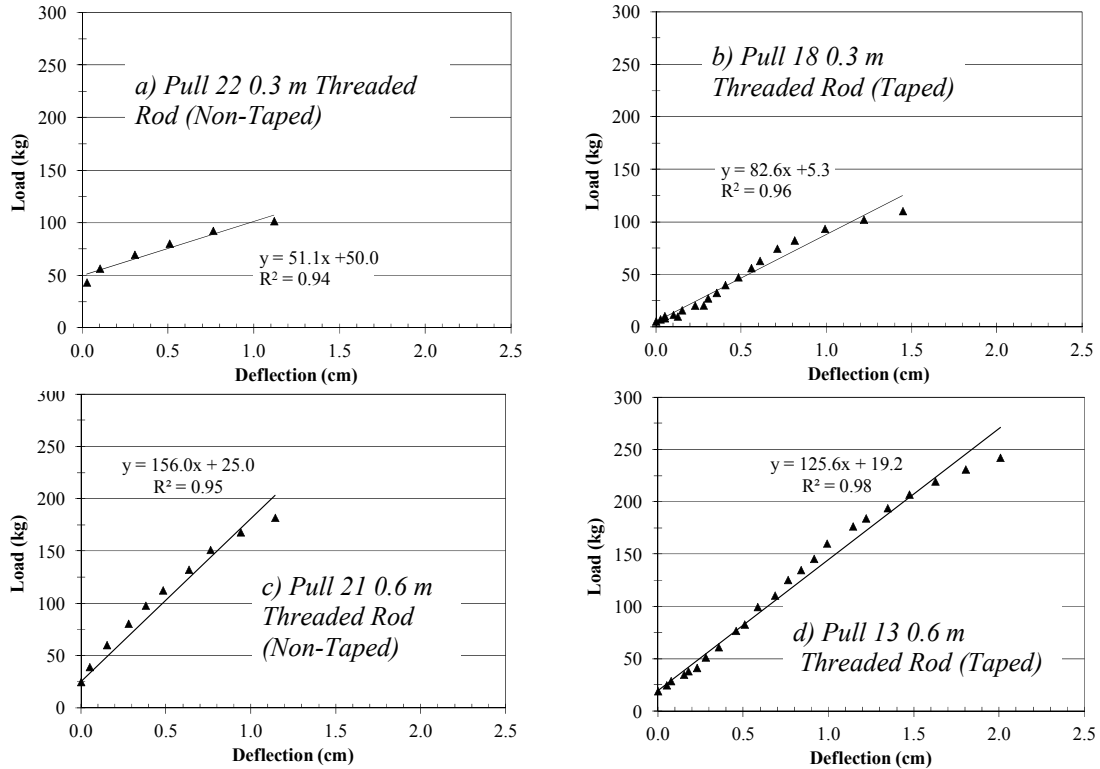


Figure 4.15. Load Deflection Behavior within Linear Portion of Curves

4.8 Simulating Sustained Loading

Three sustained loading simulation tests were conducted by pulling 0.6 m long non-taped anchors with a wench to an approximate deflection of 5 cm and holding for 2 minutes. After two minutes the anchor was pulled until it was removed from the ground. It is noted the wench was unable to keep a constant force on the anchor during the 2 minute pause. These tests were performed to simulate a longer wave loading case that might occur during a storm event to determine how the ultimate load and deflection of the anchors changed during sustained loading. Typical load deflection curves comparing continuous and sustained loading are shown in Figure 4.16 and load deflection data recorded is presented in Table 4.7.

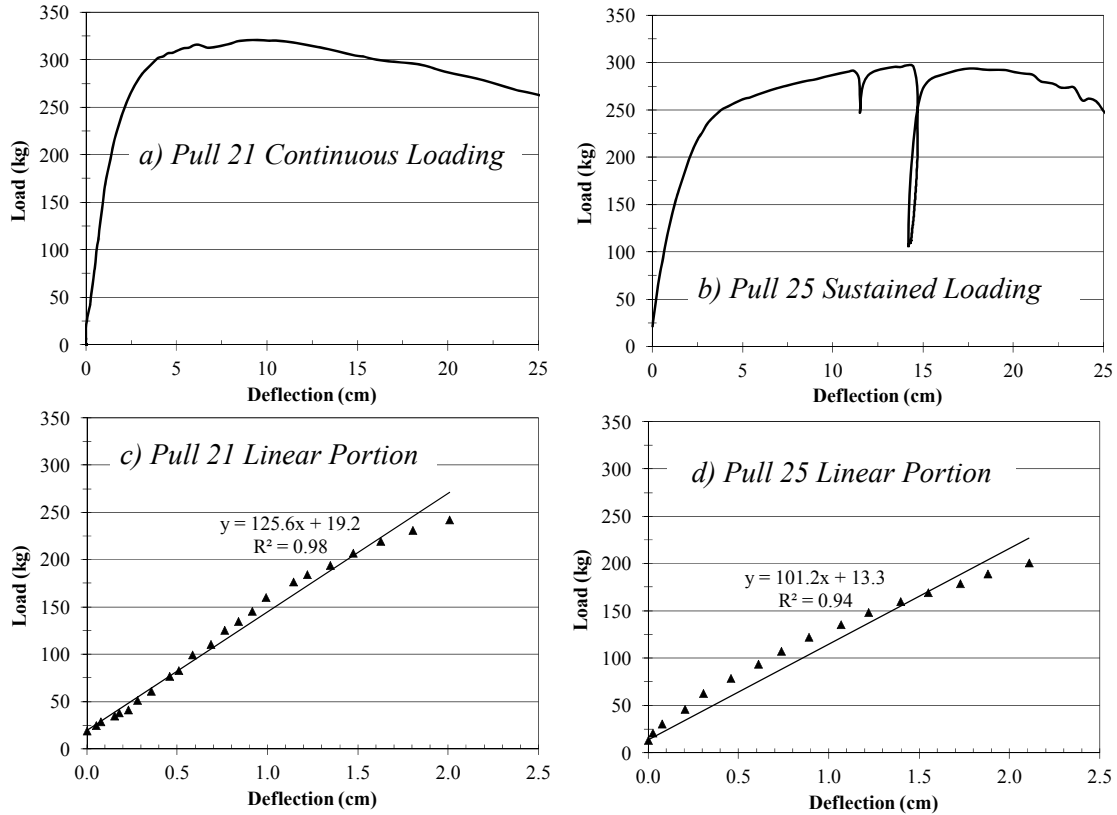


Figure 4.16. Load Deflection Behavior of Sustained Loading Comparison

Table 4.7. Load Deflection Data for Sustained Loading Effects Comparison

Pull No.	P_{Max} (kg)	$\Delta@P_{Max}$ (cm)	$\epsilon_{Max}@P_{Max}$ ($\mu\epsilon$)	S_{100} (kg/cm)	S_{100} (kg/cm)	S_{100} (kg/cm)	S_{100} (kg/cm)	TL	R^2
0.6 m Threaded Bar (Non-Taped) Continuous Loading									
19	343	15.2	3729	23	64	119	237	$y=107.0x+29.4$	0.93
20	359	10.4	5036	35	138	192	277	$y=148.3x+12.5$	0.94
21	321	9.4	3323	34	121	162	163	$y=125.6x+19.2$	0.98
0.6 m Threaded Bar (Non-Taped) Sustained loading									
25	297	14.1	4701	21	85	122	171	$y=101.2x+13.3$	0.94
26	287	11.8	7360	24	100	141	170	$y=115.2x+12.7$	0.95
27	338	12.6	12276	27	105	138	136	$y=112.2x+12.3$	0.97

Figure 4.16 comparison shows that anchors would not be expected to withstand large loads for any long period of time without pulling out of the soil. Due to limited testing, an expected time of constant loading until failure could not be established. Maximum loads were similar between continuous and sustained loading with an average P_{Max} of 341 and 307 kg, respectively. Trendlines created for the linear portion of the curves are similar in load behavior.

All 0.6 m anchors tested for continuous and sustained loading conditions experienced yielding. Although both loading conditions produced yielding, data showed the sustained loading conditions produced higher strain values than continuous loading. The sustained loading strain rate was on the upper end of continuous loading in some instances (e.g. 4702 vs. 3729 in Table 5), but much greater in others (e.g. 12276 vs. 3323).

Figure 4.16 (c-d) shows trendlines created for the linear portion of curves in parts (a-b) are similar in load behavior. Strain data from sustained loading cases was slightly higher than continuous loading cases. For modeling purposes, continuous loading cases will be used since loading changes did not produce drastically different behaviors in the linear portion of the curve. Anchors in the model will be assigned an upper allowable load less than the ultimate load results to add a safety factor for unknown anchor behaviors during sustained loading scenarios.

4.9 Summary of Anchor Tests for Use in Numerical Modeling

For modeling purposes (see Chapter 6), 0.6 m anchors were chosen to provide maximum loads ranging between 265 to 375 kg with corresponding deflections of 3.6 to 19.8 cm. Anchors measuring 0.6 m were chosen to provide a more rigorous anchor for high loading conditions because 0.3 m anchors did not provide as much load capacity and were not as repeatable. Figure 4.17a presents results for 0.6 m anchors pulls for three anchor types tested. Load deflection behaviors were similar for all anchor types, so an approximation of the average expected load deflection curve was created based on Figure 4.17a with a specified failure limit chosen based on a 1.5 cm allowed deflection to prevent anchor pullout. The approximated load deflection curve chosen for numerical modeling purposes is shown in Figure 4.17b.

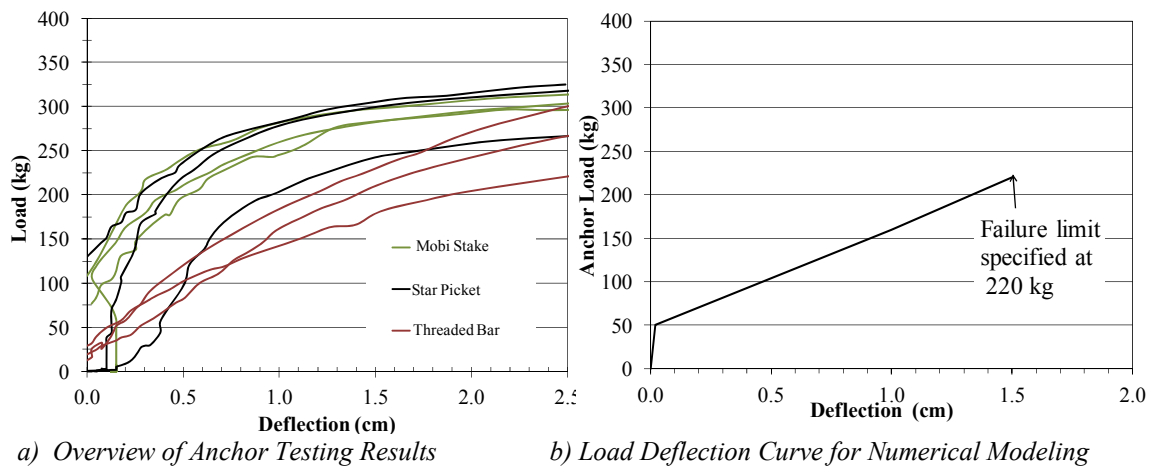


Figure 4.17. Overview of Load Deflection Curve Used in Numerical Modeling

CHAPTER 5 – CONCEPT AND CONSTRUCTION OF ARMORING SYSTEM

5.1 *RDAS* Concept

The development of a Rapidly Deployable Armoring System (*RDAS*) for emergency protection of the landward side of earthen levees would help protect against storm surge and overtopping waves. Geotextiles connected to the levee surface using small anchors are the basis of the *RDAS*. Successful *RDAS* design and implementation requires many parameters to be considered such as:

- Construction feasibility including overlapping/seaming, geotextile connection to anchors, and geotextile connection to the top and bottom of the levee.
- Anchor properties that result in a predictable load-deflection behavior (i.e. length, size, installation angle, etc.).
- Anchor spacing in x' and z' directions ($S_{x'}$ and $S_{z'}$) shown in Figure 1.2 that provide sufficient capacity for a given storm event using given materials.

The remainder of this chapter provides the *RDAS* recommended from this research. Chapters 2 through 4 were the basis for all information presented.

5.2 Preliminary Armoring Approaches

Three anchoring concepts and two end connection approaches (Figure 5.1) were considered during preliminary design that were eventually abandoned. The holes punched through the geotextile to allow anchor installation could provide access for water to enter under the geotextile within the configurations shown. Bonding the geotextile to anchored plates with adhesive (Figure 5.1a) was abandoned because adhesive bonding of polypropylene products was found to be a formidable feat even in controlled conditions. Placing the geotextile between two 20 to 30 cm square plates (Figure 5.1b) and inserting an anchor through the geotextile and both plates was abandoned because the bottom plate could be hard to locate during construction.

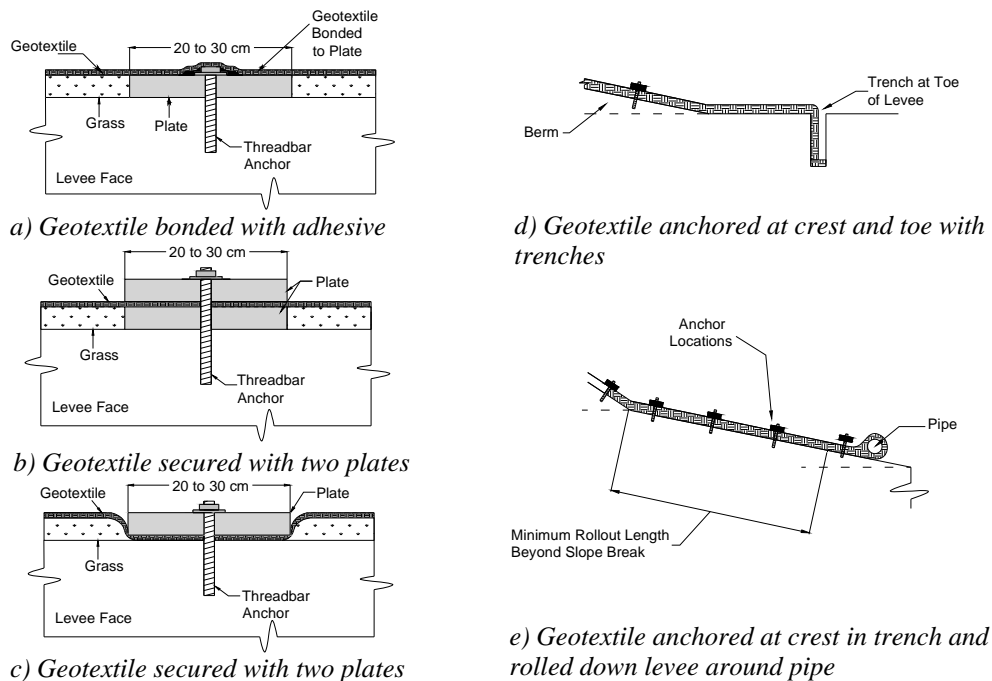


Figure 5.1. Preliminary Design Anchoring and End Connection Concepts

Placing a square plate (Figure 5.1c) on the geotextile and inserting a threadbar anchor through the tie down plate and geotextile would require tightening of a fastener to apply normal forces that could reduce the anchor capacity in some conditions. An additional issue with these approaches would be tearing the geotextile at the plate edges. Commercially available padding could be used to reduce the potential for tears, but this would add an additional time expense during installation.

Securing the geotextile in a trench at the toe of the levee (Figure 5.1d) is the most robust solution, but is likely conservative for a temporary application. Wrapping the end of the geotextile around a pipe at the levee toe is a less robust alternative (Figure 5.1e). The pipe could be useful to assist in smoothing the geotextile during placement, but could result in turbulent flow resulting in erosion that could undermine the armoring system.

5.3 RDAS Construction Materials

TenCate™ HP 570 woven geotextile (or equivalent) is a logical commercially available product for this application and was used herein. HP 570 rolls are 4.5 m by 91 m and weigh approximately 215 kg. Wider rolls could be manufactured and reduce overlapping seams, but these rolls would be heavier, more difficult to unroll, would have to be pre-ordered, and could require special storage.

Small rod shaped anchors as outlined in Chapter 4 are readily available. For a temporary application, a short object penetrating the levee is desirable for long term conditions as they would be less damaging. Three anchor types tested within this research (Chapter 4) revealed that 0.6 m long rod like anchors could withstand useable loads. Threaded bar anchors are the recommended anchor type to secure the geotextile to the levee as the bars are easy to obtain in bulk during emergency situations, they can be hauled to the site and cut to the proper length on site, and they can facilitate attachment to the geotextile.

5.4 RDAS Construction Guidance

Figure 5.2 presents *RDAS* construction sequences which are broken into 10 phases.

Phase 1: Choose Material	<ul style="list-style-type: none"> • Determine appropriate geotextile material for protection • Determine amount and type of anchors required
Phase 2: Setup	<ul style="list-style-type: none"> • Clear debris • Place roll of geotextile at crest
Phase 3: Excavate Trench	<ul style="list-style-type: none"> • Paint line along crest of levee for alignment purposes • Use large trenching device for rapid trench excavation (Fig. 3.3)
Phase 4: Roll Down Panel	<ul style="list-style-type: none"> • Place geotextile on spreader bar and position in place with excavator or with Skid Steer when site is inaccessible by heavy equipment • Cut small holes in end of geotextile to pull down slope (Fig. 3.4 and 3.5)
Phase 5: Cut Excess	<ul style="list-style-type: none"> • Cut panel from roll at crest • Reposition geotextile at crest • Place second geotextile panel down levee
Phase 6: Trench Burial 1 of 2	<ul style="list-style-type: none"> • Wrap the geotextile around a pipe or board and place in trench • Partially backfill trench with onsite material to secure geotextile during construction, the remaining portion of trench will be filled after geotextile placement
Phase 7: Anchor Geotextile Panel	<ul style="list-style-type: none"> • Anchor part of the first geotextile panel • Use wench (if needed or available) to pull and hold panel taut
Phase 8: Seam Panels	<ul style="list-style-type: none"> • Use fabric sewing machine to seam panels together • Finish anchoring first panel and part of the second panel
Phase 9: Repeat Sequence	<ul style="list-style-type: none"> • Continue placing, anchoring, and seaming panels until the stretch to be protected is covered
Phase 10: Trench Burial 2 of 2	<ul style="list-style-type: none"> • Pump or otherwise place cement stabilized onsite material into trench along entire length of the protected area filling the partially backfilled trench remaining after placing the wrapped geotextile

Figure 5.2. Summary of RDAS Construction Sequencing

5.4.1 Material Selection and Setup

The site must be cleared of debris that could damage the geotextile. To achieve this task, an All Terrain Vehicle (ATV) towing a small utility trailer could be driven down the levee as a team of workers collect debris. Debris to be removed includes but is not limited to pieces of wood, large rocks, or other objects that could tear the geotextile. One issue to this research is the surface of the levee could be paved, which could present logistical problems. Procedures outlined within this chapter assume the levee is unpaved.

5.4.2 Excavate Trench

A trench at the crest of the levee should be excavated to secure the geotextile to the levee as presented in Figure 1.2. Using a trenching device is recommended for speed and performance. Using an excavator to perform trenching is not recommended as it is challenging to produce a straight trench and is slow as outlined in the summary of the USACE Yazoo Backwater Levee protection in Chapter 3 of this document.

5.4.3 Roll Down Geotextile Panel

In preparation for construction, a geotextile roll should be moved from the temporary holding area on site to the levee crest by equipment such as a SkidSteer and spreader bar. Small grab holes can be cut in the end of the geotextile to pull down the levee. As shown by the USACE Backwater Levee protection (Chapter 3), a group of approximately 5 people is sufficient to pull the geotextile.

A second option is using an ATV to pull the geotextile panel down the levee by connecting the panel to the ATV with cables attached to a board or a pipe. This approach would wrap and secure the geotextile end around a board or pipe. A team of workers should help keep the geotextile straight and flat as it is pulled down the levee by guiding the edges of the panel as it is pulled.

5.4.4 Cut Excess and Repeat Geotextile Laydown

After the geotextile panel is pulled completely down the levee slope, the panel can be cut from the roll at the crest of the levee leaving approximately 2.4 m of excess geotextile for trench burial. The geotextile roll should be repositioned along the *z-direction* of the levee to begin placing a second segment. The second panel should be placed to ensure overlap of the previous panel for seaming. A group of workers should guide the second panel to ensure the panel is aligned correctly with the previous panel.

5.4.5 Trench Burial (1 of 2)

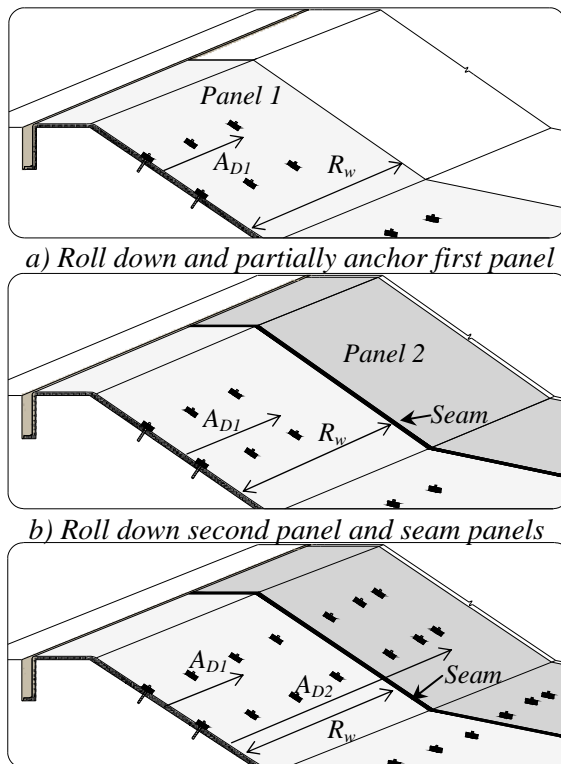
The geotextile panel ends should be wrapped around a pipe or board and placed in the bottom of the trench at the levee crest. The geotextile and pipe or board should be backfilled with material removed from the trench a sufficient amount to secure the geotextile in the trench during construction. The amount of backfill required to secure the geotextile during

construction would be determined on the first few panels placed. The remaining portion of the trench will be filled in the final steps of construction as discussed in Section 5.4.8.

5.4.6 Anchor and Seam Geotextile Panels

After the first geotextile panel is placed (Figure 5.3a), anchors can be installed to one side of the first panel, leaving the side being seamed to the next panel unanchored. The distance anchored on the first panel (A_{D1}) should be determined in the field to be the maximum distance that allows the remaining unanchored portion to be easily seamed to the second panel. To begin seaming, A Union Special 2200L (or equivalent) portable sewing machine should be attached to the rear of an ATV, and the ATV should be positioned at the levee crest between the edges of adjoining panels with the panel ends at the rear of the ATV. The ATV can be driven down the levee as the geotextile is seamed together. The geotextile should be pulled taunt with edges facing up to create a seam. In some applications, a wench could be beneficial for pulling the geotextile taunt. Figure 5.3b shows the second panel placed on the levee and seamed to the first panel with the first panel partially anchored a distance, A_{D1} .

After seaming the edges of the panels together, anchors should be installed as per guidance in the next section to the remaining portions of the first panel and only part of the second panel leaving room for connection to the subsequent panel (Figure 5.3c). The total anchored distance in this case is A_{D2} , or A_{D1} plus R_w . In high flow applications, excess material created from seaming could be pressed flat to one side of the seam and anchored. This process would be repeated to connect the required panels over the entire protection area.



a) Roll down and partially anchor first panel
b) Roll down second panel and seam panels
c) Anchor remainder of first panel and part of second
Figure 5.3. Sequences for Anchoring and Seaming of Geotextile Panels

In general, seaming could be the most logical option because it would ensure water (i.e. waves) will not penetrate under the geotextile at the connections. Overlapping in the wave overtopping direction along the landward slope is not expected to be needed because one roll of geotextile ($R_L = 91$ m) should provide enough length to cover the slope without using multiple rolls for most applications. In cases of high wind, sandbags can be used at the panel ends to prevent the panel from moving before anchors are placed. Heat seaming is an alternative to sewn seams and USACE procedures are detailed in Chapter 3.

5.4.7 Anchoring Installation Recommendations

Anchoring of the geotextile to the levee could potentially present the problem of water entering under the geotextile at the location where the anchor penetrates the geotextile provided the material was sandwiched between wood (or equivalent). In addition, the hole created by punching through the geotextile with an anchor would be an area of high stresses during wave overtopping. To mitigate the anchor hole problem, a modified version of an anchor connection cup presented by Vitton et al. (1998) is recommended. Threaded bar anchors are the recommended anchor type within this document. Modification to the connection cup includes providing the cup with metal teeth along the bottom of the cup to be pushed into the geotextile and add support to mitigate stress concentrations at the anchor hole locations as shown in Figure 5.4 (note everything but the metal prongs are the work of Vitton et al. 1998). The modified anchor cup connection is not commercially available.

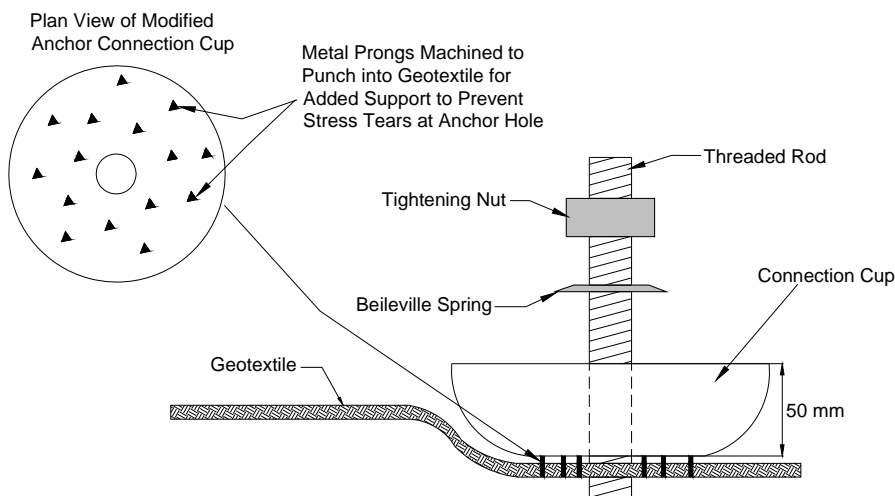


Figure 5.4. Modifications to Vitton et al. (1998) Anchor Connection Cup

An alternative option for anchoring the geotextile to the levee could be Earth percussion anchors. Lightweight earth percussion anchors can be installed with a jackhammer, while a pavement breaker could be used to install a more durable heavy anchor type. A 27 to 41 kg pavement breaker is required to drive anchors. Pins, staples, or stakes could add extra reinforcement to the geotextile between anchor locations.

5.4.8 Trench Burial (2 of 2) and End Connection

At the end of construction, the remaining portion of the trench should be filled with cement stabilized onsite soil that could be easily pumped (if slurried) into the trench in one step after construction of the protected area is complete. This will mobilize the geotextile and prevent pullout as the entire block of cement stabilized soil and pipe or board would have to fail before the geotextile would be removed from the trench. Research performed by Howard (2011) showed cement could be mixed with soils existing onsite to provide a pumpable material with fairly rapid strength gain. Desired strength of the material could be pre-estimated based on Howard et al. (2012) to ensure the material is easy to remove after the storm event occurred, but strong enough to be able to resist pullout of the geotextile from high loading.

The USACE method of trench burial included using a dozer to place random fill to 0.2 m below the top of the trench. A rubber tire backhoe was used to compact the material by placing the front tire in the trench with extra material in the front bucket for additional weight to aid in compaction. Sand bags were used to fill the remaining portion of the trench to levee with the crest of the levee. This approach was adequate for the application of small flow events, but a more sturdy connection is likely needed for large storm events.

Figure 5.5 provides the two recommended end connection details for the RDAS. Figure 5.5a stretches the geotextile roll to its maximum length and places anchors so that the geotextile coverage is maximized. Figure 5.5b anchors the geotextile a modest distance above its maximum length and overlaps the geotextile to create a scour flap. Site specific conditions will determine which configuration to use, and these configurations are expected to be intermingled along the length of an armoring project.

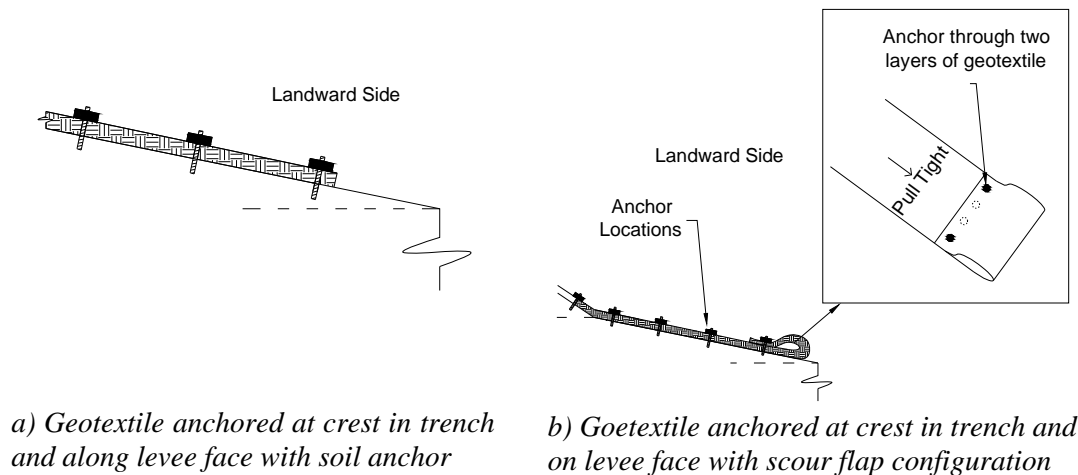


Figure 5.5. Recommended End Connection Approaches

5.5 Estimation of Installation Rates for RDAS

The USACE Yazoo Backwater Levee protection outlined in Chapter 3 provides verification that a RDAS designed for low flow conditions can be placed rather quickly with minimal equipment. Approximately 5.6 km of temporary armoring was installed in approximately 6 days. Placement of an RDAS in a high flow application could be expected to take slightly longer due to anchor placement instead of stakes.

Districts within the USACE do not have standard vegetation maintenance practices, and as a result a repeatable condition on a levee face is unlikely and could add time to placement. Additionally, the time of year a particular site experienced the need for protection could vary somewhat, and thus vary the extent of vegetation encountered.

5.6 Summary

The *RDAS* concept is viable for earthen levee protection from overtopping and waves since it can be constructed efficiently before an expected storm event. Construction would not require sophisticated equipment and the majority of the materials recommended are available in bulk. The modified anchor connectors are a notable exception that do not appear to be commercially available. Numerical calculations are required to recommend design guidelines such as required anchor spacing and geotextile strength for an expected wave load. A finite element analysis model of the *RDAS* including the design inputs is described in remaining portions of document. A finite element model could be beneficial in designing a *RDAS* system for the specific wave or overtopping loads expected.

CHAPTER 6 – FINITE ELEMENT MODELING APPROACH

6.1 Overview of Finite Element Modeling Approach

The finite element method was used to model stability of the (*RDAS*). The model took the position that erosion could be controlled if the geotextiles remained in place without experiencing excessive deflection. Membrane behavior was not efficiently modeled by the research team using Plaxis. The geogrid element in the software was not believed to be comprehensive enough to meet the needs of the project, and beam/plate elements did not provide adequate flexibility in user input of properties to simulate the geosynthetic.

Abaqus/CAE is a graphical user interface (*GUI*) that was used to create the model. The *GUI* is an environment that allows the user to graphically interact with Abaqus to create, submit, and monitor the analysis of a model. The *GUI* contains modules that allow the user to create part geometries, material properties, boundary conditions, contact interactions, loads, meshes, and analysis types. After the user completes the module inputs, Abaqus/CAE writes an input file formatted for analysis submittal.

Fortran is a general purpose programming language that was used to write a subroutine that applied dynamic wave loading to the model. Python is an object oriented programming language that was used to write programs to aid in Abaqus job submission and analysis of results. The programs automatically submitted Abaqus jobs and searched job output files to find the maximum and minimum values of shear stress and reaction forces on the geotextile.

Models were defined in general terms by the geotextile meshing method, levee configuration, and anchor rigidity. Two geotextile meshing methods were used: single layer membrane elements, *SLEMM*; and double layer membrane elements, *DLEMM*. Two levee configurations were used: flexible 3D levee, *FL*; and rigid 2D levee, *RL*. The flexible (deformable) levee brought complexities without providing advantages relative to the rigid levee shell so the majority of the effort used the rigid levee. Two anchor types were modeled: rigid anchors, *RA*; and flexible anchors, *FA*. Four model types were created based on the aforementioned terminology: *SLEMM-FL-RA*, *SLEMM-RL-RA*, *SLEMM-RL-FA* and a *DLEMM* on a square geometry without anchors. For explanation purposes, the *SLEMM-RL-RA* model includes a single layer elastic membrane model with a rigid levee and rigid anchors.

6.2 Model Type 1 - *SLEMM-FL-RA*

The levee was modeled as a three dimensional (3D) deformable body with linear elastic material properties. The purpose of a deformable levee was to model the anchor/soil interaction and include the increased soil stiffness due to anchoring at the localized area around each anchor. The geotextile was modeled as a 3D extruded deformable shell with linear elastic properties up to a failure load.

6.2.1 SLEMM-FL-RA Model Geometry

The Abaqus/CAE *Part Module* was used to create the geometries for each part in the model (Figure 6.1). The earthen levee was extruded through the assigned depth (d_1) of 22.86 m with a trench at the crest to insert anchors. The levee height (H_1) was 3.66 m. To simulate the effect of an anchor, small blocks were inserted into the levee trench that could be assigned increased stiffness values. The properties of the blocks were to be assigned based on soil/anchor interaction models.

The geotextile was modeled as a deformable shell because the thickness of the geotextile (T_g) is small relative to its width and depth. Using the shell should provide more flexibility than a solid for representing the geotextile behavior. The deformable shell was created by extruding the cross sectional sketch of the geotextile through the assigned distance (G_w) of 15.24 m. The separate geotextile and levee part geometries were combined into an assembly and positioned together.

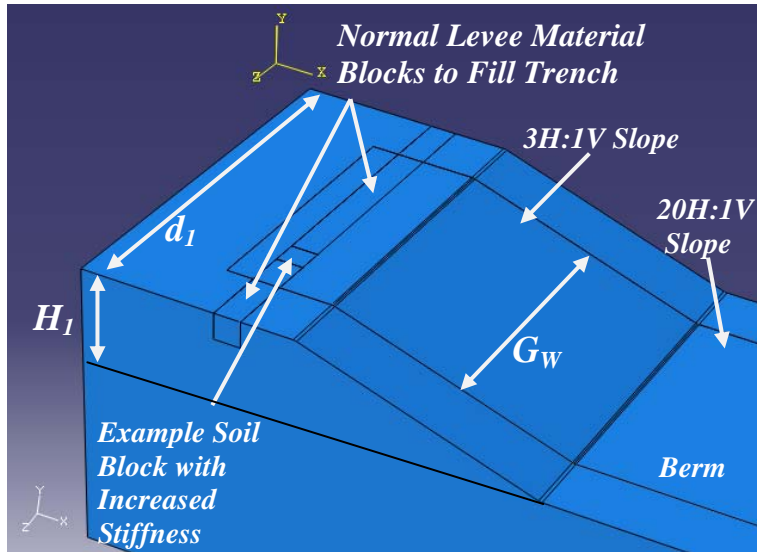


Figure 6.1. Model Type 1 – Geometry

6.2.2 SLEMM-FL-RA Material Properties

Material properties were assigned to the levee and geotextile using the *Material Module* in the *GUI*. Levee values for Young’s Modulus (E), Poisson’s ratio (ν), and density (γ) were assigned based on typical values of clay (Terzaghi et al., 1996) as seen in Table 6.1. Geotextile ν and E were taken 0.33 and 19.6 MPa, respectively, based on previous finite element modeling of geotextile reinforced banks performed by Huang (2006) as presented in Table 2.5. Soil properties near the anchors were never fully defined.

Table 6.1. Material Property Values for Earthen Levee Model

Material Parameter	Units	Value
E	MPa	6
ν	N/A	0.35
γ	kN/m ³	17.4

6.2.3 SLEMM-FL-RA Contact Interactions

The *Contact Interaction Module* was used to describe the frictional resistance of the geotextile during wave loading. A surface to surface general contact interaction was used to describe the contact between the geotextile and levee that allowed the geotextile to slide along the levee between anchor locations as governed by a friction coefficient (f). Surface to surface contact interactions can be used to describe contact between two deformable bodies or a deformable body and a rigid body (Abaqus 2009). A mechanical interaction property was assigned because this allows f to be specified; f of 0.4 was used during analysis based on friction data for grass reported by Kim et. Al (2004, 2005) shown in 2.3.2. Tied contact constraints were assigned to surfaces at anchor locations where levee material and stiffened soil blocks connected.

6.2.4 SLEMM-FL-RA Steps

Abaqus/CAE requires the user to define a sequence of steps that will be conducted to perform the analysis. In each step, the user defines the analysis type, boundary conditions, and loads that will be applied during a particular time step. For this analysis, two steps were created. Gravity and pressure loading were applied in a static general analysis step with non-linear geometry options deactivated. A dynamic, implicit step with non-linear geometry deactivated was used to apply wave loading. Unlike the static general step, the dynamic implicit step supports the dynamic wave load subroutine (*Waveload.f*) execution used in this document. In addition, the quasi-static solver application was used to regularize unstable behavior and obtain a steady state result. Results obtained without the quasi-static solver showed oscillation of the results even when an additional 10 second step was created with no applied loading. Oscillating results trends were attributed to the oscillation caused by dynamic analysis in conjunction with the material model used.

6.2.5 SLEMM-FL-RA Boundary Conditions

Boundary conditions applied to the deformable levee model included a fixed bottom of the earthen levee so that displacement was zero in the x , y , and z -directions ($U_x=U_y=U_z=0$). The boundary conditions for the sides of the levee were modeled as rollers to allow the levee to compress vertically ($U_x=U_z=0$). All anchor locations within the geotextile were also fixed ($U_x=U_y=U_z=0$).

6.2.6 SLEMM-FL-RA Mesh

The 3 dimensional, 9 node membrane element with reduced integration (M3D9R) was used in meshing the geotextile part geometry to more realistically represent flexible behavior. Membrane elements are surface elements that are used to model thin surfaces which support only in-plane strength and no bending stiffness. An example of the nodes and integration points for the membrane elements is shown in Figure 6.2. Quadrilateral structured meshing techniques in Abaqus/CAE were used in meshing the part. A total of 725 nodes and 220 elements were used to mesh the geotextile. The earthen levee was meshed with continuum 3 dimensional 9 node reduced integration elements (C3D9R) created using

the automatic structured meshing techniques in Abaqus/CAE. The mesh contained 260 nodes with 144 linear hexahedral elements as shown in Figure 6.2b.

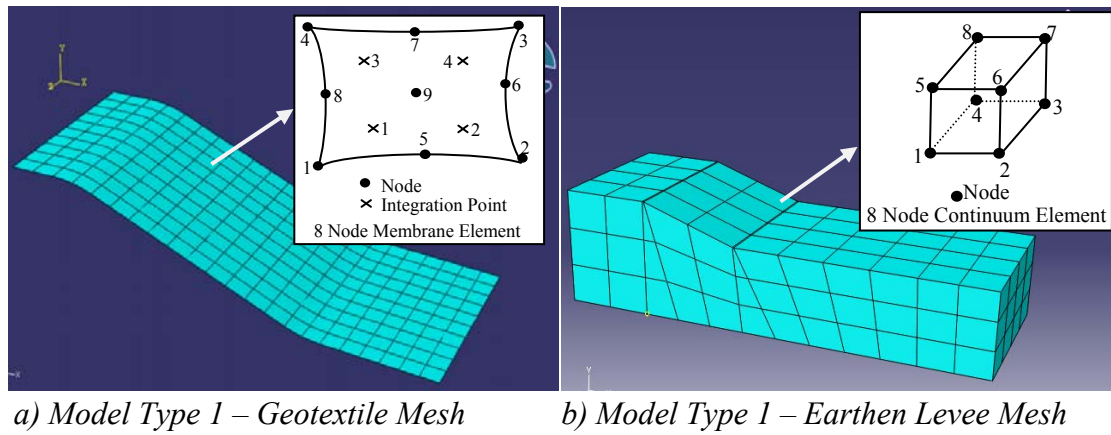


Figure 6.2. Model Type 1 – Geotextile and Earthen Levee Mesh

6.3 Model Type 2 – SLEMM-RL-RA

The second modeling approach incorporated a geotextile modeled as a thin membrane in contact with a 2 dimensional rigid levee section rather than a 3 dimensional levee section. Figure 6.3 presents a flow diagram of the rigid levee model.

The remainder of this section describes how the model was created, the material models used, boundary conditions applied, and load cases that were created to simulate the dynamic wave loads.

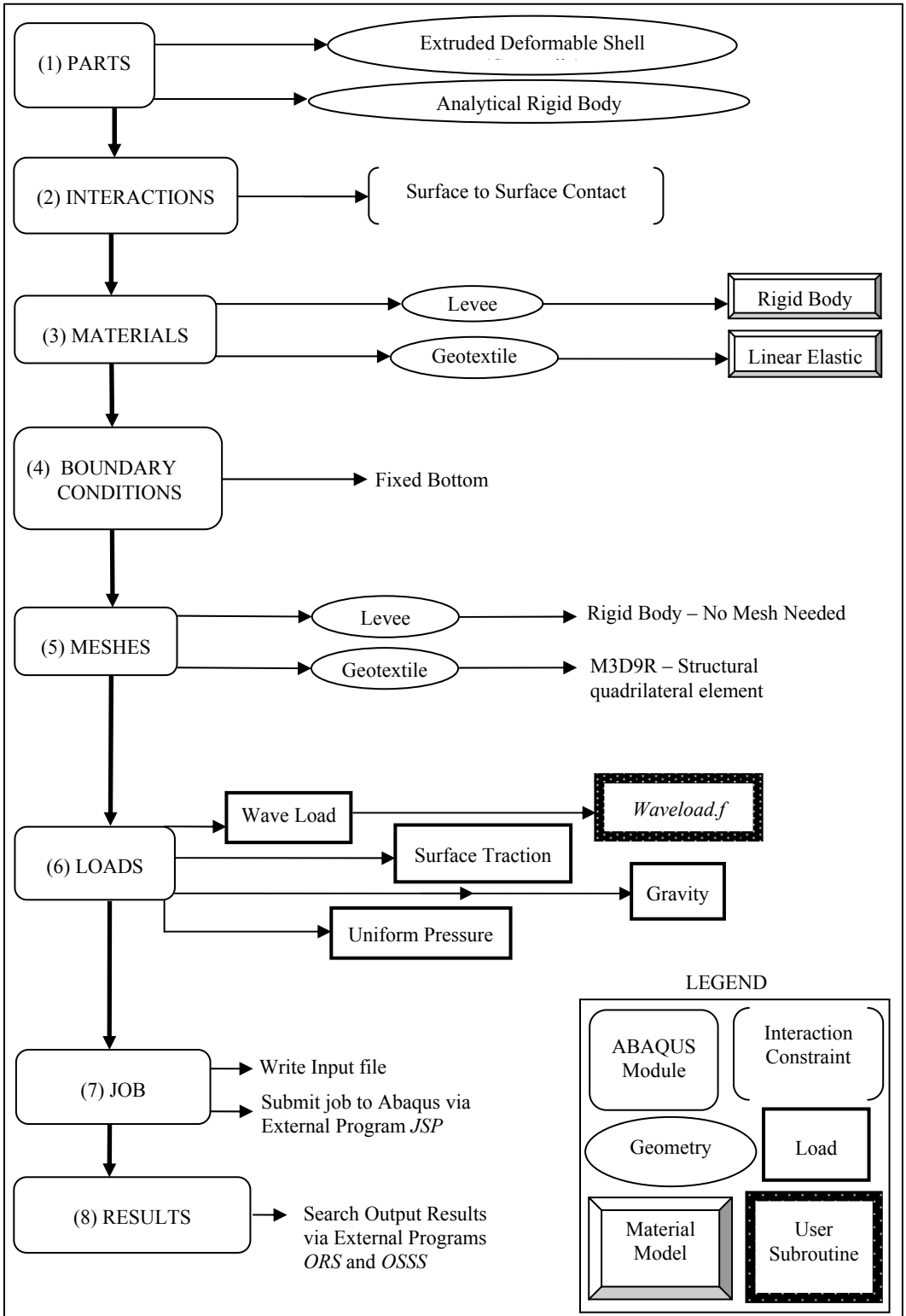


Figure 6.3. Flow Diagram of Rigid Levee Model

6.3.1 SLEMM-RL-RA Model Geometries

The levee was modeled as an analytical rigid body by sketching the two dimensional cross section of the levee in the x - y plane, extruding it through the selected depth of 9.15 m, and assigning a rigid body constraint to the part geometry. Since the part is infinitely rigid, no thickness was defined. The geotextile and levee geometries were combined into an assembly and positioned together as shown in Figure 6.4.

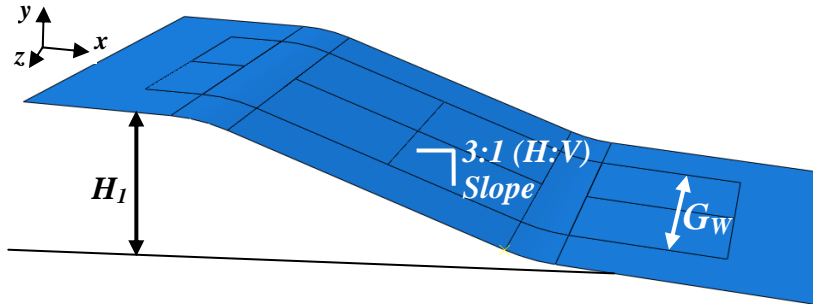


Figure 6.4. Model Type 1 – Assembly of Model Parts

6.3.2 SLEMM-RL-RA Contact Interactions

In preliminary modeling, a friction penalty contact interaction was used to describe the frictional resistance of the geotextile during wave loading. Frictional implementation produced unexpected results that could not be verified, so the frictional resistance was implemented as a pre-modeling input. Frictional behavior between geotextiles and levees when under water is not well understood. The geotextile will not be in full contact with the levee as it isn't smooth due to weathering, construction imperfections and similar. The *Contact Interaction Module* was used to enforce a frictionless surface to surface general contact interaction between the geotextile and rigid levee; i.e. friction is not a direct input into the model. Frictional resistance is implemented as user defined reduction in gross applied shear stress as shown in Figure 6.5 based on expected overtopping height (h) and unit weight of water (γ_{water}). The friction implementation approach is a good balance between rigor and practical implementation. More realistic frictional data would be needed for more rigorous simulations. The *RDAS* designer can use all, some, or partial frictional resistance.

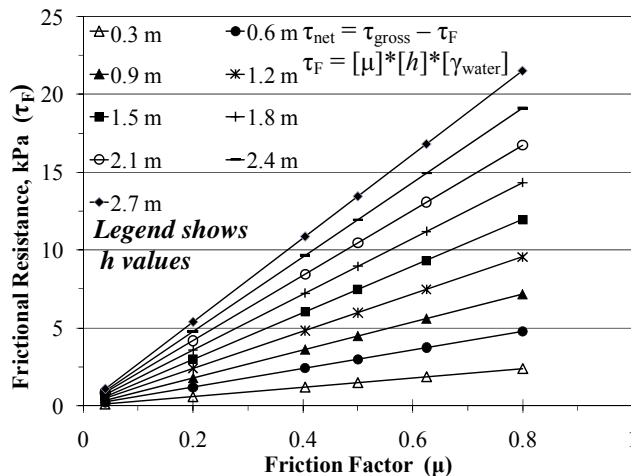


Figure 6.5. Frictional Resistance for a Range of Friction Factors

6.3.3 SLEMM-RL-RA Material Properties

It is difficult to accurately determine E for a geotextile because the geotextile dimensions change during loading. Woven geotextiles are made of different size fibers that are machine woven together to form the net-like material. The woven fibers in a relaxed state contain air voids that are reduced when load is applied and the web of fibers tighten. To estimate E , TenCate™ product data sheets from the ASTM D4595 – 05 (Wide Width Tensile Test) were used to relate load and elongation using fundamental mechanics principles.

To perform D4595, clamps are used to grip machine ends of a 20.3 cm wide strip of geotextile. An axial load P is applied to the geotextile until the fibers break, while force and elongation data are recording during testing. Figure 6.6(a) shows the specimen before testing, and Figure 6.6(b) shows the specimen during testing. During loading, the width of the specimen, L_1 , shortens as the fibers in the loading direction elongate. The change in lengths, ΔL_1 and ΔL_2 , during axial loading cause a continuous change in T_g .

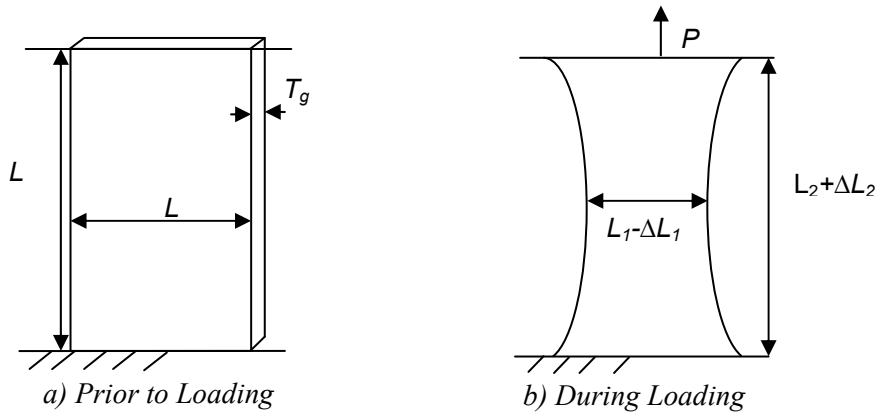


Figure 6.6. Undeformed Specimen During ASTM D4595 Testing

Figure 6.7 plots load versus strain for a variety of geotextiles. Equation 6.1 is the fundamental relationship of elongation due to axial loading and Equation 6.2 relates the elongation to the percent strain. Equation 6.3 is the result of setting the two elongations equal and solving the relationship in terms of E . A variety of geotextile products were measured using calipers while unloaded; measured values ranged from 1.2 to 3.5 mm. For model simplification purposes, the thickness of the geotextile will be assumed a constant of 2 mm; therefore, the EA term will remain constant regardless of thickness.

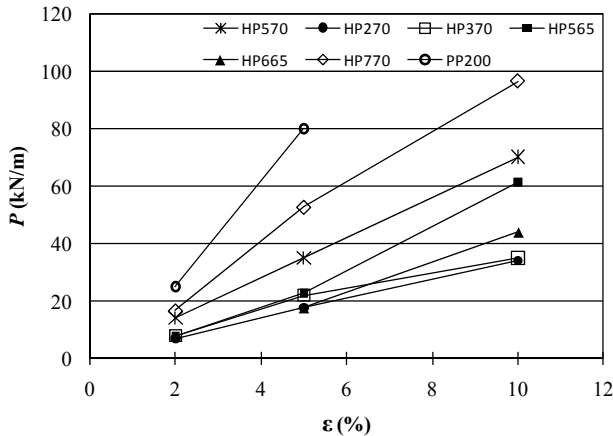


Figure 6.7. Load vs. Percent Strain Plot from Product Specifications

$$\Delta = \frac{PL_2}{AE} \quad \text{Equation (6.1)}$$

$$\Delta = \frac{\varepsilon\%L_2}{100} \quad \text{Equation (6.2)}$$

$$E = \left(\frac{100}{T_g L_1} \right) \left(\frac{P}{\varepsilon\%} \right) \quad \text{Equation (6.3)}$$

Where

E = Modulus of Elasticity

P/ε = axial force (N) per unit strain (%) reported by D4595 on a unit width basis

T_g = Geotextile thickness (taken as 0.002 m)

L_1 = Geotextile width (taken as 1 m)

6.3.4 SLEMM-RL-RA Boundary Conditions

To prevent applied loads from moving the entire levee, the levee was fixed in space. A reference node assigned to the part was fixed so that displacement was zero in the x and y -directions ($U_x=U_y$). Rigid y -direction body constraints were obtained by interaction with the rigid levee. Fixed boundary conditions were used to represent the anchors which secure the geotextile to the levee. Figure 6.8 shows all boundary conditions applied to the geometry.

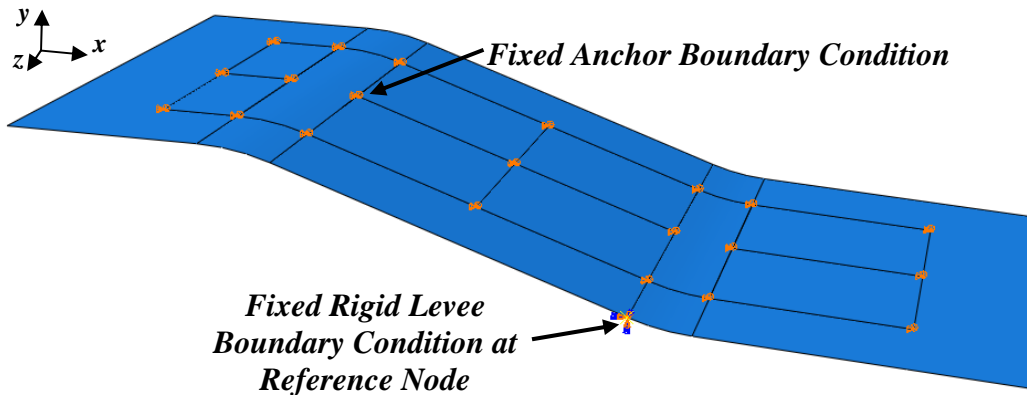


Figure 6.8. Model Type 2 – Boundary Conditions

6.3.5 SLEMM-RL-RA Mesh

The 3 dimensional, 9 node membrane element with reduced integration (M3D9R) was used in meshing the geotextile part geometry. Membrane elements are surface elements that are used to model thin surfaces which support only in-plane strength and no bending stiffness. An example of the nodes and integration points for the chosen membrane elements is shown in Figure 6.9. Quadrilateral structured automatic meshing techniques in Abaqus/CAE were used in meshing the part. A total of 3,309 nodes and 1,056 elements were

used to mesh the geotextile. Since Abaqus does not require meshing for rigid bodies, the rigid levee was not meshed.

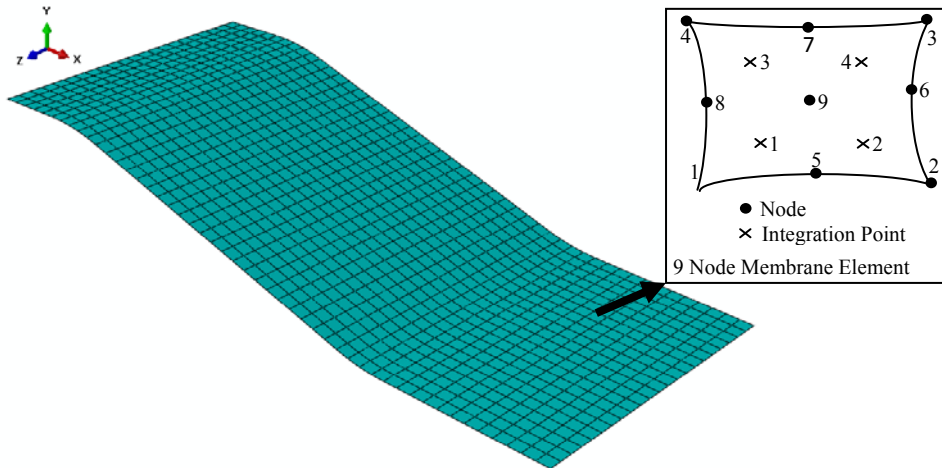


Figure 6.9. Model Type 2 – Geotextile Mesh

A mesh convergence study was performed using the full slope geometry with ≈ 4.9 m square anchor spacing, 2.99 kPa uniform pressure, and 1.0 kPa shear stress to determine a suitable mesh size to provide convergence of the solution. Five models with varying mesh sizes were performed; Figure 6.10 provides convergence results in terms of average Von Mises stress of the bottom 90% of the data ($\tau_{avg,90\%}$). A contour plot of Von Mises stress and a quilted plot of S11 stress are shown in Figures 6.11 through 6.13 for various mesh sizes. Due to increased computational time with increased mesh refinement, this mesh size was deemed sufficient. As the mesh is refined, the model produces solutions that show a spike in shear stresses only in a very close proximity to the fixed anchor boundary conditions.

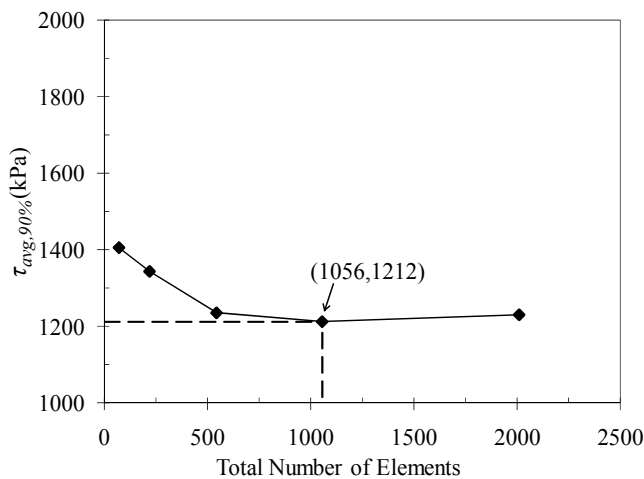
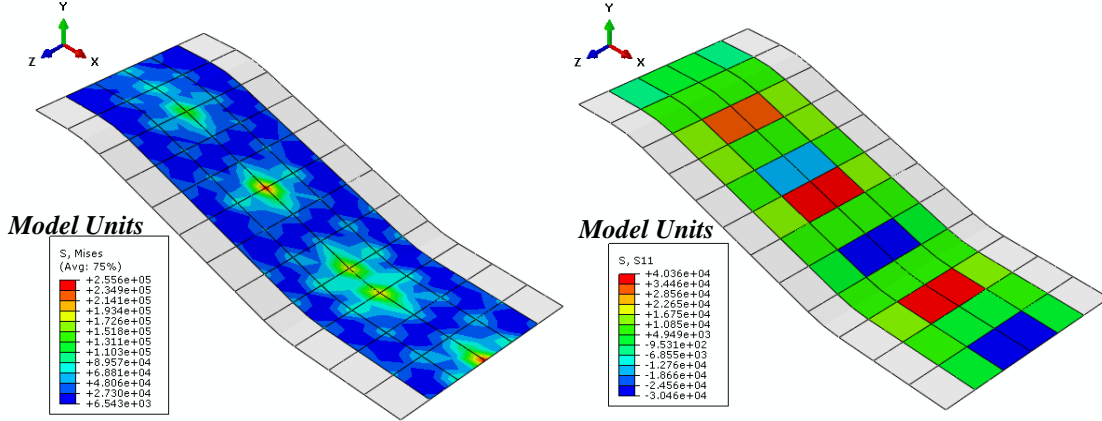


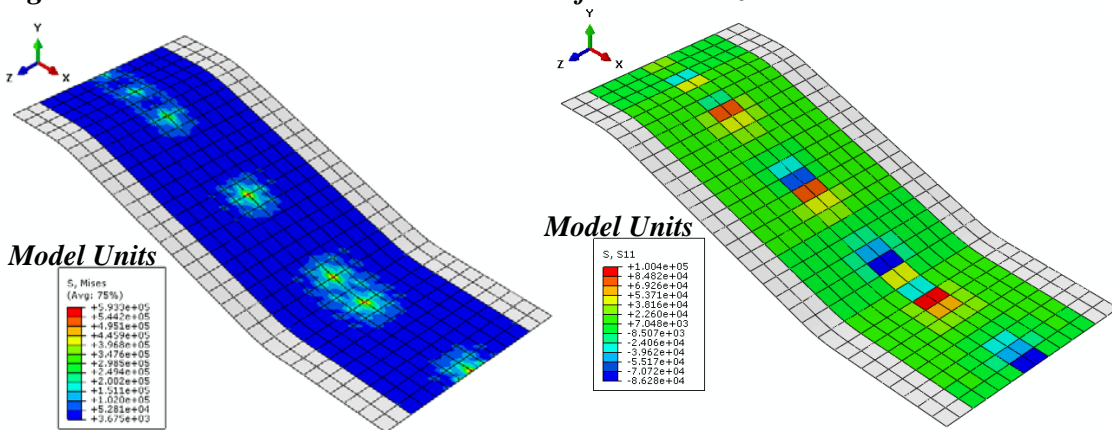
Figure 6.10. Mesh Convergence Curve

As shown in the quilted plots, areas at the anchors experience the largest tensile stresses at one element and the largest compressive stresses at the next connected element. This model does not appear to yield physically meaningful predictions of the mechanical response of a thin geotextile subjected to normal pressure and distributed shear traction. In

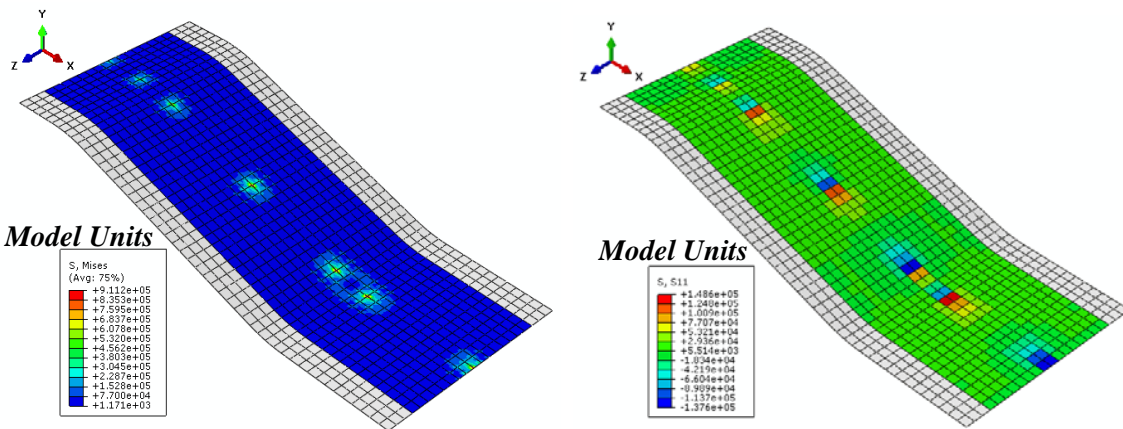
particular, the surface shear tractions applied to the membrane elements are equilibrated by uniform, in-plane normal stresses only. The resulting stress distributions include compressive stress levels that suggest buckling of the membrane near anchor points. Because compressive buckling is not represented by the membrane elements, the current model does not predict a physically meaningful response.



a) Von Mises Banded Stress Plot b) S11 Quilted Stress Plot
Figure 6.11. Shear Stress Distribution Plot for Mesh Size = 2.47 m²



a) Von Mises Banded Stress Plot b) S11 Quilted Stress Plot
Figure 6.12. Shear Stress Distribution Plot for Mesh Size = 0.45 m²



a) Von Mises Banded Stress Plot b) S11 Quilted Stress Plot
Figure 6.13. Shear Stress Distribution Plot for Mesh Size = 0.18 m²

6.3.6 SLEMM-RL-RA Loads

Observations suggest normal stresses on the levee protection fabric are almost always compressive. Lift forces probably would be difficult on the sloped portion of the levee unless water accumulated behind the protection membrane. With this in mind, four loads were applied to the rigid body levee model: gravity, uniformly distributed pressure, surface traction, and user defined pressure. Gravity, uniformly distributed pressure, and traction loads were applied to the selected geometries using the *Load Module*. All loads applied were increased linearly over the step during analysis. Gravity was applied to the entire model in the negative *y-direction*. Pressure of 3 kPa was applied as a uniformly distributed load over the entire face of the geotextile surface perpendicular to the fabric to represent the pressure of 0.3 m of water. A surface traction load was applied as a uniformly distributed load to the geotextile surface using a vector $\langle -1, 0, 0 \rangle$ to describe the direction of the force moving along the face of the geotextile. The traction load was used to simulate any constant shear stresses due to surge loading. The space and time dependent pressures produced by dynamic wave loading from overtopping cannot be defined graphically in Abaqus/CAE. The dynamic pressure distribution profile caused by the wave loading was defined using a Fortran DLOAD subroutine as discussed further in the following paragraphs. Figure 6.14 shows the rigid body model with the gravity, uniformly distributed pressure, and traction loads applied.

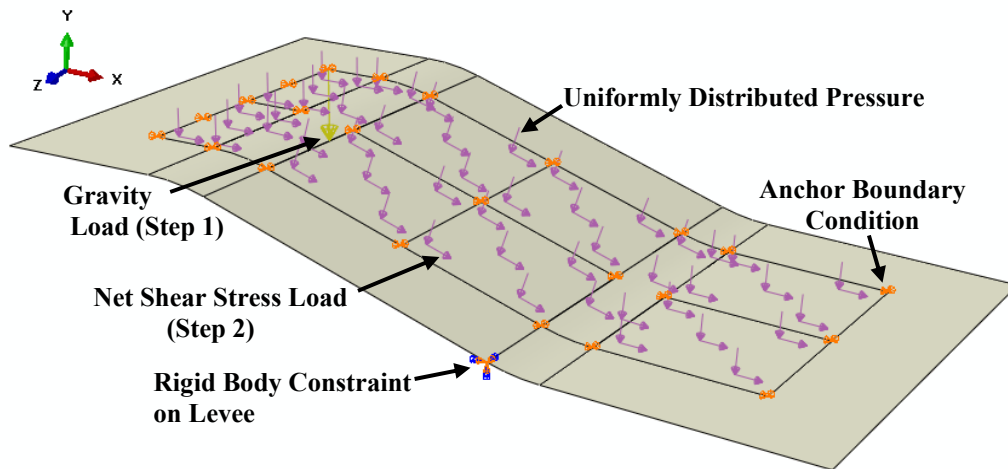


Figure 6.14. Model Type 2 – Applied Loads

Flume testing was performed by Hughes et al. (2011) to determine expected velocity and depth profiles along the levee during wave overtopping. Results from this testing provided empirical formulations for estimating the magnitude of shear stresses on the landward side of levees. The shear stress profiles obtained were incorporated in this model to represent the dynamic distribution of loading caused by the wave action on the levee (overtopping conditions). Shear stress calculations were given in two zones along the landward levee face.

An example shear stress profile for Wave Case 1 (WC-1) with 0.3 m of surge is shown in Figure 6.15. Shear stress is constant 1000 Pa and 1420 Pa in Zones 1 and 2, respectively based on Hughes et al. (2011). The model included a transition zone between Zone 1 and Zone 2 to increase the shear stress along the levee without creating a discontinuity in the modeling. Within the transition zone, the shear stress varies linearly

according to the x -coordinate at each integration point. Hughes et al. (2011) estimated Zone 2 to begin at 7.1 m down the levee from the crest, and the transition zone was incorporated into the model between 6 and 7.5 m down levee.

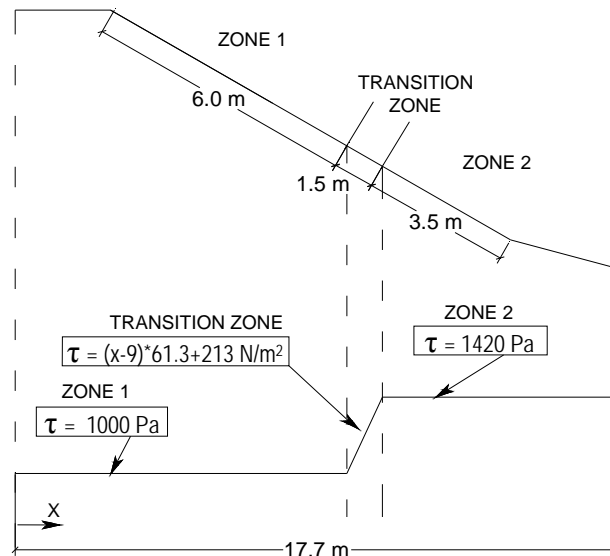


Figure 6.15. Shear Stress Profiles on Levee

Since Abaqus does not allow the user to define loads that vary with position and time in the *GUI*, the wave loading profile was defined manually through a subroutine. Abaqus can execute subroutines written in the FORTRAN programming language to manually define parameters such as loads. Specifically, a UTRACLOAD subroutine was written to create a user defined load case. As an example, Figure 6.16 presents the UTRACLOAD subroutine for a net applied shear stress of 1,000 Pa in Zone 1 and 1,420 Pa in Zone 2.

```

1 c  WAVELOAD Subroutine
2  Subroutine UTRACLOAD(ALPHA,T_USER,KSTEP,KINC,TIME,NOEL,NPT,
3  * COORDS,DIRCOS, JLTP,SNAME)
4
5  Include 'ABA_PARAM.INC'
6
7  Dimension T_USER(3), TIME(2), COORDS(3), DIRCOS(3,3)
8  Character*80 SNAME
9
10 T_USER(1)=1
11 T_USER(2)=0
12 T_USER(3)=0
13
14 IF (Coords(1)<28.63) THEN
15   ALPHA=20.9
16
17 ELSE IF (Coords(1)<33.318) THEN
18   ALPHA=((Coords(1)-28.63)*1.873+20.9)
19
20 ELSE IF (Coords(1)<67) THEN
21   ALPHA=29.68
22
23 END IF
24 RETURN
25 END

```

Note: Model units are shown.

Figure 6.16. UTRACLOAD Subroutine (Waveload.f)

Lines 2-8 of the subroutine are standard declarations required in any subroutine called by the program. These lines allow required variables and information to be passed into the program for job analysis. Beginning with line 10, user code was written to describe an example loading profile. Lines 10-12 initialize a beginning direction vector for the applied shear stress. After the initial direction, the shear stress is applied using a “*follower*” option so the direction corresponds to each element face. An *IF ELSE* logic statement was used to describe the wave loading profile. The code requires the program to identify the position of each node along the levee to determine the magnitude of force to apply. For example, lines 24-25 require all nodes with *x-coordinates* that are less than 28.63 (model units) be assigned a shear stress of 20.9 (model units). As shown in lines 17-18, if the *x-coordinate* falls between 28.63 and 33.318, the stress applied is ramped linearly from 20.9 to 29.68 according to nodal position; therefore, the load applied to a node with an *x-coordinate* of 30 is 23.47 (in model units). Every node where the subroutine *Waveload.f* is called falls into one of the regions, which allows the correct load function to be defined. The goal of this approach is to be able to specify how the wave load changes with magnitude along *x-direction* of the levee using the loading functions.

6.3.7 SLEMM-RL-RA External Python Job Submittal Program

To analyze the levee model, multiple loading cases and anchoring patterns were considered. An Abaqus input file for each case was created. To expedite the process of submitting each input file to Abaqus, a computer programming language (Python) was used to write an external program named *Job Submittal Program (JSP)* that would submit each Abaqus job from the Linux command prompt. A flowchart describing the *JSP* is shown in Figure 6.17 and program code is presented in Figures 6.18 and 6.19.

The *JSP* begins by creating a directory for each input file which will be used as a place to save Abaqus output files related to each appropriate input file. Next, the program loops through the input directories and submits the Abaqus input file located in each directory. To determine if the job has been completed, the program polls each input directory for a *.lck* file which Abaqus returns until the job is completed. If a *.lck* file is detected, the program pauses for 10 seconds and polls the file again until the job completes. Once the jobs are complete, the program calls the results search programs described in the following section.

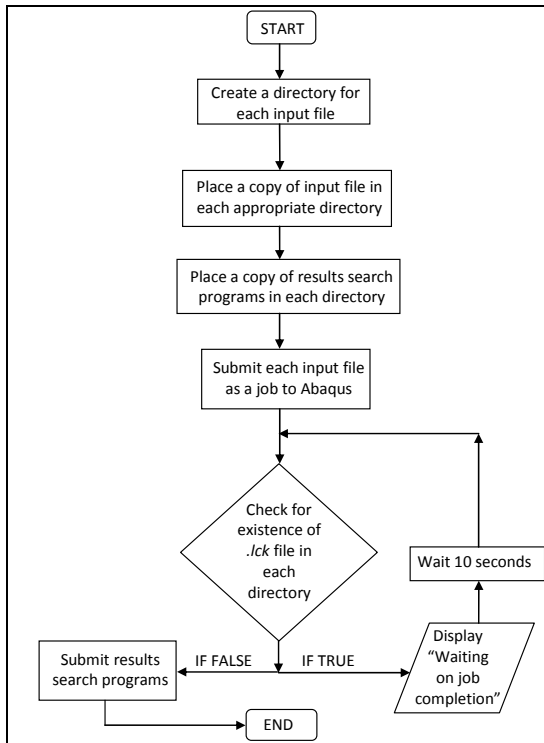


Figure 6.17. Job Submittal Program (JSP) Flowchart

```

1 #!/usr/bin/env python
2 ##!/usr/local/bin/python
3 """
4 setup.py
5 execute using:
6 python setup.py
7 http://docs.python.org/modindex.html
8 """
9
10 import os
11 import platform
12 import shutil
13 import string
14 import subprocess
15 import time
16
17 # creates variables for path to list input files
18 leveePath = "/home/ach217/Levee/"
19 inputPath = "/home/ach217/Levee/InputFiles"
20 nameList = os.listdir(inputPath)
21
22 # creates logfile to write to
23 logfile = open('./setup.log','w')
24
25 rootList = []
26 suffix = ".inp"
27
28 logfile.write(platform.system()+'\n')
29
30 for fname in nameList:
31

```

Figure 6.18. JSP Code Lines 1 to 31 of 91

```

32 # changes to lowercase version of input filename
33 fnameRoot = fname.lower()[::-len(suffix)]
34
35 # creates a list of needed directories to create from input files
36 rootList.append(fnameRoot)
37
38 # writes a list of input files to the logfile created
39 logfile.write('\nInputfiles\n')
40
41 for fname in nameList:
42     logfile.write(fname+'\n')
43
44 # create a directory for each input file
45 logfile.write('\nDirectories\n')
46 for fname in rootList:
47     logfile.write('./'+fname+'\n')
48
49 # check existence of directories
50 if os.access('./'+fname,os.F_OK) != True:
51     print 'creating: ./'+fname
52     os.mkdir('./'+fname)
53
54 # copy each input file to its appropriate directory
55 logfile.write('\nLinks\n')
56 for fname in nameList:
57     source = inputPath + '/' + fname
58     link_name = './'+fname.lower()[::-len(suffix)] + '/' + fname.lower()
59     logfile.write(link_name+'\n')
60     if os.access(link_name,os.F_OK) == False:
61         os.link(source,link_name)
62
63 # Copy fortran files for Dload Subroutine
64 for each in rootList:
65     shutil.copy2('/home/ach217/Levee/waveload.f',leveePath + each)
66
67 # create a copy of the reactions program in each directory to be able
68 # to run on the .odb file that abaqus creates in the same directory
69 for each in rootList:
70     shutil.copy2('/home/ach217/Levee/Latest_Reactions1.py',leveePath + each)
71     shutil.copy2('/home/ach217/Levee/Search_Shear_Mises.py',leveePath + each)
72
73 # changes to the directory of the appropriate input file
74 # and submits the abaqus job for each input file
75 for each in rootList:
76     os.chdir(leveePath + each)
77     os.system('abaqus analysis job='+each+' input='+ each + '.inp' 'user=waveload.f')
78
79 for each in rootList:
80     os.chdir(leveePath + each)
81     while os.access(each + '.lck',os.F_OK) == True:
82         print 'Waiting on job completion...'
83         time.sleep(10)
84     os.system('abaqus python Latest_Reactions1.py')
85
86 for each in rootList:
87     os.chdir(leveePath + each)
88     while os.access(each + '.lck',os.F_OK) == True:
89         print 'Waiting on job completion...'
90         time.sleep(10)
91     os.system('abaqus python Search_Shear_Mises.py')

```

Figure 6.19. JSP Code Lines 32 to 91 of 91

6.3.8 SLEMM-RL-RA External Python Results Search Programs

Results search programs were written that would automatically search Abaqus output results for reaction forces and shear stresses. The search programs were named *Output Reactions Search (ORS)* and *Output Shear Stress Search (OSSS)*, respectively. A flowchart describing the *ORS* and *OSSS* are presented in Figure 6.20. The *ORS* and *OSSS* programs increased modeling time efficiency since the modeler was not required to submit each job or sort through results manually. Program codes for *ORS* and *OSSS* are presented in Figures 6.21 through 6.25.

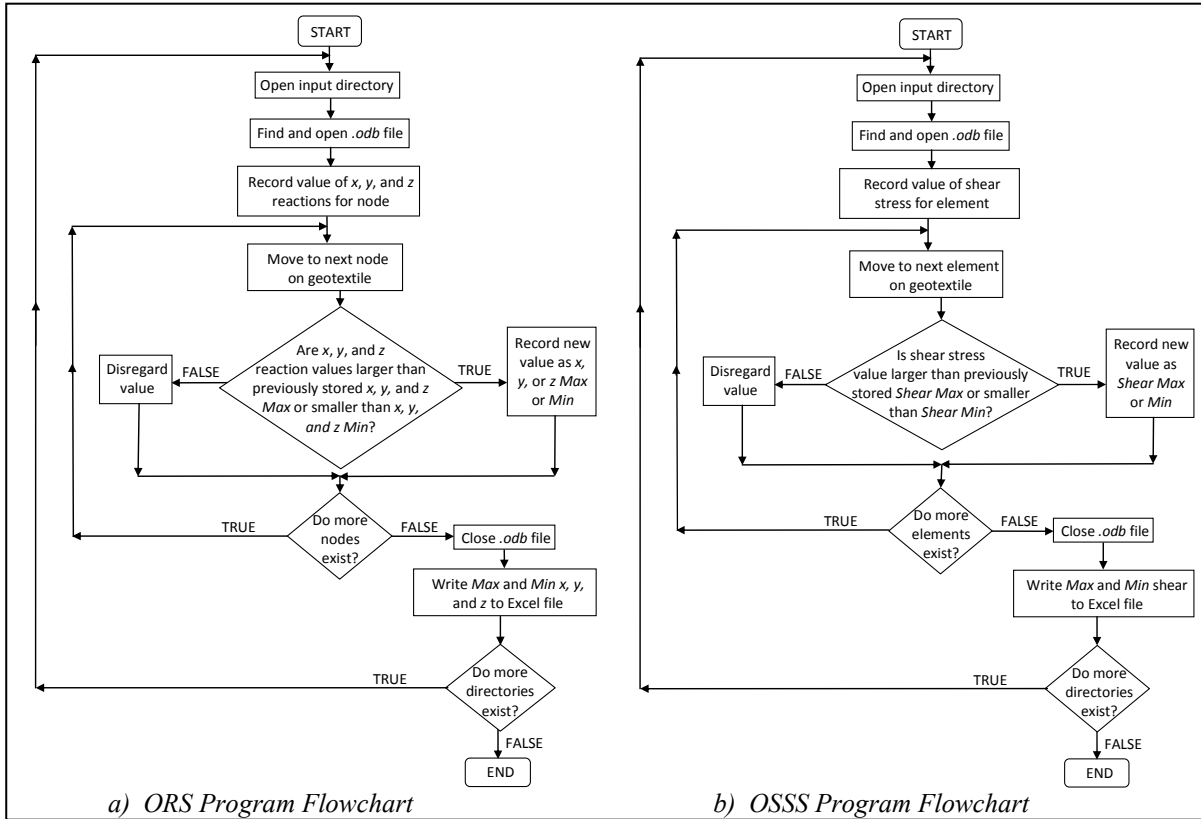


Figure 6.20. Flowcharts of Output Search Programs

The results search programs were written to automatically search the output data and record the maximum (*Max*) and minimum (*Min*) reaction forces (*RF*) and shear stresses (τ) in the *x*, *y*, and *z*-directions on the geotextile. Both search programs begin by locating and opening the *.odb* output file created by Abaqus within the input directories. The *ORS* program loops over all nodes on the geotextile. The values for the minimum and maximum reaction forces in all directions are originally set to equal 1×10^{100} and 0, respectively. As the program loops over all nodes, the *RF* in each direction is compared to the current maximum and minimum *RF* in the respective direction to determine if the value should replace the current minimum or maximum values. Once the program has looped over all nodes on the geotextile, the *.odb* file is closed and the values recorded for reaction forces in each direction and nodal locations are written to an Excel file for further use. The *OSSS* program operates in the same manner as the *ORS* program, with the exception that it loops over the elements located on the geotextile and records the integration point and element location of maximum

and minimum in-plane Von Mises Shear Stress values. Both programs loops through all input directories to provide output results for each job submitted.

```

1  """
2  odbExample.py
3  execute using:
4  abaqus python scriptname.py
5  Script to open an output database and read information. References:
6  Abaqus Scripting User's Manual
7  9.3.1 Model data
8  9.5.6 Reading field output data
9  Abaqus Scripting Reference Manual
10 31.11 JobData object
11 31.19 OdbMeshNode object
12 """
13
14 # from abaqus import *
15 import odbAccess
16 import sys
17 import csv
18 import os
19
20 inputPath = "/home/ach217/Levee/InputFiles"
21 nameList = os.listdir(inputPath)
22 leveePath = "/home/ach217/Levee/"
23 rootList = []
24 suffix = ".inp"
25
26 for fname in nameList:
27     fnameRoot = fname.lower()[::-len(suffix)]
28     rootList.append(fnameRoot)
29
30 for each in rootList:
31     # name of odbfile
32     odbName = leveePath + each + '/' + each + '.odb'
33     odb = odbAccess.openOdb(odbName)
34
35     # open logfile
36     logfile = open('./' + each + 'shear.log','w')
37
38     # loop over steps ASM
39     logfile.write('Load steps available = '+str(odb.steps))
40
41     # access the nodes from desired part
42     nodes = odb.rootAssembly.instances['GEOTEXTILE'].nodes
43
44     # note that 0 refers to the first step, -1 refers to the last step
45     # take the last frame (increment) of the last step
46     for stepName in odb.steps.keys():
47
48         step = odb.steps[stepName]
49
50         logfile.write('\n')
51         logfile.write("\n*****")
52         logfile.write("\nCurrent Step = " + stepName)
53         logfile.write("\n*****")
54         logfile.write("\nFrames in Current Step = " + str(len(step.frames)))
55         print 'processing step: ', stepName
56
57         shear=0
58         shear_node = 0
59         shearMin=1e100
60         shearMax=0
61         inodemin = 0
62         inodemax = 0
63         inode = 0
64         elementMin=0
65         pointMin=0
66         elementMax=0
67         pointMax=0
68         elementAverage=0
69         elementTotal=0

```

Figure 6.21. OSSS Program Code Lines 1 to 69 of 113

```

70
71     for frameNum in range(1,len(step.frames)):
72         logfile.write('\n\nFrame = ' + str(frameNum))
73
74         frame=step.frames[frameNum]
75         shear_stress=frame.fieldOutputs['S']
76         fieldValues=shear_stress.values
77
78     # loop over all nodes
79     for v in fieldValues:
80         shear = v.mises
81
82     # check for extreme values
83     if v.mises < shearMin:
84         shearMin = v.mises
85         elementMin = v.elementLabel
86         pointMin = v.integrationPoint
87
88     # elementAverage=
89     if v.mises > shearMax:
90         shearMax = v.mises
91         elementMax = v.elementLabel
92         pointMax = v.integrationPoint
93
94     logfile.write('\n\n')
95     logfile.write('\n shearMin %f ' % (shearMin))
96     logfile.write('\n element %f ' % (elementMin))
97     logfile.write('\n integration pt %f' % (pointMin))
98     logfile.write('\n shearMax %f ' % (shearMax))
99     logfile.write('\n element %f ' % (elementMax))
100    logfile.write('\n integration pt %f' % (pointMax))
101
102    # write to excel compatible csv file
103    spamWriter = csv.writer(open('shear' + each + '.csv','wb'), delimiter=',', quotechar='|', quoting=csv.QUOTE_MINIMAL)
104    spamWriter.writerow(['odbName      ': ' + odbName])
105    spamWriter.writerow(['job name      ': ' + odb.jobData.name])
106    spamWriter.writerow(['creation time: ' + odb.jobData.creationTime])
107    spamWriter.writerow(['\n','Stress (psf)', 'Element', 'Integration Pt'])
108    spamWriter.writerow(['Min. Shear Stress',shearMin, elementMin, pointMin])
109    spamWriter.writerow(['Max Shear Stress', shearMax, elementMax, pointMax])
110
111    print 'Shear Stress Search Completed'
112
113    odb.close()

```

Figure 6.22. OSSS Program Code Lines 69 to 113 of 113

```

1    """
2    odbExample.py
3    execute using:
4    abaqus python scriptname.py
5    Script to open an output database and read information. References:
6    Abaqus Scripting User's Manual
7    9.3.1 Model data
8    9.5.6 Reading field output data
9    Abaqus Scripting Reference Manual
10   31.11 JobData object
11   31.19 OdbMeshNode object
12   """
13
14   # from abaqus import *
15   import odbAccess
16   import sys
17   import csv
18   import os
19
20   inputPath = "/home/ach217/Levee/InputFiles"
21   nameList = os.listdir(inputPath)
22   leveePath = "/home/ach217/Levee/"
23   rootList = []
24   suffix = ".inp"

```

Figure 6.23. ORS Program Code Lines 1 to 24 of 143

```

25
26 for fname in nameList:
27     fnameRoot = fname.lower()[:-len(suffix)]
28     rootList.append(fnameRoot)
29
30 for each in rootList:
31     ##name of odbfile
32     odbName = leveePath + each + '/' + each + '.odb'
33     odb = odbAccess.openOdb(odbName)
34
35     # open logfile
36     logfile = open('./' + each + 'reactions.log', 'w')
37
38     # loop over steps ASM
39     logfile.write('Load steps available = ' + str(odb.steps))
40
41     # access the nodes from desired part
42     nodes = odb.rootAssembly.instances['GEOTEXTILE'].nodes
43
44     # note that 0 refers to the first step, -1 refers to the last step
45     # take the last frame (increment) of the last step
46     for stepName in odb.steps.keys():
47
48         step = odb.steps[stepName]
49
50         logfile.write('\n')
51         logfile.write('\n*****')
52         logfile.write('\nCurrent Step = ' + stepName)
53         logfile.write('\n*****')
54         logfile.write('\nFrames in Current Step = ' + str(len(step.frames)))
55         print 'processing step: ', stepName
56
57         rxMax = 0
58         ryMax = 0
59         rzMax = 0
60         rxMin = 1e100
61         ryMin = 1e100
62         rzMin = 1e100
63         inodexmin = 0
64         inodeymin = 0
65         inodezmin = 0
66         inodexmax = 0
67         inodeymax = 0
68         inodezmax = 0
69
70         for frameNum in range(1, len(step.frames)):
71             logfile.write('\n\nFrame = ' + str(frameNum))
72             frame = step.frames[frameNum]
73             reactions = frame.fieldOutputs['RF']
74             fieldValues = reactions.values
75
76             # zero the total reaction forces
77             rxt = 0.0
78             ryt = 0.0
79             rzt = 0.0
80
81             # loop over all nodes
82             for v in fieldValues:
83
84                 # calculate the nodal reaction force magnitude
85                 rmag = v.data[0] + v.data[1] + v.data[2]
86                 rmag = rmag * rmag
87

```

Figure 6.24. ORS Program Code Lines 25 to 87 of 143

```

88 # consider nodes with non-zero reaction forces
89     if rmag > 0.1:
90
91 # sum reaction forces
92     rxt = rxt + v.data[0]
93     ryt = ryt + v.data[1]
94     rzt = rzt + v.data[2]
95
96 # current node number
97     inode = v.nodeLabel
98
99 # check for extreme values
100    if v.data[0] < rxMin :
101        rxMin = v.data[0]
102        inodexmin = inode
103    if v.data[1] < ryMin :
104        ryMin = v.data[1]
105        inodexmin = inode
106    if v.data[2] < rzMin :
107        rzMin = v.data[2]
108        inodezmin = inode
109    if v.data[0] > rxMax :
110        rxMax = v.data[0]
111        inodexmax = inode
112    if v.data[1] > ryMax :
113        ryMax = v.data[1]
114        inodeymax = inode
115    if v.data[2] > rzMax :
116        rzMax = v.data[2]
117        inodezmax = inode
118
119 # write results to log file
120    logfile.write('\n\n')
121    logfile.write('\n rxMin %8d ' % (rxMin))
122    logfile.write('\n rxMax %8d ' % (rxMax))
123    logfile.write('\n ryMin %8d ' % (ryMin))
124    logfile.write('\n ryMax %8d ' % (ryMax))
125    logfile.write('\n rzMin %8d ' % (rzMin))
126    logfile.write('\n rzMax %8d ' % (rzMax))
127
128 # write to excel compatible csv file
129    spamWriter = csv.writer(open('reactions' + each + '.csv','wb'), delimiter=',', quotechar='|', quoting=csv.QUOTE_MINIMAL)
130    spamWriter.writerow(['odbName      ': ' + odbName])
131    spamWriter.writerow(['job name      ': ' + odb.jobData.name])
132    spamWriter.writerow(['creation time: ' + odb.jobData.creationTime])
133    spamWriter.writerow(['\n','Value','Node Location',])
134    spamWriter.writerow(['rxMin',rxMin,inodexmin])
135    spamWriter.writerow(['ryMin',ryMin,inodeymin])
136    spamWriter.writerow(['rzMin',rzMin,inodezmin])
137    spamWriter.writerow(['rxMax',rxMax,inodexmax])
138    spamWriter.writerow(['ryMax',ryMax,inodeymax])
139    spamWriter.writerow(['rzMax',rzMax,inodezmax])
140
141    print 'Reactions Search Complete'
142
143    odb.close()

```

Figure 6.25. ORS Program Code Lines 88 to 143 of 143

6.4 Model Type 3 – SLEMM-RL-FA

A third model type was created to simulate the flexible anchors that attached the geotextile to the levee. Model type 3 was similar to type 2 with exception of the anchors. To better represent anchor pullout resistance, the boundary conditions at the anchor nodes were changed from fixed (Model Types 1 and 2) to basic connector elements (CONN3D2 elements). The connector elements were assigned a non linear force displacement behavior with a 220 kg failure limit at 1.5 cm of deflection to describe the anchor flexibility based on physical anchor testing (see Figure 4.17b for the load deflection curve used). Loads and contact interactions remained the same as in Model Type 2 for this analysis.

A mesh convergence study was performed for Model Type 3 using shear stresses of 1000 Pa in Zone 1 to 1,420 Pa in Zone 2, gravity, and uniform pressure of 0.3 m of water over the geotextile. Figure 6.26 provides convergence results in terms of average Von Mises stress of the bottom 90% of data ($\tau_{avg,90\%}$). Von Mises stress values ($\tau_{max,90\%}$) excluding the top 10% of values to account for stress peaks at anchors were compared to the number of elements to determine an acceptable number of elements to be 1,056 (approximately 9 elements/m²). Considering computation time, establishing a search area, and viewing results, further mesh refinement produced a change in stress in the flexible anchor model which is not a first order effect of the modeling problem. Variability present during *RDAS* field placement such as soil strength, moisture content, and compaction density could present larger changes in expected results than the accuracy change provided by doubling the number of elements used in modeling. The same number of elements were used for models 2 and 3.

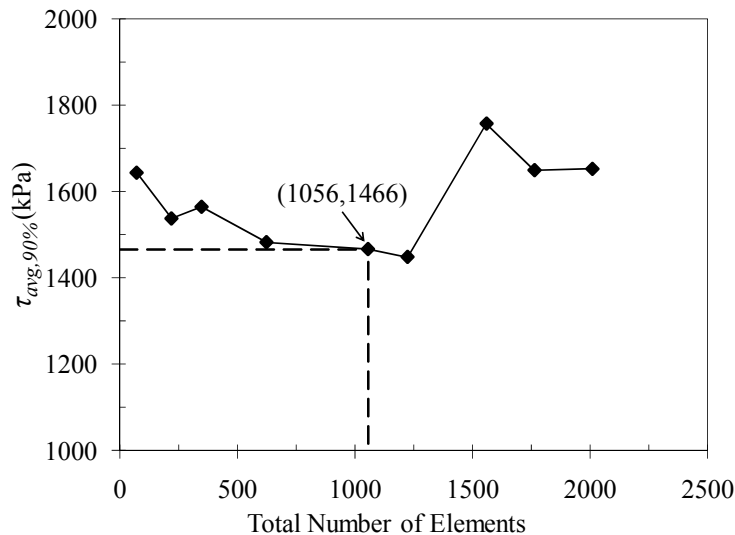


Figure 6.26. Model Type 3 Mesh Convergence

It is noted that the same trend of compressive and tensile stresses were present as were shown in Figures 6.11 to 6.12 of the rigid model. These results show the need for a more complicated model to sufficiently model the geotextile. To avoid the significant computational effort associated with explicitly modeling thin shell buckling, an enhanced membrane model is needed. In this model, the effects of the buckling instability are captured by an asymmetric tension-compression response in which tensile stresses are developed as linear functions of applied strain while compressive strains produce no membrane stress. In

order to minimize computational instabilities associated with the asymmetric material response, a second membrane layer was introduced as discussed in Section 6.5.

6.5 Model Type 4 – DLEMM

The fourth model type attempted included introducing a dual layer geotextile model to obtain more physically meaningful results. The additional layer was modeled as a compliant isotropic, linear elastic material that provides the compressive stiffness required for simulation convergence without introducing unrealistically large compressive resistance. To evaluate dual layer model, a rectangle was used with fixed nodes on one end and concentrated loads applied at the other end in the x -direction (Figure 6.27). The Top Layer was a replicate of the geotextile layer except a Young’s Modulus of 479 kPa was assigned. Corresponding nodes on each layer were tied so the layers rest on top of each other. Verification results for this model type are presented in the following results section.

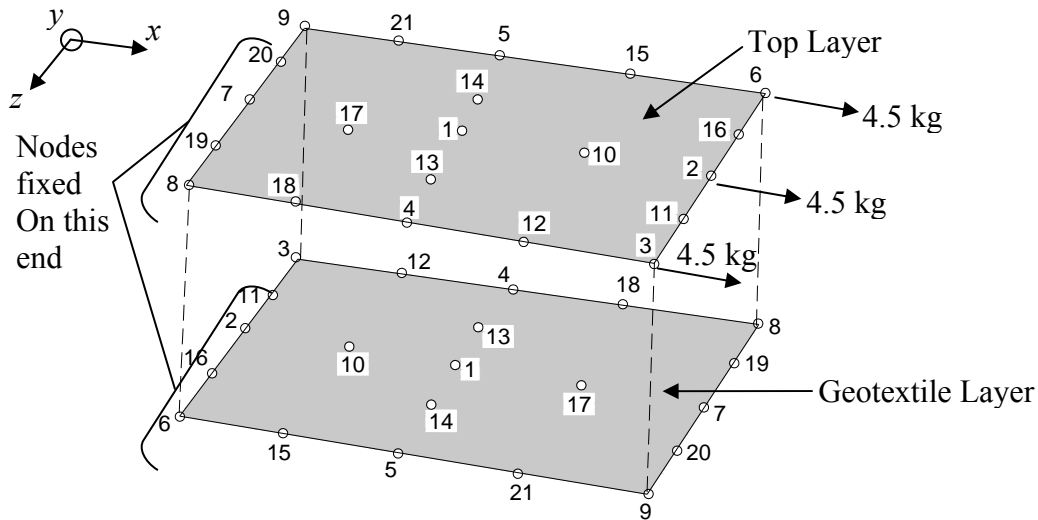


Figure 6.27. Model Evaluation Rectangle for Dual Layer Geotextile Model

6.6 Modeling Results

The *SLEMM-FL-RA* 3D levee model resulted in solution difficulties which were contributed to the contact between the geotextile and the large levee mass. The contact between the stiffened soil block, levee, and geotextile was modeled by a surface to surface contact with f of 0.4. The analysis was completed only after adjusting the general solution settings. The step time increment was changed to 1×10^{-20} and a half step residual of 1×10^{20} to be able to complete the analysis. This resulted in a pillowing effect in the geotextile when completely unloaded, which could imply the contact between the bodies could be a source of error in the results. Analysis results with these solution settings were not counted as viable because unreasonable values were required to allow the job to run. When using a reasonable half step residual of 10, the model would not complete the analysis.

Abaqus contact algorithms were originally created for large object interactions (e.g. car collisions). A reaction force is assigned to nodes on a contacting body to prevent the bodies from passing through one other. The contact compensation forces applied to nodes

from the contact algorithm could be erroneous for a lightweight membrane contacting a large levee soil mass since it was originally meant for large bodies.

Six simulations were performed using the *SLEMM-RL-RA* and *SLEMM-RL-FA*. Simulations performed included 3 geotextile types: GT-1, GT-2, and GT-3 (Table 2.1) which have machine direction tension strength at ultimate strain of 38.5, 70, and 200 kN/m, respectively. Two boundary conditions were used in the simulations: fixed anchors and flexible anchors based on experimental results presented in Chapter 4, The loading condition applied was a shear stress beginning at 1,000 Pa at the top portion of the levee face (Zone 1) and ramped linearly over a 1.5 m transition zone to 1,420 Pa the bottom portion of the levee face (Zone 2). For details of the load ramping and Zones refer to Chapter 6.3.6.

Geotextile stress and anchor reactions are presented in Table 6.1. Geotextile stresses include the maximum Von Mises stress in the entire geotextile ($\tau_{\max,all}$), the average Von Mises stress of the bottom 90% of data ($\tau_{\text{avg},90\%}$) (top 10% removed to capture field values away from anchor locations), the maximum Von Mises stress in the bottom 90% of data ($\tau_{\max,90\%}$), and the maximum *x-direction* reaction force at any anchor (RF_{\max}).

Comparing flexible anchor and rigid anchor simulations show that the over constraint associated with rigid anchor assumptions adversely affects maximum stress as well as field values. On average, the rigid anchor over constraint produces maximum stress values ($\tau_{\max,all}$) approximately 8 times higher than the flexible anchors and average field stress values ($\tau_{\text{avg},90\%}$) 1.5 times higher. The field stress deviations between rigid and flexible predictions render the rigid results physically meaningless. Comparing the rigid simulations for the three geotextiles shows average field stresses vary by less than 2% difference. For flexible anchor models, the values differ by approximately 10%.

Table 6.2. Results of SLEMM

Simulation	Geotextile	$\tau_{\text{avg},90\%}$ (kPa)	$\tau_{\max,90\%}$ (kPa)	$\tau_{\max,all}$ (kPa)	RF_{\max} (kg)
<i>Rigid Anchor Simulations</i>					
R-1	GT-1	1,182	3,350	24,122	2,448
R-2	GT-2	1,198	3,391	24,375	2,484
R-3	GT-3	1,204	3,412	24,477	2,499
<i>Flexible Anchor Simulations</i>					
F-1	GT-1	789	1,697	4,775	---*
F-2	GT-2	727	1,549	2,838	---*
F-3	GT-3	710	1,519	2,501	---*

*All anchors reached the failure limit for the given simulations.

Note: Predictions of SLEMM do not appear to be physically realistic.

DLEMM verification was performed by applying concentrated loads to the tied nodes at one end (as previously shown in Figure 6.29) and recording the reaction forces at the fixed nodes (simulating anchors); results for the verification are shown in Table 6.2. The summation of reaction forces shows that the *x-direction* reaction forces are 1.66 kg higher than the applied concentrated loading to the model. A dual layer model for full slope geometry was not attempted because the membrane elements do not produce valid results using dual layers. To obtain more physically meaningful results, a new element formulation could be required that will accommodate both surface and shear loading.

Table 6.3. Reaction Forces from Dual Layer Rectangle Validation Model

Node No.	RF_{x-dir}	RF_{y-dir}	RF_{z-dir}
6	0.95	0	0.19
16	5.99	0	0.51
2	1.28	0	0.00
11	5.99	0	0.51
3	0.95	0	0.19
Total	15.16	0	0

6.7 Modeling Summary

Four model types were created to aide in the design of an *RDAS* system. Although the modeling performed is more rigorous than currently found in literature for anchored geotextile systems, it should not be used for *RDAS* design since the results are suspect. The *SLEMM-RL-FA* model successfully simulated the material models and conditions entered (a useful step for research and development), but the results indicate it did not represent the true physical nature of an *RDAS* system. The *DLEMM* model unsuccessfully attempted to improve results of the *SLEMM-RL-FA* model.

The model framework created within this research, including the 3 external Python programs, successfully increases modeling efficiency. The programs could also be applied to other modeling applications to greatly reduce the computing time and results searching time. In addition, the incorporation of flexible anchors boundary conditions, wave loading conditions, and contact interactions is a significant advancement in modeling an *RDAS* as compared to current models found in literature.

A model that could represent an *RDAS* has merit if a more physically realistic simulation approach can be developed. Incorporation of flexible anchors improved the simulation, but not enough to rely on the results for material selection and anchor spacing design for a temporary application. It is possible that a new element formulation will be needed to model the geotextile that can accommodate shear and surface loading but prevent compressive strains from producing geotextile stress.

CHAPTER 7 – CONCLUSIONS AND RECOMMENDATIONS

7.1 Summary of Research

The primary objective of this document was to develop guidance for an *RDAS* for the landward side of earthen levees. This objective was partially met. All components needed to provide the guidance were successful with exception of the finite element model, which was partially successful.

The research presented herein is part of a larger project that is broken into 4 major portions. The details and status of each portion of work are detailed in bullet form below.

- 1) Collect shear stress profiles for wave and surge overtopping. This portion of the research was completed by Hughes et al. (2011) in a separate effort.
- 2) Determine the construction feasibility of an *RDAS*. A case study was performed on the Yazoo Backwater levee protection performed by the USACE (presented in Chapter 3) to show that construction of a *RDAS* is feasible for emergency construction.
- 3) Perform anchor testing to determine load deflection behavior in soil representative of a levee face soil during overtopping. Full scale anchoring testing on three types of rod shaped anchors (0.3 and 0.6 m lengths) was performed, and detailed load deflection behavior is provided in Chapter 4.
- 4) Conduct numerical modeling of an *RDAS* system with typical levee dimensions, anchor load deflection behaviors determined from physical testing, and applied shear stresses from flume testing data performed by Hughes et al. (2011). Writing user subroutines to increase modeling efficiency and incorporate wave loading was also part of this secondary objective. The model developed during this work should not currently be used for design; rather, it provides an advancement in the research area of modeling geotextiles and levee protection. Further advancements of the current model are needed in the future to provide physically meaningful results for use in design.

Actual design S_x' and S_z' values (Figure 1.2) were not determined within this research because the Finite Element Analysis (FEA) model is not suitable for design at this point. It is the author's opinion that static equilibrium calculations taking into consideration friction resistance, anchor resistance, geotextile strength, and applied shear loading would not be able to provide a realistic estimate of design spacing and as a result they weren't performed in place of finite element simulations. The *RDAS* is a deflection driven problem with full geotextile strength only being mobilized at ultimate strain. Anchors are incorporated into the system to provide many functions including preventing geotextile creep and adding serviceability to the system.

7.2 Conclusions

The model framework developed within this research successfully increases computing efficiency, and could easily be applied to other modeling applications. The incorporation of anchor testing data, shear stress wave data, surface to surface contact interactions, and the automated modeling framework into an *RDAS* model is a significant advancement from the modeling approaches found in literature. Specific conclusions drawn from the research are presented in bulleted form below.

- All three anchor types resulted in similar load deflection behavior. Average ultimate loads ranged from 145 to 155 kg for 0.3 m anchors and 280 to 360 kg for 0.6 m anchors. Maximum loads were consistent among all anchor types.
- Maximum load achieved for 0.6 m threaded bar anchors was consistent for both loading types. 307 kg was achieved for sustained loading as compared to 279 kg for continuous loading.
- All three small rod shaped anchors types tested proved to be easy to install by hand with a sledge hammer. High soil moisture contents that could be encountered during a disaster event would make anchor installation easier.
- Anchor capacity could very likely be increased easily by installing a plate to the front of anchors to increase the bearing area of the soil.
- Taping specimens did not produce drastic changes in load or deflection of the anchors. Taping proved beneficial to protect strain gauges during testing of the threaded bar anchors.
- Sustained load anchor testing showed anchors would not be expected to withstand maximum load for any long period of time without pulling out of the soil. An expected time could not be determined from the amount of testing performed.
- The USACE case study of the Yazoo Backwater Levee protection validated the feasibility of constructing an *RDAS* quickly and with minimal equipment.
- Flexible anchor simulations were preferred over rigid anchors as they more accurately modeled the physical behavior.
- Flexible anchors relieved geotextile stresses as expected, but the magnitude of results was governed by the peak stresses at the boundary conditions.
- A single-layer elastic membrane model (*SLEMM*) was created that incorporated levee and geotextile contact interactions, flexible anchors, and wave loading. The *SLEMM* appears to perform the finite element formulations correctly, but does not appear to be adequate to provide physically meaningful results even though it is a more complicated approach than typical.
- A double layer elastic membrane model (*DLEMM*) was attempted to provide compressive stiffness required for simulation convergence without introducing unrealistically large compressive resistance. The *DLEMM* model did not improve model quality.
- The current FEA model needs improvements before being used for design of an *RDAS*.

7.3 Recommendations

Research performed for this document validated a *RDAS* to have merit for emergency applications for levee protection, although further research is needed to be able to use a *RDAS* in the field. Recommendations for needed improvements are provided in bullet list below.

- Overall, it is recommended to give an *RDAS* serious consideration for temporary protection of select levee sections. Improvements are needed, but results to date are promising.
- It is recommended to use Briaud et al. (2008) to determine where to deploy an *RDAS*. For example, an erosion rate category I high erodibility soil would be deemed a critical area of a levee system where *RDAS* deployment could be useful.
- The modified Vitton et al. (1998) connection cup suggested by the author to connect anchors to the geotextile during placement should be machined and tested to verify its applicability to the system.
- Full scale testing of the *RDAS* system is needed to determine the interactions and behaviors of the anchors, geotextile strength mobilization, frictional resistance, and wave conditions.
- Further modeling is required for the current model to be able to provide design guidance. A new element formulation could be required to accommodate shear and surface loading to further develop the model for use in design.

CHAPTER 8 - REFERENCES

Abaqus, (2009). *Abaqus Version 6.9 PDF Documentation*.

ArmorMax[®] (2010a). *Installation Guidelines for ArmorMax[®] Anchored Reinforced Vegetation System*. Geosynthetics Limited, United Kingdom. http://www.geosyn.co.uk/brochures/installation_specification/armormaxinstallationguidelines.pdf. Accessed: June 15, 2010.

ArmorMax[®] (2010b). *Case Studies: Penn and DeCamp Street Levees – Jefferson Parish, South Louisiana Levee Armoring*. <http://armormax.geotextile.com/case-studies.aspx>. Accessed: June 15, 2010.

Austin, D. N., and Theisen, M. S. (1996). "Three-Dimensional Woven Geotextiles for Containment Dike Construction." *Geotextiles and Geomembranes*, 14, 265-275.

Bilberry, A.C., (2012). "Rapidly Deployable Armoring System for Temporary Protection of Earthen Levees During Overtopping." Master's Thesis. Mississippi State University.

Brandon, T.L., Wright, S.G., and Duncan, J.M. (2008). "Analysis of the Stability of I-Walls with Gaps between the I-Wall and the Levee Fill." *Journal of Geotechnical and Geoenvironmental Engineering*, 134 (5), 692-700.

Briaud, J.-L., Chen, H.-C., Govindasamy, A. V., and Storesund, R. (2008). "Levee Erosion by Overtopping in New Orleans During the Katrina Hurricane." *Journal of Geotechnical and Geoenvironmental Engineering*, 134 (5), 618-632.

Broms, B.B. (1964a). "Lateral Resistance of Piles in Cohesive Soils." *Journal of Soil Mechanics and Foundations Division*, 90 (2), 27-63.

Broms, B.B. (1964b). "Lateral Resistance of Piles in Cohesive Soils." *Journal of Soil Mechanics and Foundations Division*, 90 (3), 123-156.

Broms, B.B. (1965). "Design of Laterally Loaded Piles." *Journal of Soil Mechanics and Foundations Division*, 90 (2), 27-63.

Bygness, R. (2008). "Geosynthetic-Reinforced Levees Performed Well." *Geosynthetics*, 26 (3), 56.

California Stormwater BMP Handbook (2003). *Geotextiles and Mats*. California Stormwater Quality Association[®]: Menlo Park, California. www.cabmphandbooks.com/Documents/Construction?EC-7.pdf. Accessed: June 14, 2010.

Carter N. (2005). *New Orleans Levees and Flood Walls: Hurricane Damage Protection*. CRS Report for Congress, <http://www.fas.org/sgp/crs/misc/RS22238.pdf>. Accessed: July 14, 2010.

Chen, S. C., Chang, K. T., Wang, S. H., and Lin, J. Y. (2010). "The Efficiency of Artificial Materials Used for Erosion Control on Steep Slopes." *Environmental Earth Sciences*, 62 (1), 197-206.

Cheung, Y.K., and Lee, P.K. (1991). "Elastoplastic Analysis of Soil-Pile Interaction." *Computers and Geotechnics*, 12 (2), 115-132.

Das, M. B., and Puri, V.K. (1989). "Holding Capacity of Inclined Square Plate Anchors in Clay." *Soils and Foundations Japanese Society of Soil Mechanics and Foundation Engineering*, 29 (3), 138-144.

Duncan, M.J., Brandon, T.L., Wright, S.G., and Vroman, N. (2008). "Stability of I-Walls in New Orleans During Hurricane Katrina." *Journal of Geotechnical and Geoenvironmental Engineering*, 134 (5), 681-691.

El Sawwaf, M. and Nazir, A. (2006). "The Effect of Soil Reinforcement on Pullout Resistance of an Existing Vertical Anchor Plate in Sand." *Computers and Geotechnics*, 33, 167-176.

FEMA (2009). *Protecting Manufactured Homes from Floods and Other Hazards: A Multi-Hazard Foundation and Installation Guide*. Report FEMA P-85, Second Edition, pp. 266.

Foresight[®] Products (2001a). *An Introduction to Manta Ray and Stingray Earth Anchors*. Foresight[®] Products, LLC, Commerce City, Colorado. http://foresightproducts.com/pdfs/intro_mr_sr.pdf. Accessed: June 10, 2010.

Foresight[®] Products (2001b). *Multipurpose Specifications*. Foresight[®] Products, LLC, Commerce City, Colorado. <http://foresightproducts.com/duckspec.html>. Accessed: June 10, 2010.

Fritz, H.M., Blount, C., Sokoloski, R., Singleton, J., Fuggle, A., McAdoo, B.G., Moore, A., Grass, C., and Tate, B. (2008). "Hurricane Katrina Storm Surge Reconnaissance." *Journal of Geotechnical and Geoenvironmental Engineering*, 134 (5), 644-656.

Ghiassian, H. (1995). *Stabilization of Sandy Slopes with Anchored Geosynthetic Systems*. Doctoral Dissertation, The University of Michigan.

Ghiassian, H., Gray, D., and Hryciw, R. (1997). "Stabilization of Coastal Slopes by Anchored Geosynthetic Systems." *Journal of Geotechnical and Geoenvironmental Engineering*, 123 (8), 736-743.

Gray, D. H., Hryciw, R. D., and Ghiassian, H. (1996). "Protection of Coastal Sand Dunes with Anchored Geonets." *Proceedings of the Conference on Florida Beach Protection*, St. Petersburg, FL, 255-270.

Hartl, H., and Pernthaner, M. (2002). "Soil Anchors Modeled by an Embedded Formulation Allowing Slip." *Proceedings of 2nd International Conference on Soil Structure Interaction in Urban Civil Engineering*. March 7-8, Zurich.

Hayes, A. (2010). "Synthetic Turf System Stops Erosion...for Starters: Quest for Erosion Control Delivers Additional Benefits." *Geosynthetics*, 28 (10), 21-30.

Heerden, V. (2007). "The Failure of the New Orleans Levee System Following Hurricane Katrina and the Pathway Forward." *Public Administration Review*, 67 (1), 24-35.

Hill, D. M. (1997). "Alternative Materials for Overtopping Protection." *Proceedings of the International Conference on Hydropower*, August 5-8, Atlanta, GA, 2215-2224.

Howard, I.L. (2011). *Guidance for Using Cementitiously Stabilized Emergency Construction Materials*. SERRI Report 70015-008, US Dept. of Homeland Security Science and Technology Directorate.

Howard, I.L., Carruth, W.D., Sullivan, W.G., Bilberry, A.C., Cost, T., Badran, W., and Jordan, B.D. (2012). *Development of an Emergency Construction Material for Disaster Recovery*. SERRI Report 70015-006, US Dept. of Homeland Security Science and Technology Directorate.

Hryciw, R. D. (1991). "Anchor Design for Slope Stabilization by Surface Loading." *Journal of Geotechnical Engineering*, 117 (8), 1260-1274.

Hryciw, R. D., and Haji-Ahmad, K. (1992). "Design of Anchored Geosynthetic Systems for Slope Stabilization." *Proceedings of the Specialty Conference Stability and Performance of Slopes and Embankments II*, New York, N.Y., 1464-1480.

Hsiung, Y. (2003). "Theoretical Elastic-Plastic Solution for Laterally Loaded Piles." *Journal of Geotechnical and Geoenvironmental Engineering*, 129 (6), 475-480.

Huang, Y., Sawada, K., Moriguchi, S., Yashima, A., and Zhang, F. (2006). "Numerical Assessment of the Effect of Reinforcement on the Performance of Reinforced Soil Dikes." *Geotextiles and Geomembranes*, 24 (3), 169-174.

Hughes, S.A., Ward, D.L., Wibowo, J.L., and Lee, L.T. (2006). *Protection Alternatives for levees and Floodwalls in Southeast Louisiana: Phase One Evaluation*. Unpublished final draft technical report for New Orleans District, Corps of Engineers. 228p.

Hughes, S.A., Sharp, J.A., Shaw, J.M., Howard, I.L., and McAnally, W.H. (2011). *Physical Testing and Hydraulic Simulation of Wave Overtopping of Earthen Levees*. SERRI Report 70015-009, US Dept. of Homeland Security Science and Technology Directorate, pp. 144.

Kilgore, R.T, and Cotton, G.K. (2005). "Design of Roadside Channels with Flexible Linings." *Hydraulic Engineering Circular*, 15 (3). <http://www.fhwa.dot.gov/engineering/Hydraulics/pubs/05114/05114.pdf>. Accessed: June 23, 2010.

Kim, M., Freeman, M., FitzPatrick, B.T., Nevius, D.B., Plaut, R.H., and Filz, G.M. (2004). "Use of an Apron to Stabilize Geomembrane Tubes for Fighting Floods." *Geotextiles and Goemembranes*, 22, 239-254.

Kim, M., Moler, M., Freeman, M., Filz, G.M., and Plaut, R.H. (2005). Stacked Geomembrane Tubes for Flood Control: Experiments and Analysis. *Geosynthetics International*, 12 (5), 253-259.

Kim, N.K., Park, J.S., and Kim, S.K. (2007). "Numerical Simulation of Ground Anchors." *Computers and Geotechnics*, 34 (6), 498-507.

Klar, A., and Frydman, S. (2002). "Three-Dimensional Analysis of Lateral Pile Response Using Two-Dimensional Explicit Numerical Scheme." *Journal of Geotechnical and Geoenvironmental Engineering*, 128 (9), 775-784.

Koerner, R. M. (2005). *Designing with Geosynthetics*. Prentice-Hall, Inc., 5th Edition. Upper Saddle River, New Jersey.

Koerner, R. M., and Robbins, J. C. (1986). "In-situ Stabilization of Slopes Using Nailed Geosynthetics." *Proceedings of the 3rd International Conference on Geotextiles*, days April Vienna, Austria, 395-400.

Liang, R.Y., and Feng, Y. (2002). "Development and Application of Anchor-Soil Interface Models." *Soils and Foundations*, 42 (2), 59-70.

Matlock, H., and Reese, L.C. (1960). "Generalized Solutions for Laterally Loaded Piles." *Journal of Soil Mechanics Foundation Division*, 86 (5), 63-91.

Manous, J., Basham, D., Brumund, W.F., Dalton, M., Galloway, G.E., Gilbert, R.B., Hatch, S., Herrmann, A.W., Izzo, D., Link, L.E., Moran, K., Roth, L.H., and Smith, R.E. (2009). "Guiding Principles for Critical Infrastructure." *Civil Engineering*, 79 (2), 56-61.

Merifield, R.S., Sloan, S.W., and Lyamin, A.V. (2003). *The Stability of Inclined Plate Anchors in Purely Cohesive Soil*. Faculty of Engineering & Surveying Technical Reports, Report TR-2003-03, University of Southern Queensland, Australia, pp. 23.

Ng, C.W.W., and Zhang, L.M. (2001). "Three-Dimensional Analysis of Performance of Laterally Loaded Sleeved Piles in Sloping Ground." *Journal of Geotechnical and Geoenvironmental Engineering*, 127 (6), 499-509.

Nicholson, P.G. (2006). "Special Report: Observations of a Broken System: New Orleans' Levees." *Geo-Strata*, January/February, 13-17.

North American Green[®] (2004). *Erosion Control Products*. Product Literature, North American Green, Evansville, IN, www.nagreen.com.

North American Green[®] (2009a). *SC250 Turf Reinforcement Mat*. North American Green[®], Evansville, Indiana. http://www.nagreen.com/assets/specification-sheets/SC250_Spec.pdf. Accessed: July 9, 2010.

North American Green[®] (2009b). *C350 Turf Reinforcement Mat*. North American Green[®], Evansville, Indiana. http://www.nagreen.com/assets/specification-sheets/C350_Spec.pdf. Accessed: July 9, 2010.

North American Green[®] (2009c). *P550 Turf Reinforcement Mat*. North American Green[®], Evansville, Indiana. http://www.nagreen.com/assets/specification-sheets/P550_Spec.pdf. Accessed: July 9, 2010.

North American Green[®] (2009d). *P300 Turf Reinforcement Mat*. North American Green[®], Evansville, Indiana. http://www.nagreen.com/assets/specification-sheets/P300_Spec.pdf. Accessed: July 9, 2010.

NRF (2008). *National Response Framework*. US Department of Homeland Security, Washington, DC, pp. 82.

Platipus[™] Anchors (2010a). *Stealth Anchor Specifications*. Platipus Anchors, Unlimited. http://www.platipus-anchors.com/earth_anchoring_systems/stealth_earth_anchor_specifications.php. Accessed: June 16, 2010.

Platipus[™] Anchors (2010b). *The Earth Anchor*. Platipus Anchors, Unlimited. http://www.platipus-anchors.com/earth_anchoring_systems/stealth_earth_anchor_specifications.php. Accessed: June 16, 2010.

Platipus[™] Anchors (2010c). *Top Accessories*. Platipus Anchors, Unlimited. http://www.platipus-anchors.com/earth_anchoring_systems/earth_anchor_top_accessories.php. Accessed: June 16, 2010.

ProPex[®], (2010a). *Installation Guidelines for LANDLOK[®] TRMs and PYRAMAT[®] HPTRMs*. ProPex[®] Geosynthetics, Chattanooga, TN. www.geotextile.com/downloads/Propex_InstGuide_TRMS.pdf. Accessed: June 16, 2010.

ProPex[®], (2010b). *The Exceptional Choice for Sustainable Erosion Control to Replace Hard Armour*. ProPex[®] Geosynthetics, Chattanooga, TN. http://www.globalsynthetics.com.au/files/datasheet_propex_erosion.pdf. Accessed: July 12, 2010.

Reese, L.C., Cox, W.R., and Koop, R.D. (1974). "Analysis of Laterally Loaded Piles in Sand." *Proceedings of the 6th Offshore Technology Conference*, May 6-8, 1974. Houston, TX.

Sasanakul, I., Vanadit-Ellis, W., Sharp, M., Abdoun, T., Ubilla, J., Steedman, S., and Stone, K. (2008). "New Orleans Levee System Performance during Hurricane Katrina: 17th Street Canal and Orleans Canal North." *Journal of Geotechnical and Geoenvironmental Engineering*, 134 (5), 657-667.

Seay, P.A. (1998). *Finite Element Analysis of Geotextile Tubes*. Masters Thesis, Virginia Polytechnic Institute and State University.

Seed, R.B., Athanasopoulos-Zekkos, A., Cobos-Roa, D., Pestana, J.M., and Inamine, M., "U.S. Levee Flood Protection Engineering in the Wake of Hurricane Katrina." (2012). *Proceedings of GeoCongress 2012: State of the Art and Practice in Geotechnical Engineering (GSP 226)*, Mar 25-29, Oakland, CA, pp 294-334.

Seed, R.B., Bea, R.G., Abdelmalak, R.I., Athanasopoulos-Zekkos, A., Boutwell, G.P., Briaud, J.-L., Cheung, C., Cobos-Roa, D., Ehrensing, L., Govindasamy, A.V., Harder Jr., L.F., Inkabi, K.S., Nicks, J., Pestana, J.M., Porter, J., Rhee, K., Riemer, M.F., Rogers, J.D., Storesund, R., Vera-Grunauer, X., and Wartman, J. (2008). "New Orleans and Hurricane Katrina. I: Introduction, Overview, and the East Bank." *Journal of Geotechnical and Geoenvironmental Engineering*, 134 (5), 701-717.

Seed, R.B., Bea, R.G., Athanasopoulos-Zekkos, A., Boutwell, G.P., Bray, J.D., Cheung, C., Cobos-Roa, D., Ehrensing, L., Harder Jr., L.F., Pestana, J.M., Riemer, M.F., Rogers, J.D., Storesund, R., Vera-Grunauer, X., and Wartman, J. (2008). "New Orleans and Hurricane Katrina. II: The Central Region and the Lower Ninth Ward." *Journal of Geotechnical and Geoenvironmental Engineering*, 134 (5), 718-739.

Seed, R.B., Bea, R.G., Athanasopoulos-Zekkos, A., Boutwell, G.P., Bray, J.D., Cheung, C., Cobos-Roa, D., Harder Jr., L.F., Moss, R.E.S., Pestana, J.M., Riemer, M.F., Rogers, J.D., Storesund, R., Vera-Grunauer, X., and Wartman, J. (2008). "New Orleans and Hurricane Katrina. III: The 17th Street Drainage Canal." *Journal of Geotechnical and Geoenvironmental Engineering*, 134 (5), 740-761.

Seed, R.B., Bea, R.G., Athanasopoulos-Zekkos, A., Boutwell, G.P., Bray, J.D., Cheung, C., Cobos-Roa, D., Cohen-Waeber, J., Collins, B.D., Harder Jr., L.F., Kayen, R.E., Pestana, J.M., Riemer, M.F., Rogers, J.D., Storesund, R., Vera-Grunauer, X., and Wartman, J. (2008). "New Orleans and Hurricane Katrina. IV: Orleans East Bank (Metro) Protected Basin." *Journal of Geotechnical and Geoenvironmental Engineering*, 134 (5), 762-779.

Shen, W.Y., and Teh, C.I. (2004). "Analysis of Laterally Loaded Piles in Soil with Stiffness Increasing with Depth." *Journal of Geotechnical and Geoenvironmental Engineering*, 130 (8), 878-882.

Sills G.L., Vroman N.D., Wahl R.E., and Schwanz N.T. (2008). "Overview of New Orleans Levee Failures: Lessons Learned and Their Impact on National Levee Design and Assessment." *Journal of Geotechnical and Geoenvironmental Engineering*, 134 (5), 556-565.

Smith, I.M., and Su, N. (1997). "Three-Dimensional FE Analysis of a Nailed Soil Wall Curved in Plan." *International Journal for Numerical and Analytical Methods in Geomechanics*, 21 (9), 583-597.

Sprague, C.J., Carver, C.A., and Allen, S. (2002). "Development of RECP Performance Test Methods." *Journal of Geotechnical Testing*, 25 (4), 1-10.

Synthetic Industries (1995). PYRAMAT™ *Permanent Erosion and Reinforcement Matrix*. Product Literature. Chattanooga, Tennessee.

TenCate Mirafi® (2001). *Seaming of Geosynthetics*. TenCate Mirafi®. <http://www.tencate.com/smartsite.dws?id=4462>. Accessed: June 15, 2010.

TenCate Mirafi® (2010a). *Mirafi® HP270*. TenCate Mirafi®. [www.tencate.com/TenCate/Geosynthetics/documents/HP Series/TDS_HP270A.pdf](http://www.tencate.com/TenCate/Geosynthetics/documents/HP%20Series/TDS_HP270A.pdf). Accessed: July 8, 2010.

TenCate Mirafi® (2010b). *Mirafi® HP370*. TenCate Mirafi®. [www.tencate.com/TenCate/Geosynthetics/documents/HP Series/TDS_HP370A.pdf](http://www.tencate.com/TenCate/Geosynthetics/documents/HP%20Series/TDS_HP370A.pdf). Accessed: July 8, 2010.

TenCate Mirafi® (2010c). *Mirafi® HP565*. TenCate Mirafi®. [www.tencate.com/TenCate/Geosynthetics/documents/HP Series/TDS_HP565A.pdf](http://www.tencate.com/TenCate/Geosynthetics/documents/HP%20Series/TDS_HP565A.pdf). Accessed: July 8, 2010.

TenCate Mirafi® (2010d). *Mirafi® HP570*. TenCate Mirafi®. [www.tencate.com/TenCate/Geosynthetics/documents/HP Series/TDS_HP570A.pdf](http://www.tencate.com/TenCate/Geosynthetics/documents/HP%20Series/TDS_HP570A.pdf). Accessed: July 8, 2010.

TenCate Mirafi® (2010e). *Mirafi® HP665*. TenCate Mirafi®. [www.tencate.com/TenCate/Geosynthetics/documents/HP Series/TDS_HP665A.pdf](http://www.tencate.com/TenCate/Geosynthetics/documents/HP%20Series/TDS_HP665A.pdf). Accessed: July 8, 2010.

TenCate Mirafi® (2010f). *Mirafi® HP770*. TenCate Mirafi®. [www.tencate.com/TenCate/Geosynthetics/documents/HP Series/TDS_HP770A.pdf](http://www.tencate.com/TenCate/Geosynthetics/documents/HP%20Series/TDS_HP770A.pdf). Accessed: July 8, 2010.

TenCate Mirafi® (2010g). *Mirafi® HP465*. TenCate Mirafi®. [www.tencate.com/TenCate/Geosynthetics/documents/HP Series/TDS_HP465A.pdf](http://www.tencate.com/TenCate/Geosynthetics/documents/HP%20Series/TDS_HP465A.pdf). Accessed: July 8, 2010.

TenCate Mirafi® (2010h). *Mirafi® PP200/40*. TenCate Mirafi®. [www.tencate.com/TenCate/Geosynthetics/documents/HP Series/TDS_PP200x40.pdf](http://www.tencate.com/TenCate/Geosynthetics/documents/HP%20Series/TDS_PP200x40.pdf). Accessed: July 8, 2010.

Terzaghi, K., Peck, R.B., Mesri, G. (1996). *Soil Mechanics in Engineering Practice*. John Wiley and Sons, Inc., 3rd Edition. New York, New York.

Thiesen, M.S. (1992). "The Role of Geosynthetics in Erosion and Sediment Control: An Overview." *Geotextiles and Geomembranes*, 11, 535-550.

USACE (2000). *Engineering and Design: Design and Construction of Levees*. United States Army Corps of Engineers Technical Manual EM 1110-2-1913.

USACE (1995). *Engineering Use of Geotextiles*. Technical Manual No. 5-818-8, United States Army Corps of Engineers Air Force Manual No. 32-1030.

USACE (2007). *Hurricane and Storm Damage Reduction System Design Guidelines*. Interim Document from New Orleans District Engineering Division, October 2007.

Vitton, S., Harris, W., Whitman, M., and Liang, R. (1998). "Application of Anchored Geosynthetic Systems for In Situ Slope Stabilization of Fine-Grained Soils." *Transportation Research Record: Journal of the Transportation Research Board*, 1633, 94-101.

Wisconsin Transportation Bulletin (2010). *Geotextiles in Road Construction/Maintenance and Erosion Control*. Transportation Information Center. Bulletin No. 16, Madison, Wisconsin. http://epdfiles.engr.wisc.edu/pdf_web_files/tic/bulletin/Bltn_016_Geotextiles.pdf. Accessed: June 9, 2010.

Woodward, M.L., and Dendurent, J.L. (2009a). "Part 1 of 2: History, Performance and Design of Geotextiles in Levees: A report from New Orleans." *Geosynthetics*, 27 (2), 38-43.

Woodward, M.L., and Dendurent, J.L. (2009b). "Part 2 of 2: History, Performance and Design of Geotextiles in Levees." *Geosynthetics*, 27 (3), 38-44.

Xue, L.K. (2003). Numerical Modeling of Anchor-Soil Interaction. PhD Dissertation, National University of Singapore.

Zhang, M., Song, E., and Chen, Z. (1999). "Ground Movement Analysis of Soil Nailing Construction by Three-Dimensional (3-D) Finite Element Modeling (FEM)." *Computers and Geotechnics*, 25 (4), 191-204.



"An Industry, Agency & University Partnership"

